Search for Rare and Lepton Flavour Violating Decays of the Higgs Boson with the ATLAS Detector

Eric Drechsler
Simon Fraser University
On behalf of the ATLAS Collaboration

10. February 2020
Lake Louise Winter Institute
Lake Louise, AB

ATLAS EXPERIMENT

SFU SIMON FRASER UNIVERSITY
ENGAGING THE WORLD

Production Modes

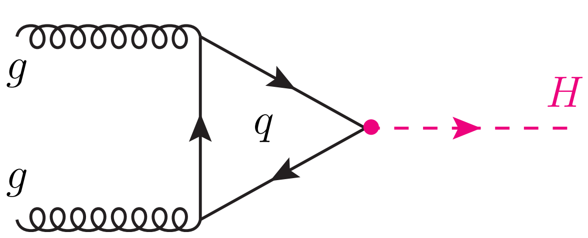

gluon-gluon-Fusion (ggF)

$\sigma^{\text{SM}}_{\text{ggF}}(pp \to H) = 48.6$ pb

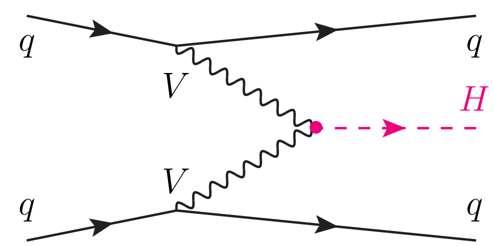

Vectorboson-Fusion (VBF)

$\sigma^{\text{SM}}_{\text{VBF}}(pp \to qqH) = 3.8$ pb

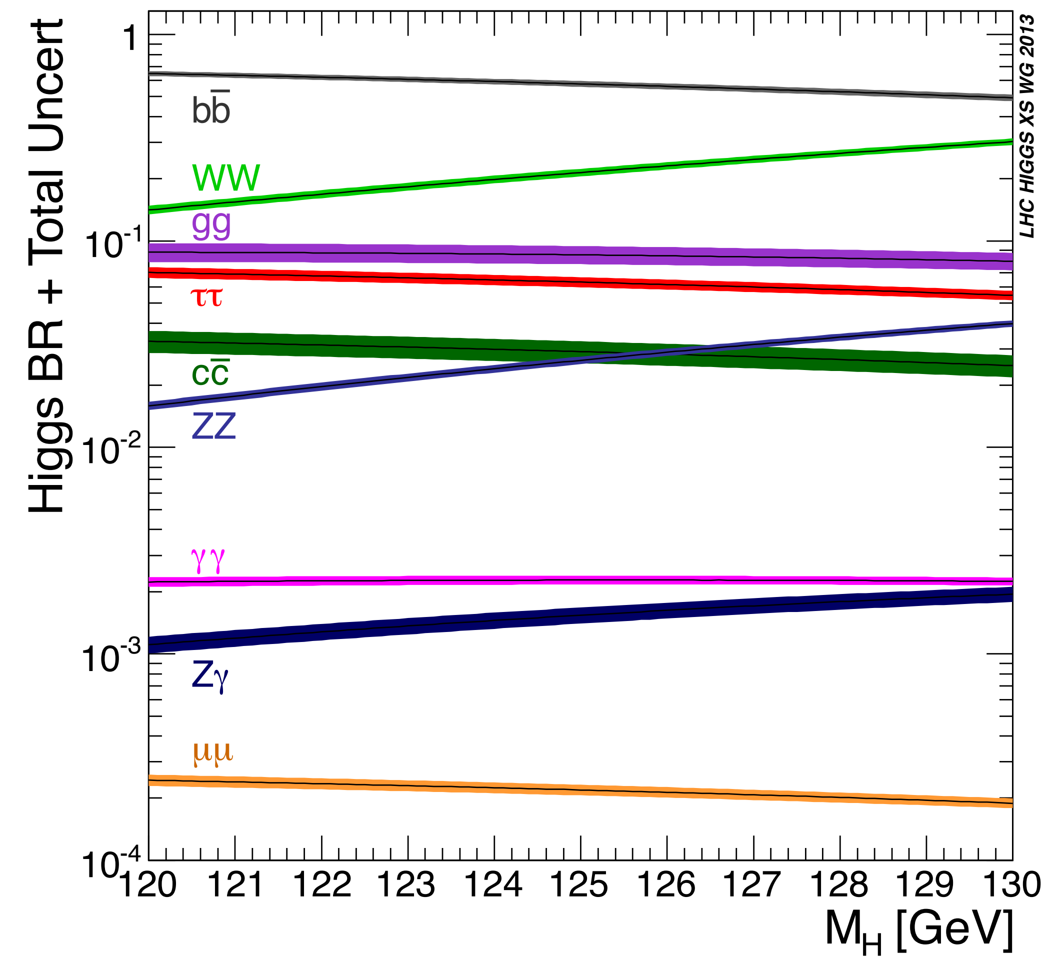

Production Modes

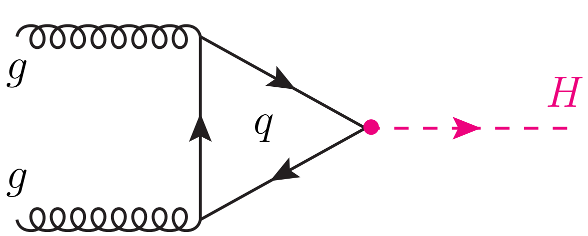

gluon-gluon-Fusion (ggF)

$\sigma_{\text{ggF}}^{\text{SM}}(pp \to H) = 48.6$ pb

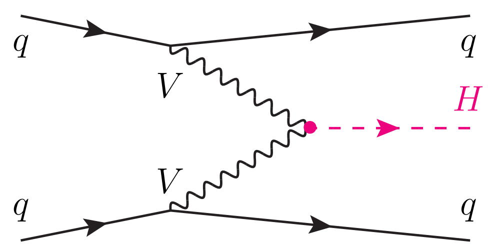

Vectorboson-Fusion (VBF)

$\sigma_{\text{VBF}}^{\text{SM}}(pp \to qqH) = 3.8$ pb

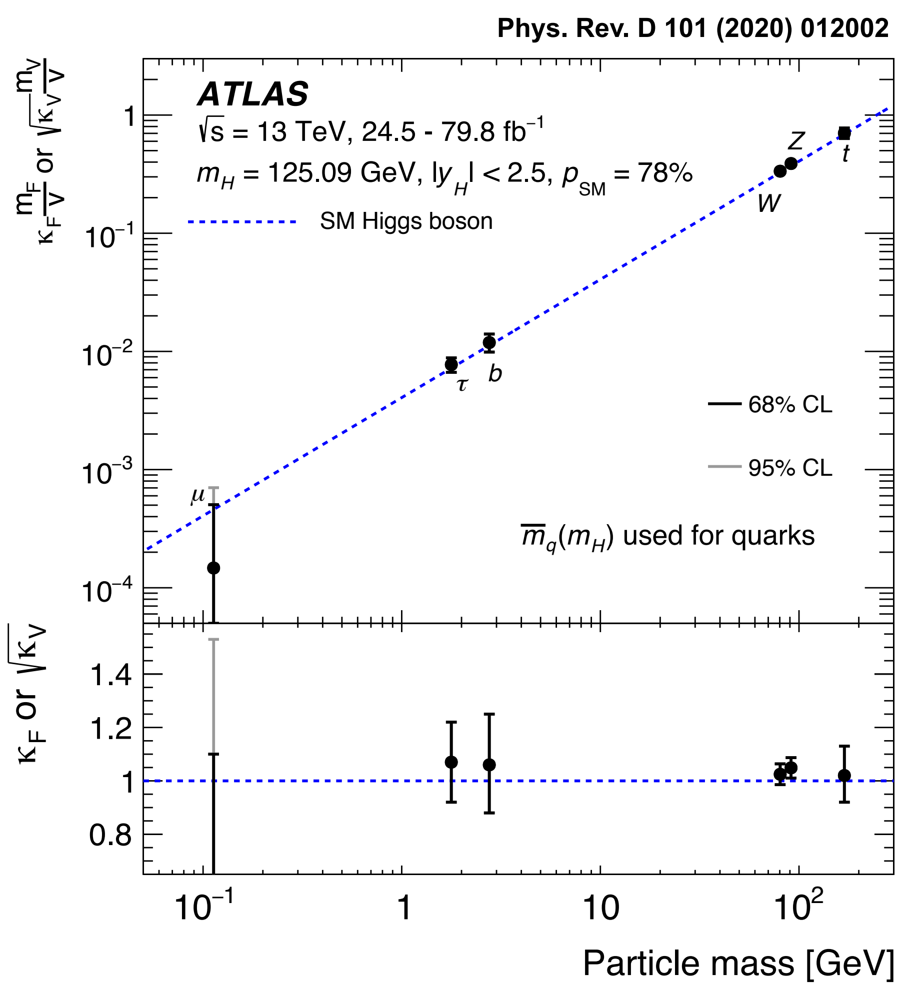

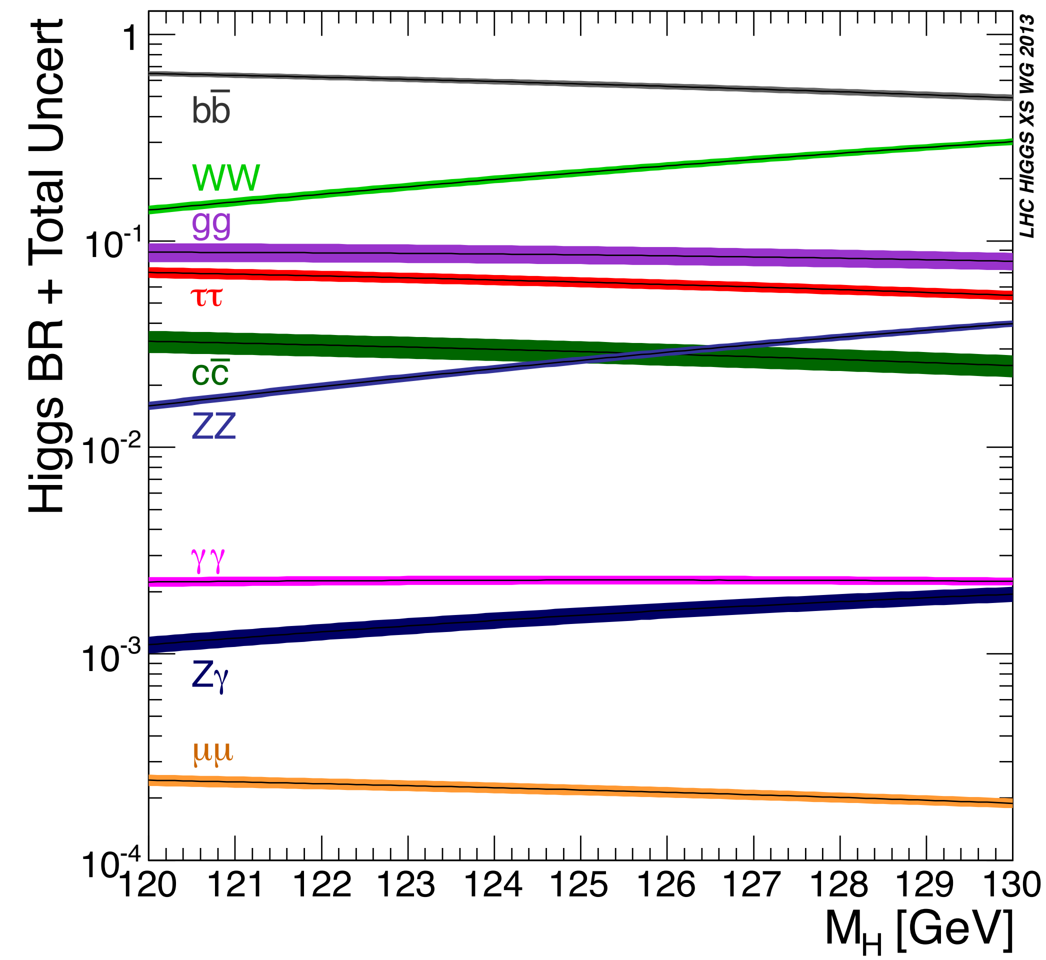

Yukawa-Coupling

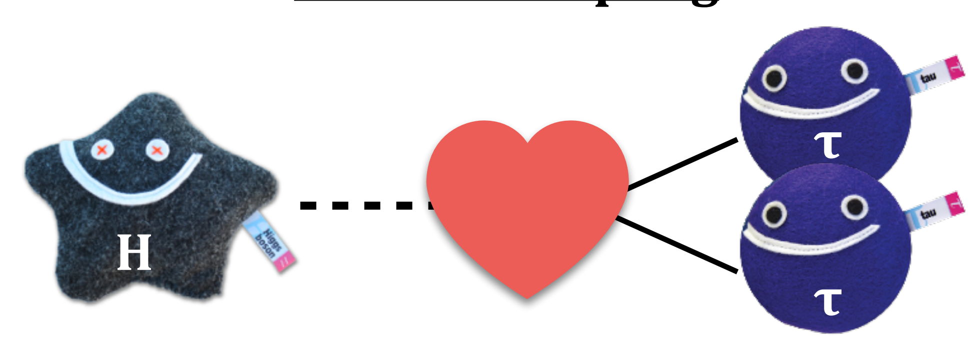

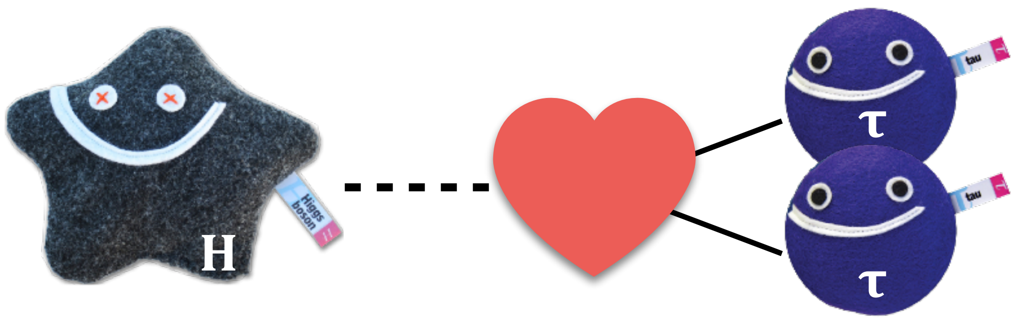

$BR^{SM}(H \to \tau\tau) \approx 6.3 \times 10^{-4}$

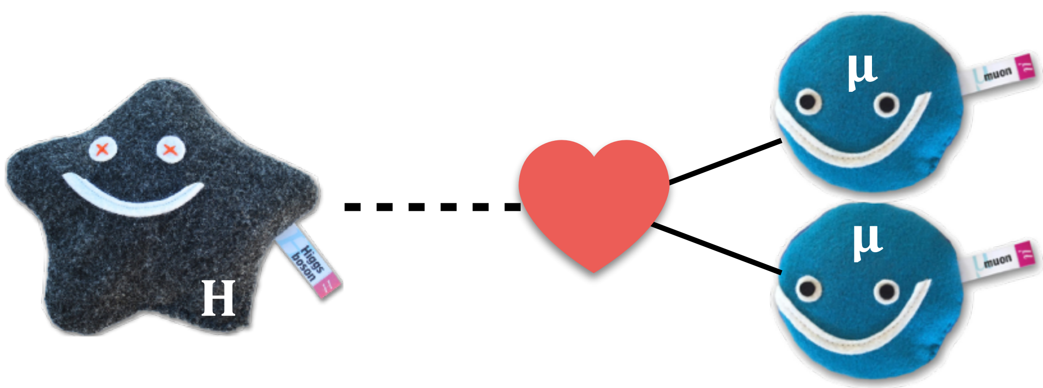

$BR^{SM}(H \to \mu\mu) \approx 2.2 \times 10^{-4}$

https://www.particlezoo.net/

Search for H→μμ Decays

2019: ATLAS-CONF-2019-028 (**139 fb^{-1}, √s=13 TeV**)

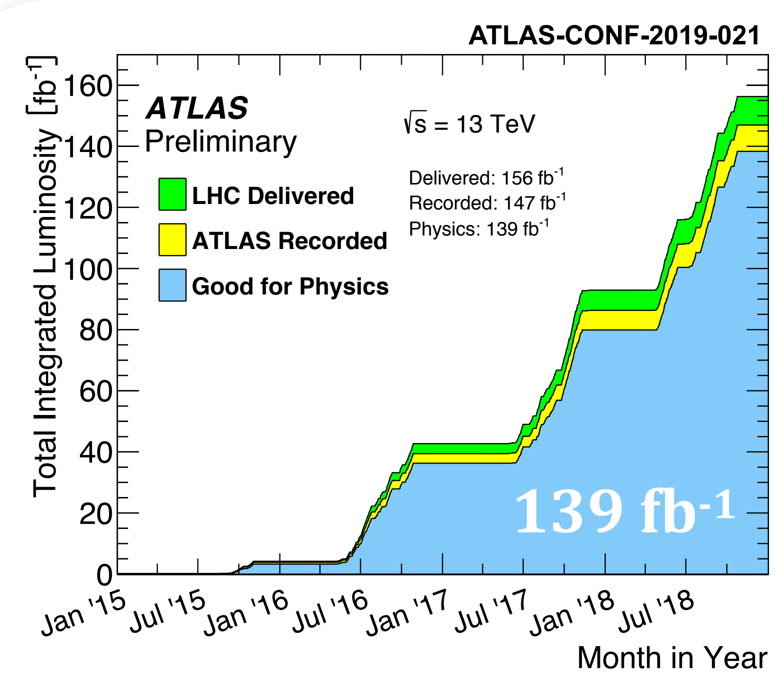

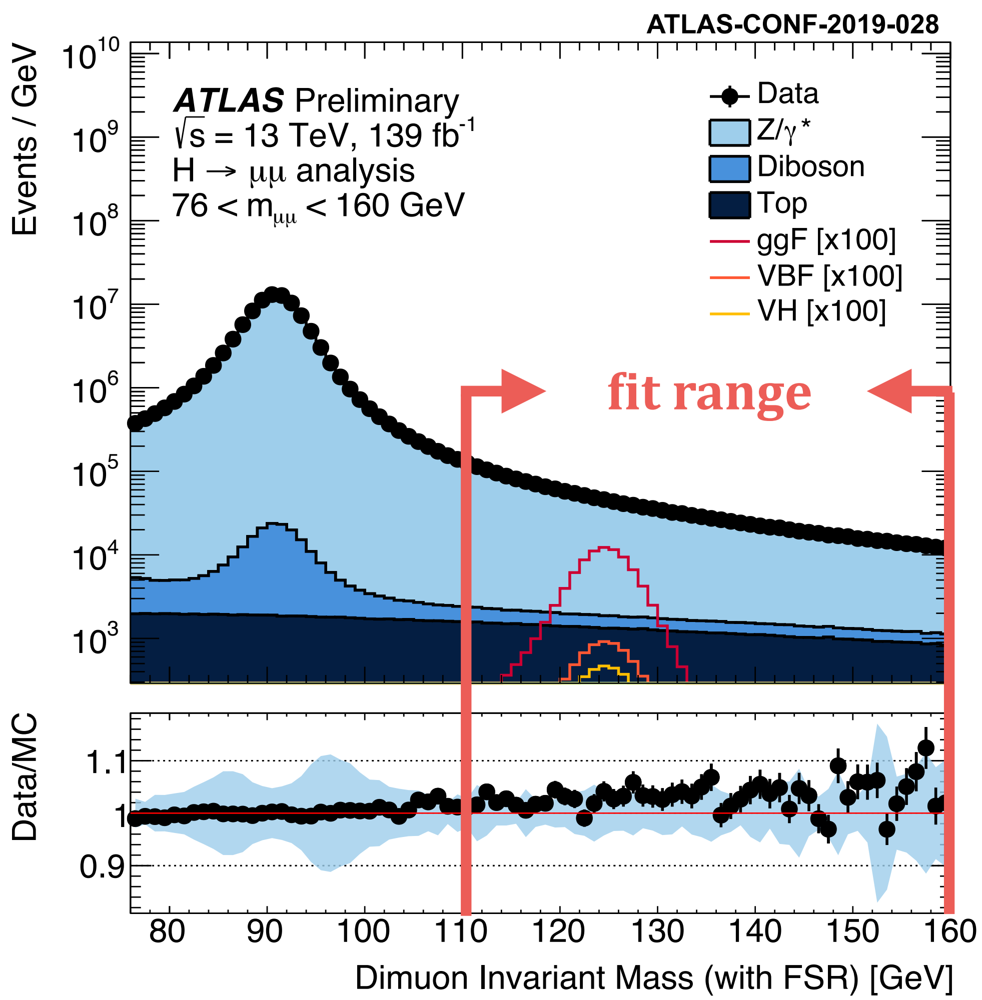

- dominating background source: $Z/\gamma^{*} \rightarrow \mu\mu$
  - 100 ab^{-1} simulation used to determine analytical model
- very small **S/B ratio ~0.2%** (120-130 GeV)
- 3% signal mass resolution improvement:
  - final state radiation recovery

Search for H→μμ Decays with ATLAS

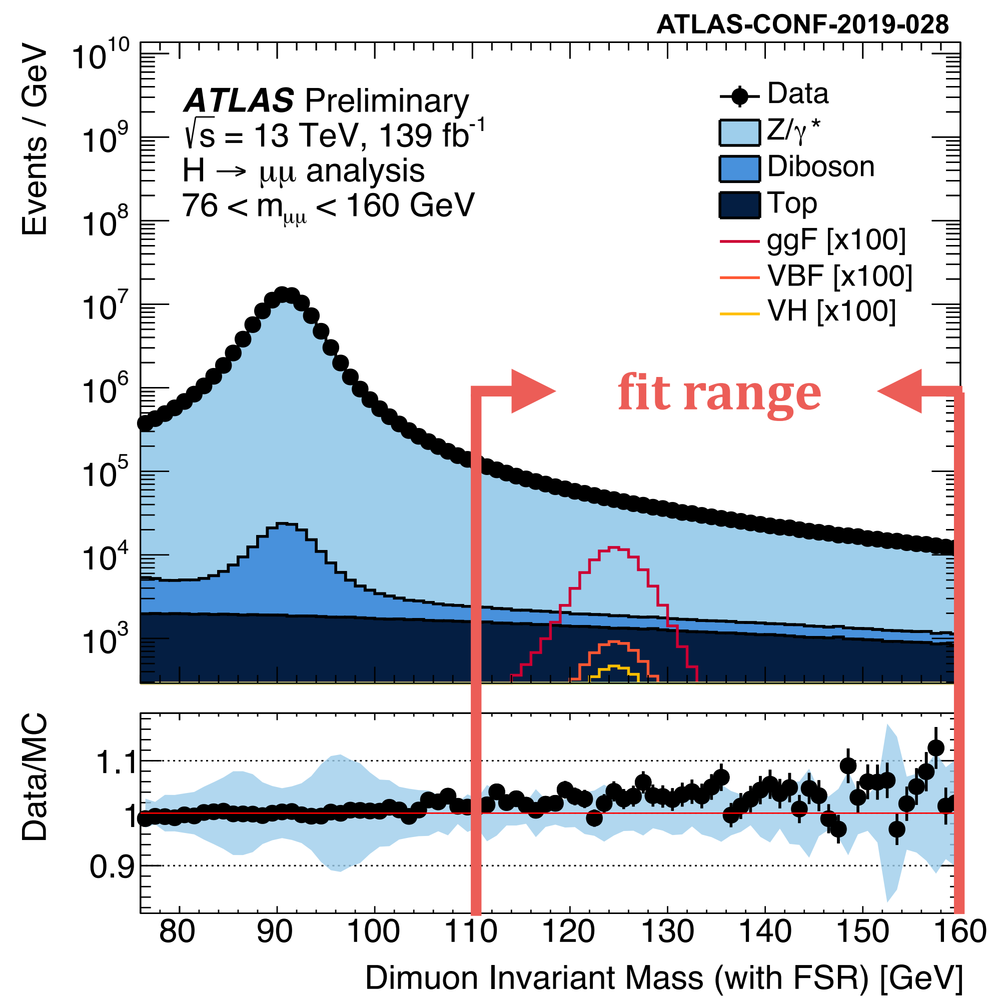

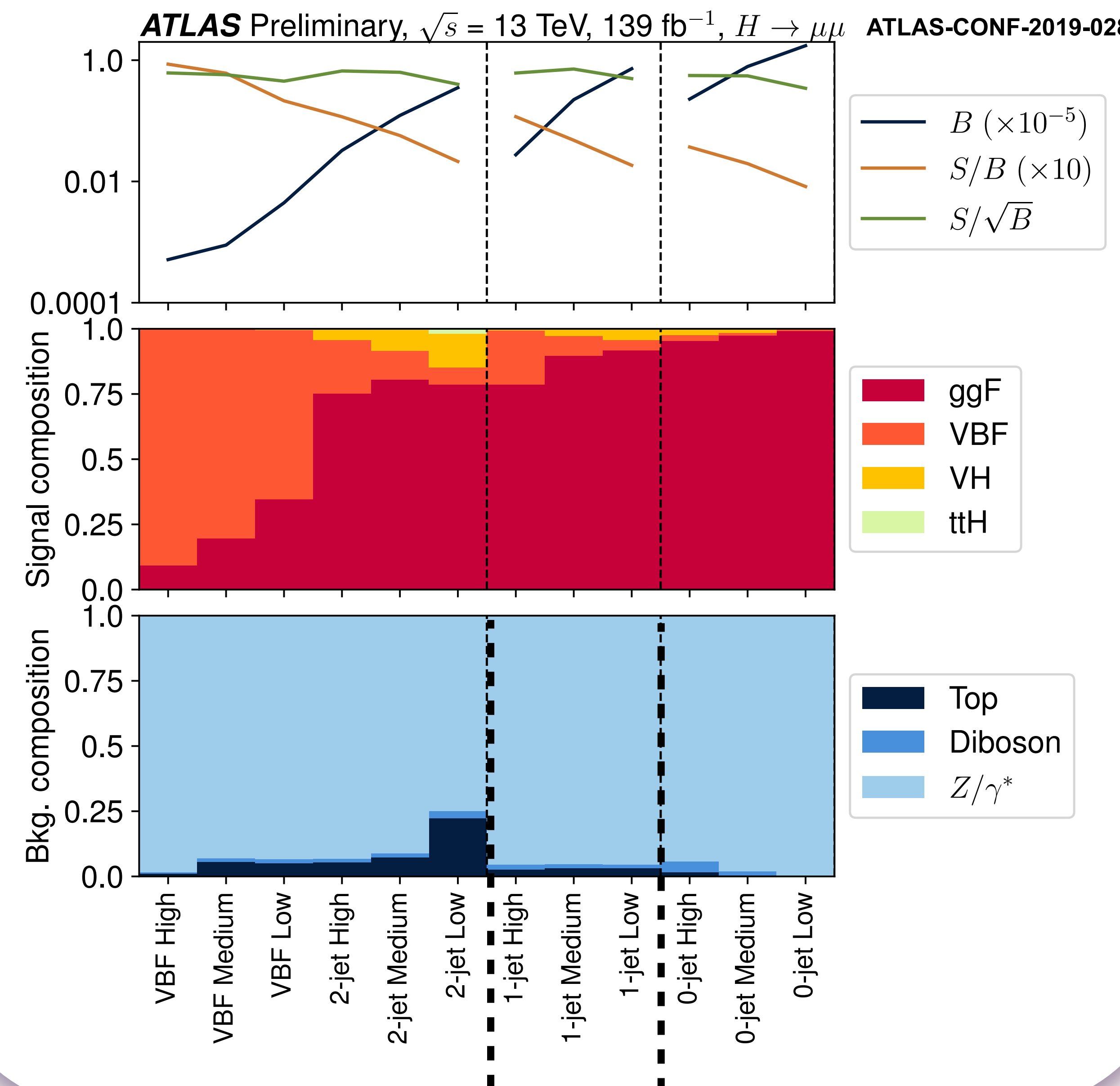

- dominating background source: Z/γ*→μμ
  - 100 ab^{-1} simulation used to determine analytical model
- very small **S/B ratio ~0.2%** (120-130 GeV)
- 3% signal mass resolution improvement:
  - final state radiation recovery

- **12** exclusive **BDT**-score based **categories**
- training separation of **signal** region vs **data sidebands**
- main **discriminating features** (14 in total)
  - **μμ-centrality** and **-transverse momentum**

- **analytical functions** in binned **Likelihood fit**
  - background: core fct+empirical components
  - signal: double sided Crystal Ball
  - signal yield, bkgd norm free floating
- **statistical uncertainty dominates**
- best fit signal strength:
  - μ = 0.5 ± 0.7

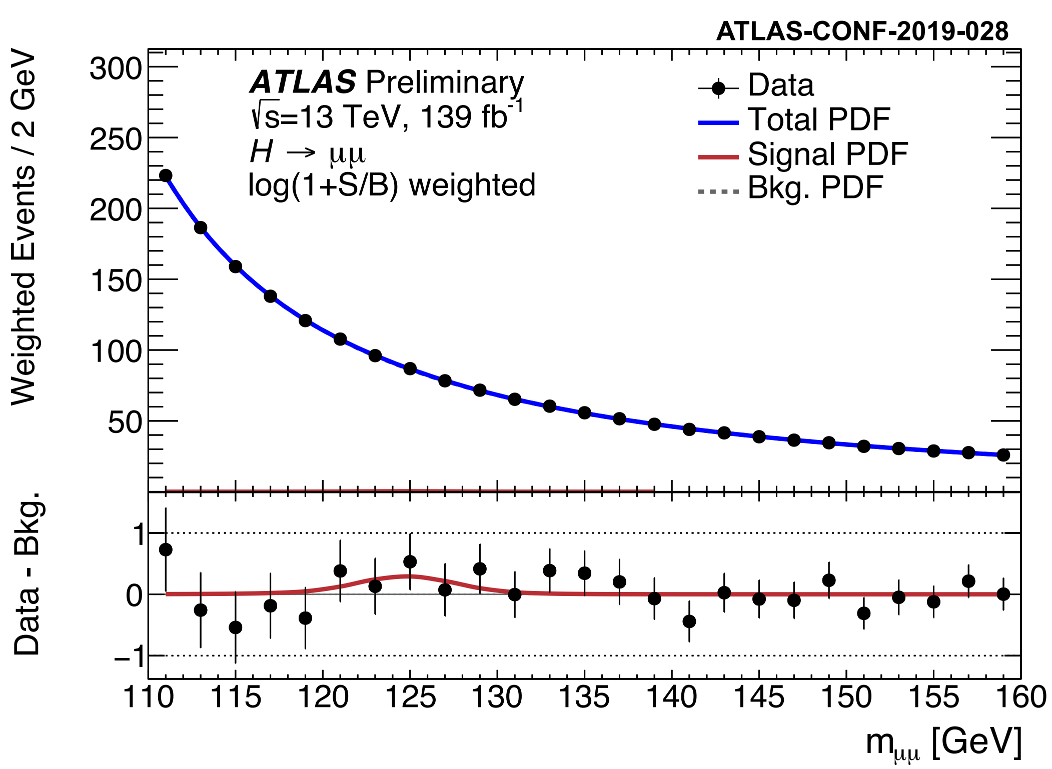

- **analytical functions** in binned **Likelihood fit**
  - background: core fct+empirical components
  - signal: double sided Crystal Ball
  - signal yield, bkgd norm free floating
- **statistical uncertainty dominates**
- best fit signal strength:
  - $\mu = 0.5 \pm 0.7$

- background-only hypothesis test:
  - 0.8σ observed (1.5σ expected)
- upper limit on branching ratio (CL@95%)
  - BR(H→μμ) < $3.8 \cdot 10^{-4}$
  - **~1.7 times SM prediction** (1.3 expected)
- **50% higher sensitivity** wrt previous ATLAS result
- CMS limit: 2.9 times SM (7+8+13 TeV, 20+36 fb^{-1})

PRL 122 (2019) 021801

ATLAS-CONF-2019-028

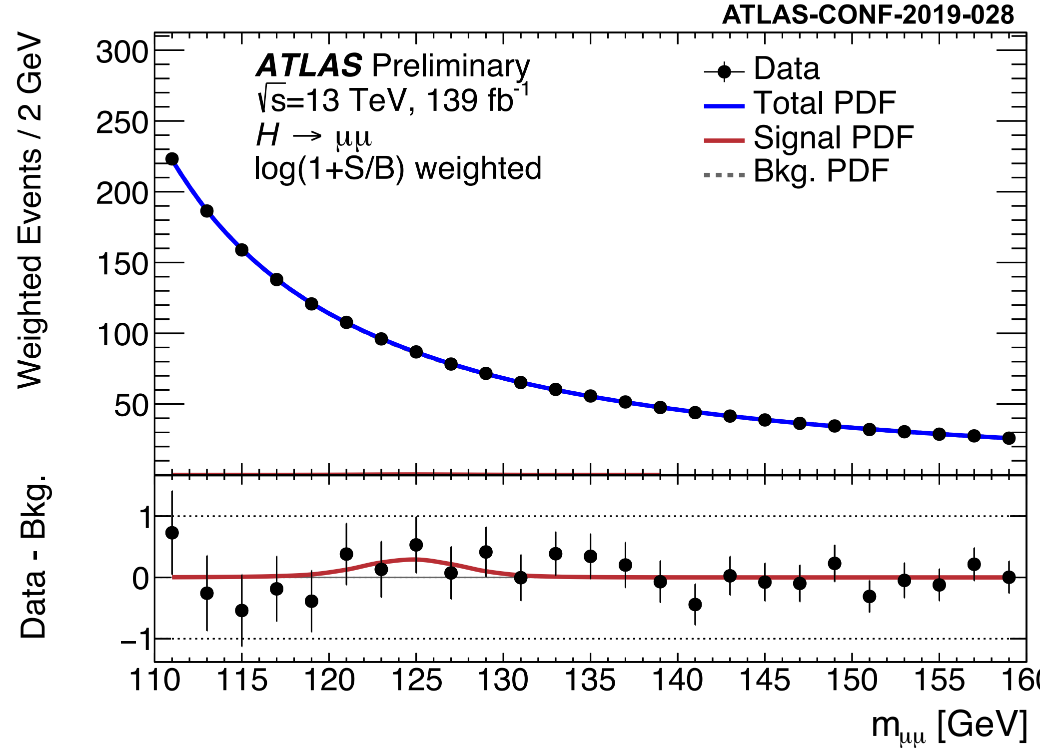

ATLAS-CONF-2019-028

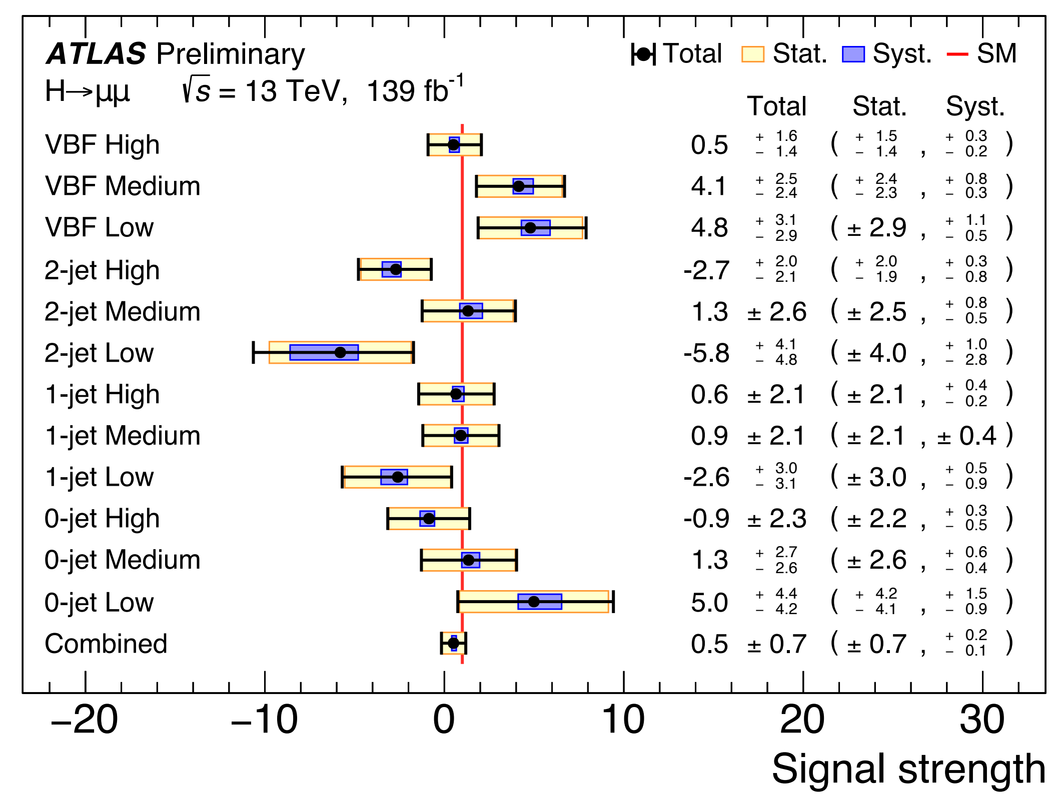

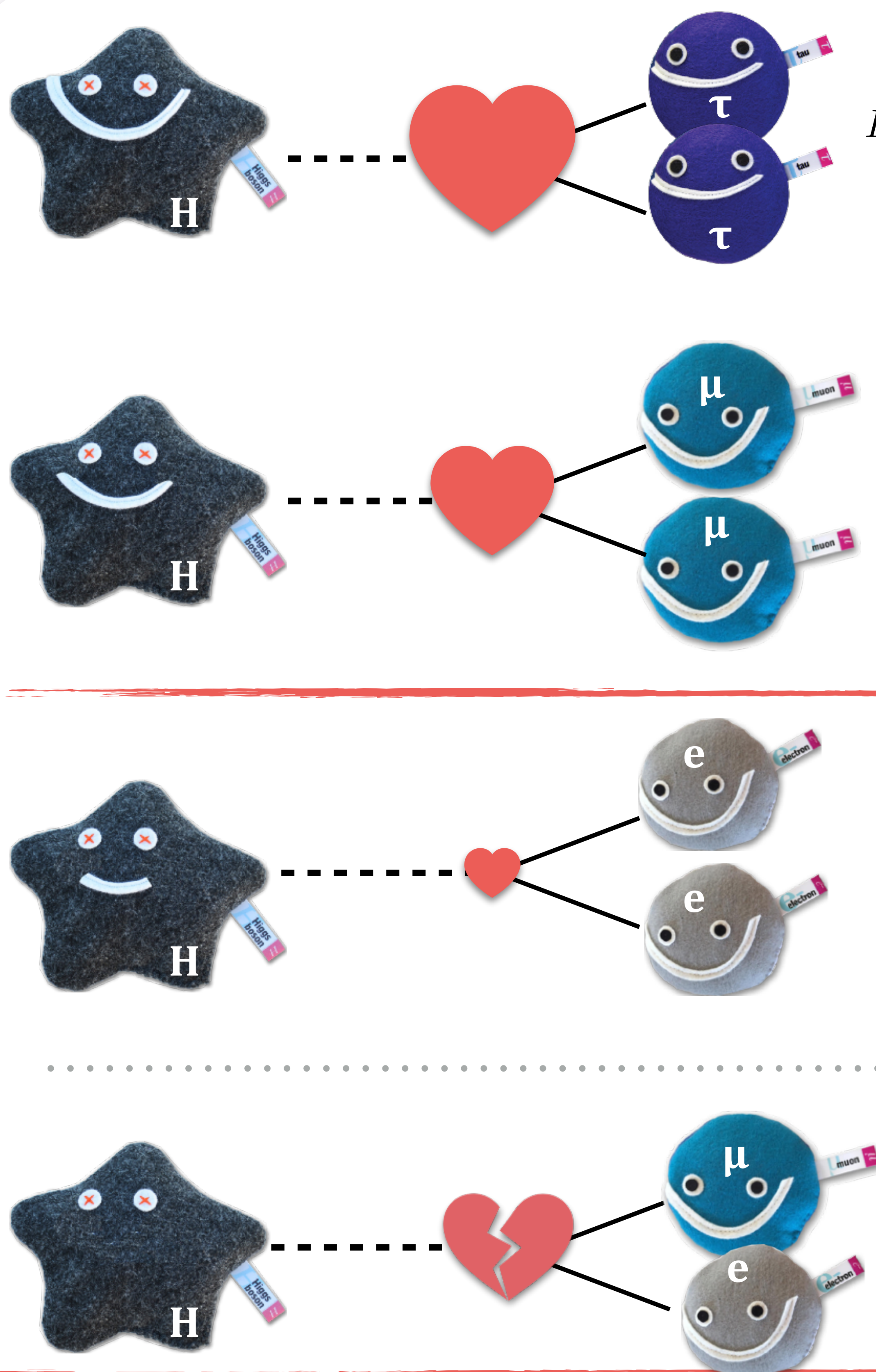

$BR^{SM}(H \to \tau\tau) \approx 6.3 \times 10^{-4}$

$BR^{SM}(H \to \mu\mu) \approx 2.2 \times 10^{-4}$

$BR^{SM}(H \to ee) \approx 5.0 \times 10^{-9}$

$BR^{SM}(H \to \ell\ell') \sim 0$

https://www.particlezoo.net/

Search for H→μμ Decays

2019: ATLAS-CONF-2019-028 (**139 fb^{-1}, √s=13 TeV**)

Search for H→ee and H→eμ

2019: Phys. Lett. B 801 (2020) 135148 (**139 fb^{-1}, √s=13 TeV**)

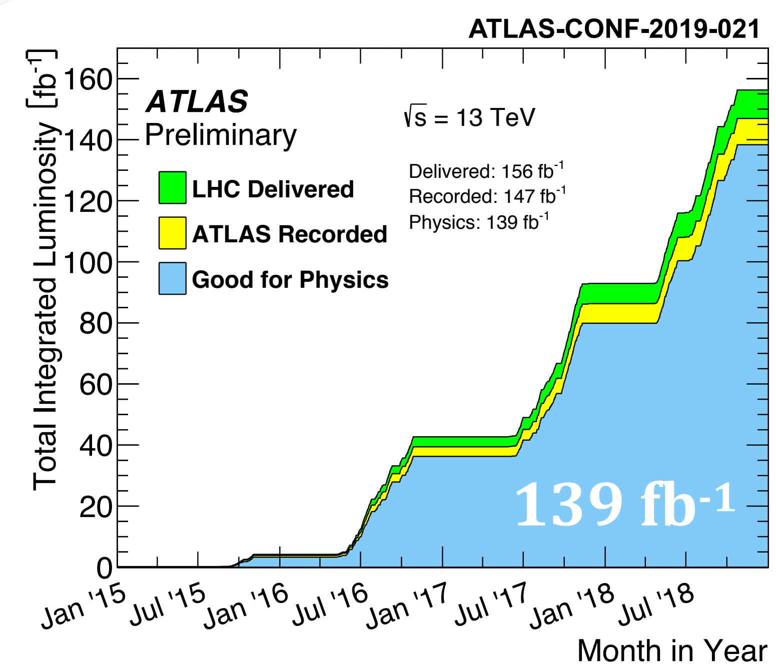

Baseline

- object selection
- MET suppression
- 110 GeV < m_{ll} < 160 GeV

Low-p_T

H→eμ only

- subleading lepton p_T < 27 GeV
- multijet background enriched

VBF

- jets in opposite hemisphere
- $|\Delta\eta_{jj}|>3$. m_{jj} > 500 GeV

Central

- each lepton: $|\eta| < 1$

Low-p_T(ll) | **Mid-p_T(ll)** | **High-p_T(ll)**

Non-Central

- otherwise

Low-p_T(ll) | **Mid-p_T(ll)** | **High-p_T(ll)**

Baseline

- object selection
- MET suppression
- 110 GeV < m_{ll} < 160 GeV

Low-p_T H→eμ only

- subleading lepton p_T < 27 GeV
- multijet background enriched

VBF

- jets in opposite hemisphere
- $|\Delta\eta_{jj}|>3$. m_{jj} > 500 GeV

Central

- each lepton: $|\eta|$ < 1

Low-p_T(ll) **Mid-p_T(ll)** **High-p_T(ll)**

Non-Central

- otherwise

Low-p_T(ll) **Mid-p_T(ll)** **High-p_T(ll)**

H→ee

Category	S	B	S/B	Data
Central Low $p_T^{\ell\ell}$	230	39200	0.0057	39872
Forward Low $p_T^{\ell\ell}$	390	98500	0.0039	100844
Central Medium $p_T^{\ell\ell}$	420	30700	0.014	31182
Forward Medium $p_T^{\ell\ell}$	710	74900	0.0095	76477
Central High $p_T^{\ell\ell}$	380	13400	0.028	13625
Forward High $p_T^{\ell\ell}$	590	29900	0.020	30164
VBF	120	2530	0.049	2561

Phys. Lett. B 801 (2020) 135148

H→eμ

Category	S	B	S/B	Data
Central Low $p_T^{\ell\ell}$	210	150	1.35	171
Forward Low $p_T^{\ell\ell}$	400	560	0.72	532
Central Medium $p_T^{\ell\ell}$	250	290	0.86	277
Forward Medium $p_T^{\ell\ell}$	450	830	0.54	854
Central High $p_T^{\ell\ell}$	180	280	0.65	299
Forward High $p_T^{\ell\ell}$	300	700	0.43	707
VBF	83	100	0.82	102
Low p_T^{ℓ}	89	600	0.15	558

Phys. Lett. B 801 (2020) 135148

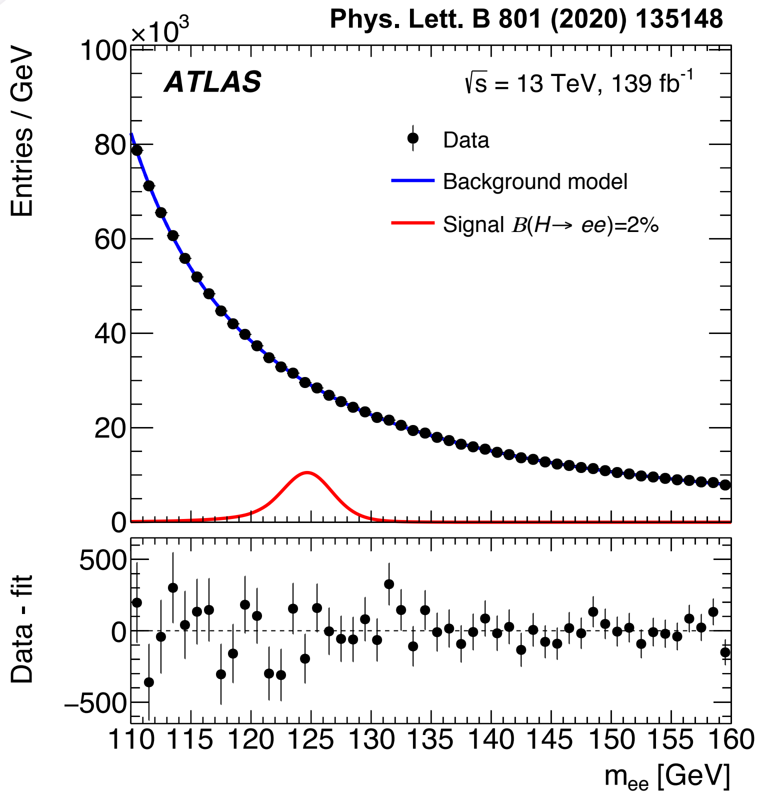

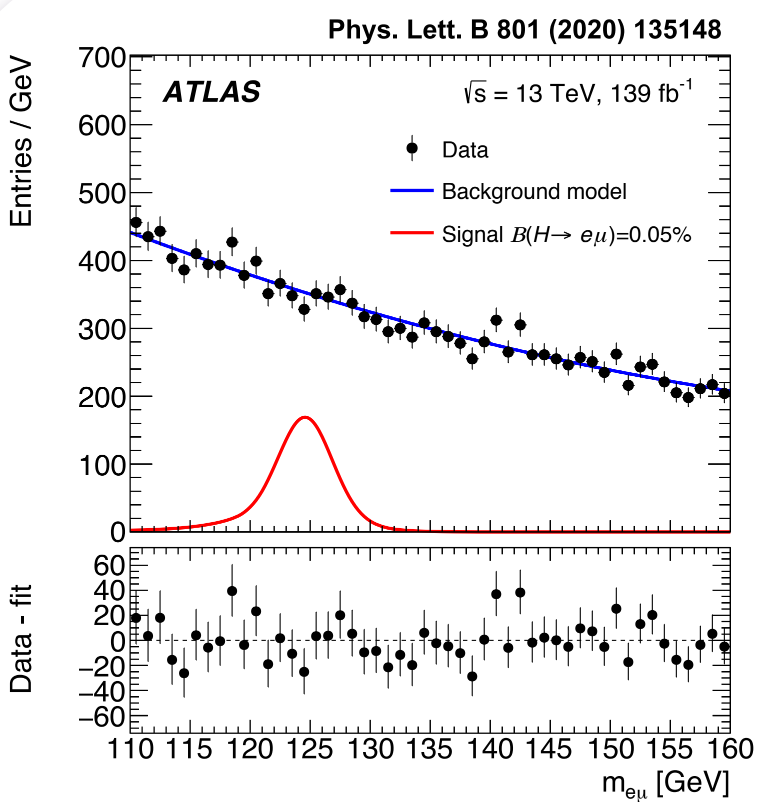

- **H→ee background processes:**
  - **Z/γ*→ee,** top-quark pair, Diboson
  - analytical model similar to H→μμ:
    - Breit-Wigner x Gaussian function
- **H→eμ background processes:**
  - smaller SM background contributions
  - Z/γ*→ττ, top, dibosons (**WW**), W+jets and multijet events
  - Bernstein polynomial (degree 2)
- parameters uncorrelated across categories

- detector resolution determining signal peak shape
  - modelled by sum of Crystal Ball + Gaussian fct
  - parameters fitted to simulation/category
- final fit per channel
  - **Likelihood fit** simultaneously for all categories
  - bkgd norm and BR(signal) free parameters

Results H→ee

- statistical uncertainty dominates
- observed (exp.) upper limit (CL@95%):
  - **BR(H → ee) < 3.6×10^{-4} (3.5×10^{-4})**
- **72,000** times SM prediction
- ~5× improvement on CMS *Run I* limit of 1.9×10^{-3}

Phys. Lett. B 744 (2015) 184

Phys. Lett. B 801 (2020) 135148

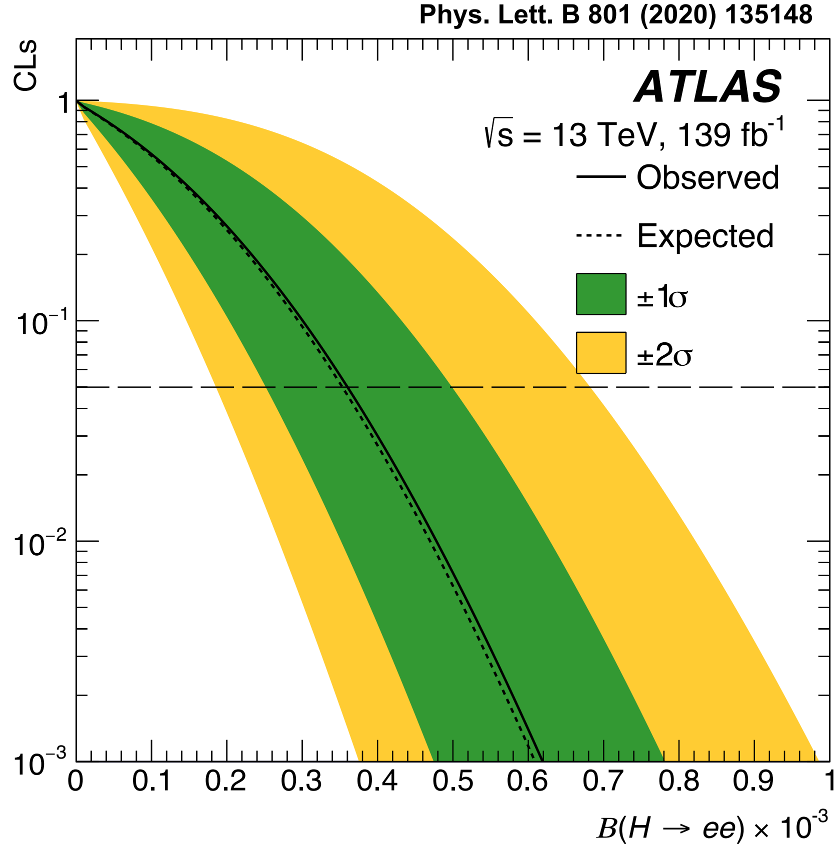

Results H→ee

- statistical uncertainty dominates
- observed (exp.) upper limit (CL@95%):
  - **BR(H → ee) < 3.6×10^{-4} (3.5×10^{-4})**
- **72,000** times SM prediction
- ~5× improvement on CMS *Run I* limit of 1.9×10^{-3}

Phys. Lett. B 744 (2015) 184

Results H→eμ

- statistical uncertainty dominates
- observed (exp.) upper limit (CL@95%):
  - **BR(H → eμ) < 6.1×10^{-5} (5.8×10^{-5})**
- ~6× improvement on CMS *Run I* limit of 3.5×10^{-4}

Phys. Lett. B 763 (2016) 472

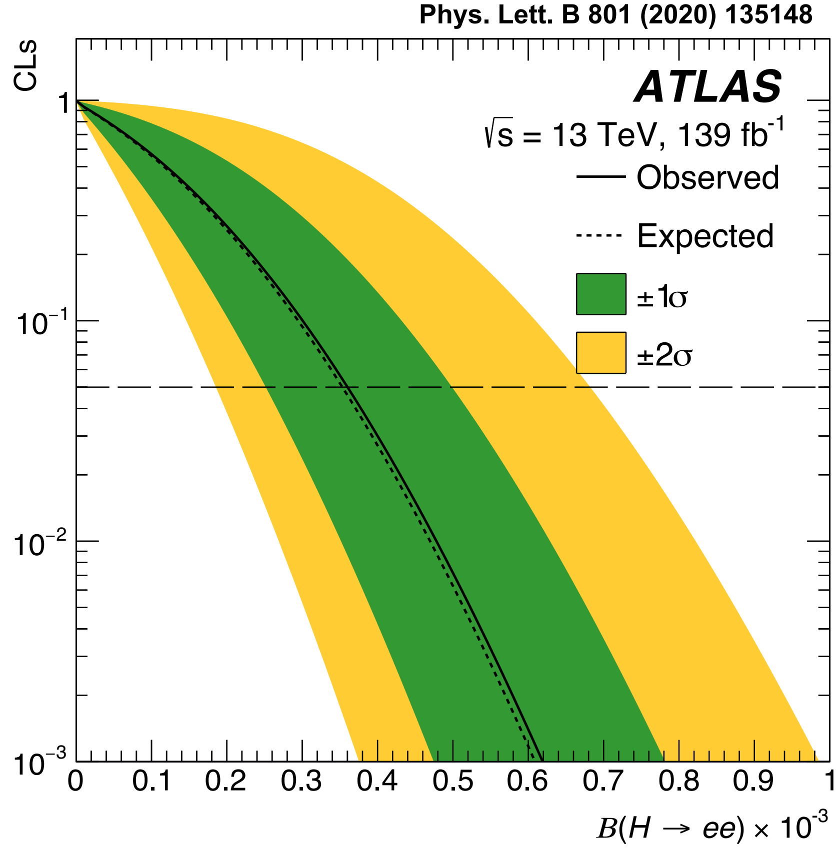

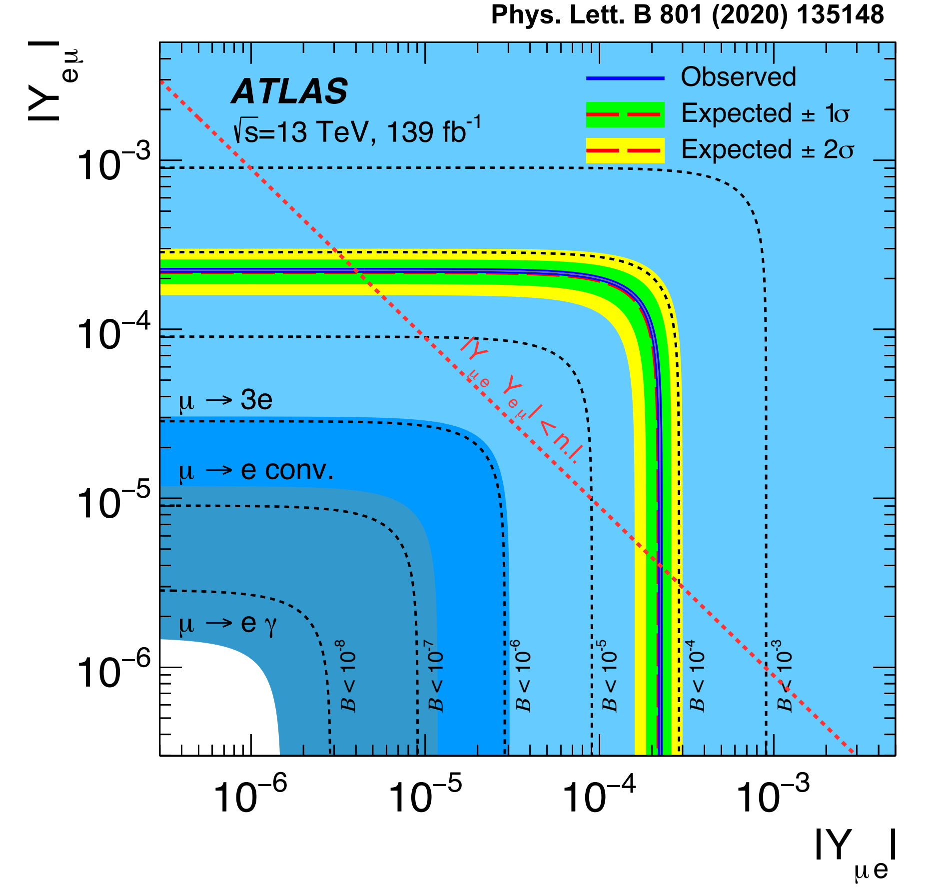

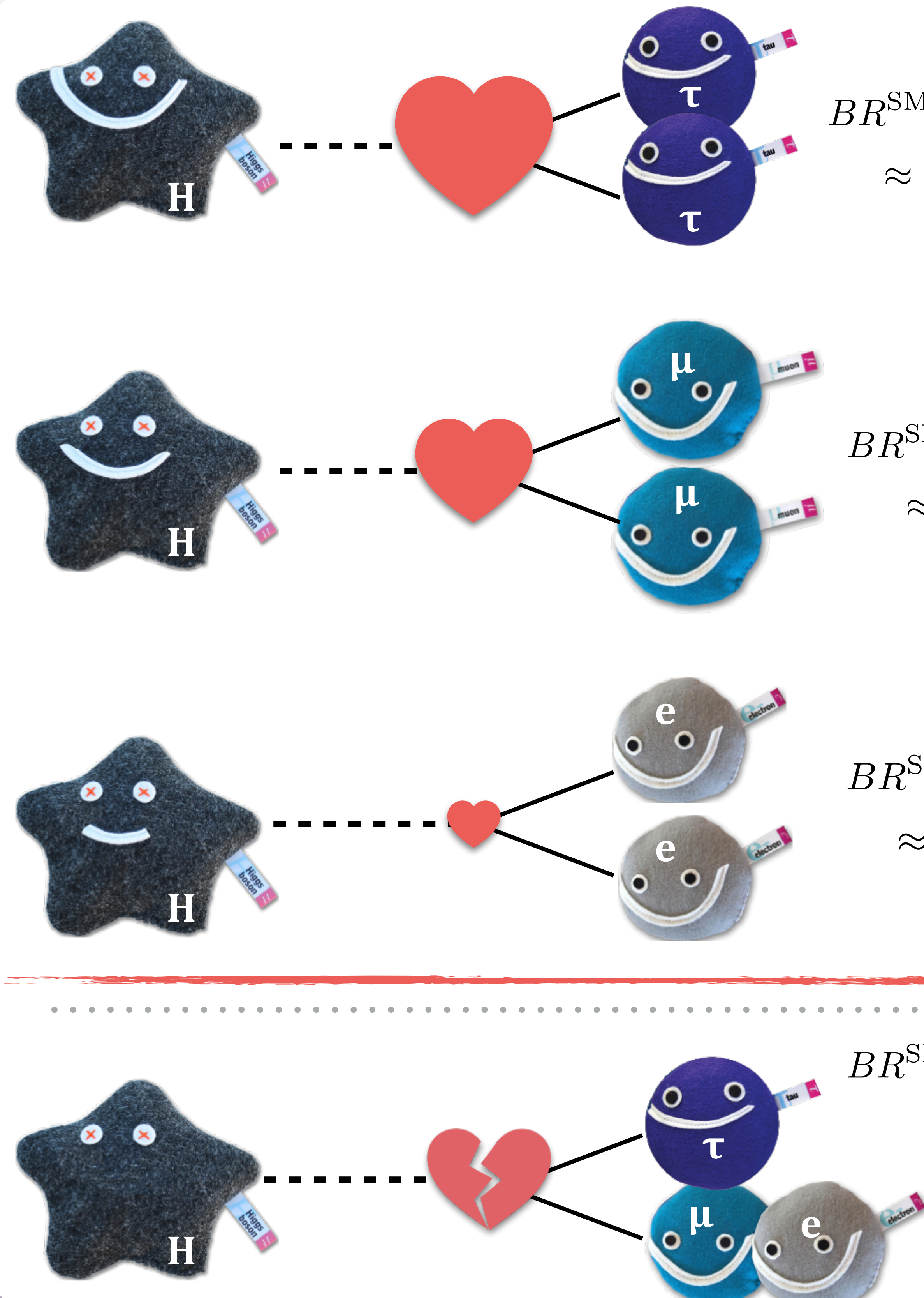

$BR^{SM}(H \to \tau\tau) \approx 6.3 \times 10^{-4}$

$BR^{SM}(H \to \mu\mu) \approx 2.2 \times 10^{-4}$

$BR^{SM}(H \to ee) \approx 5.0 \times 10^{-9}$

$BR^{SM}(H \to \ell\ell') \sim 0$

https://www.particlezoo.net/

Search for H→μμ Decays

2019: ATLAS-CONF-2019-028 **(139 fb^{-1}, √s=13 TeV)**

Search for H→ee and H→eμ

2019: Phys. Lett. B 801 (2020) 135148 **(139 fb^{-1}, √s=13 TeV)**

Search for H→τl

2019: Phys. Lett. B 800 (2020) 135069 **(36 fb^{-1}, √s=13 TeV)**

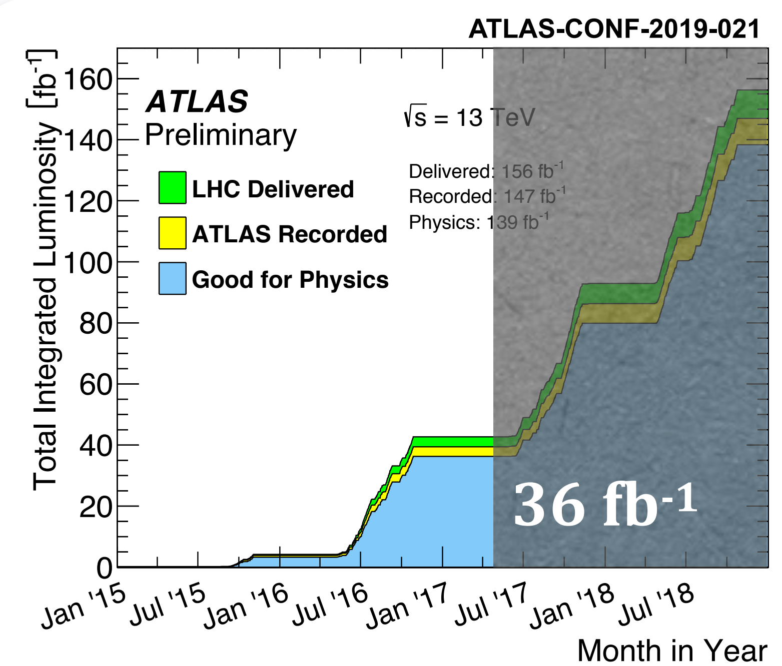

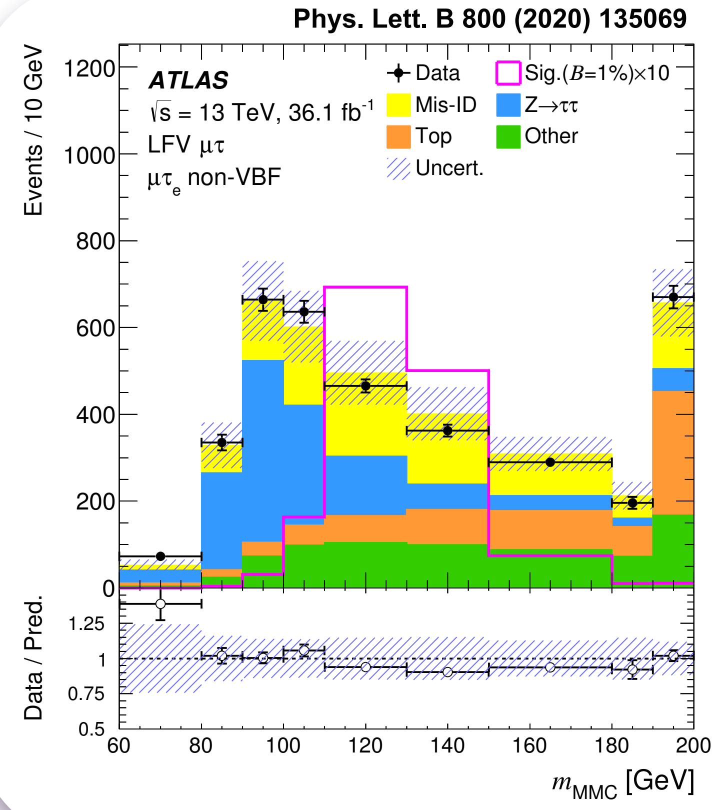

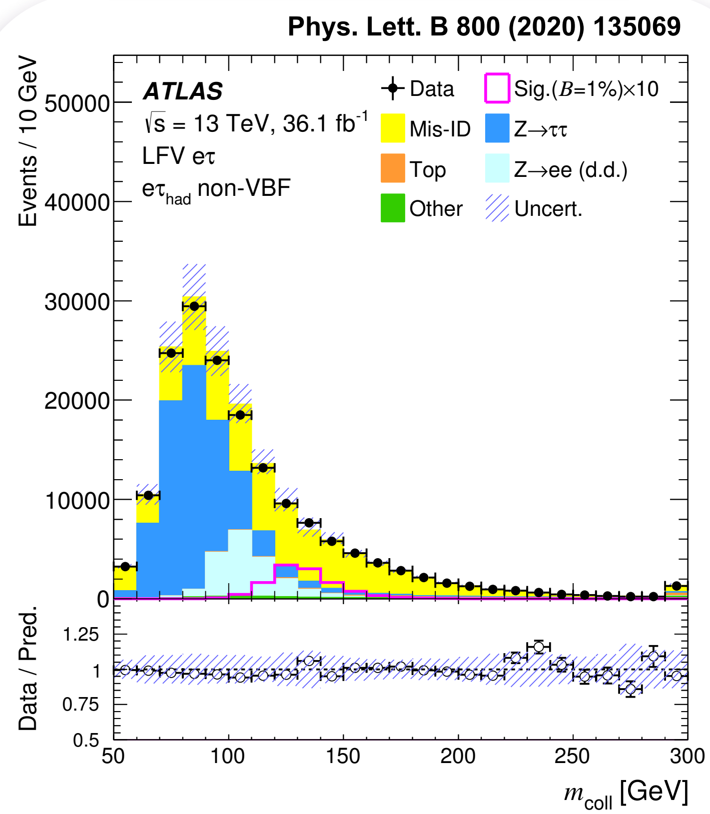

$Z/\gamma^* \to \tau\tau$ - dedicated CR
- shape from simulation
- normalisation in final fit + CR

top backgrounds - dedicated CR
- shape from simulation
- normalisation in final fit + CR

Diboson, W/Z+jets, H→ττ, H→WW
- shape & normalisation from simulation

misidentified jets - fully data driven
- Fake Factor method in multijet enriched control regions

$Z/\gamma^* \to ee$ - fully data driven
- Fake Factor method in $Z/\gamma^* \to ee$ enriched control regions

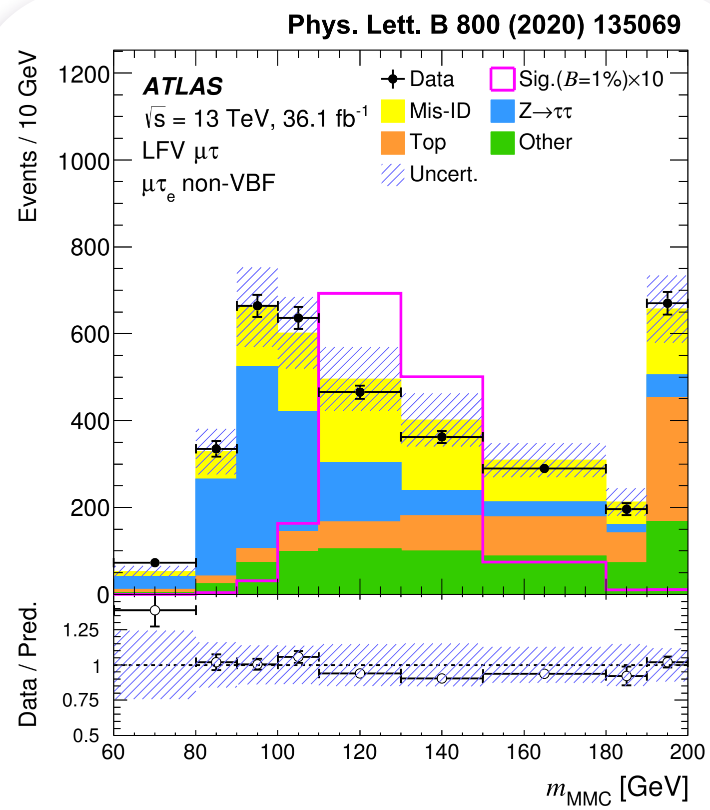

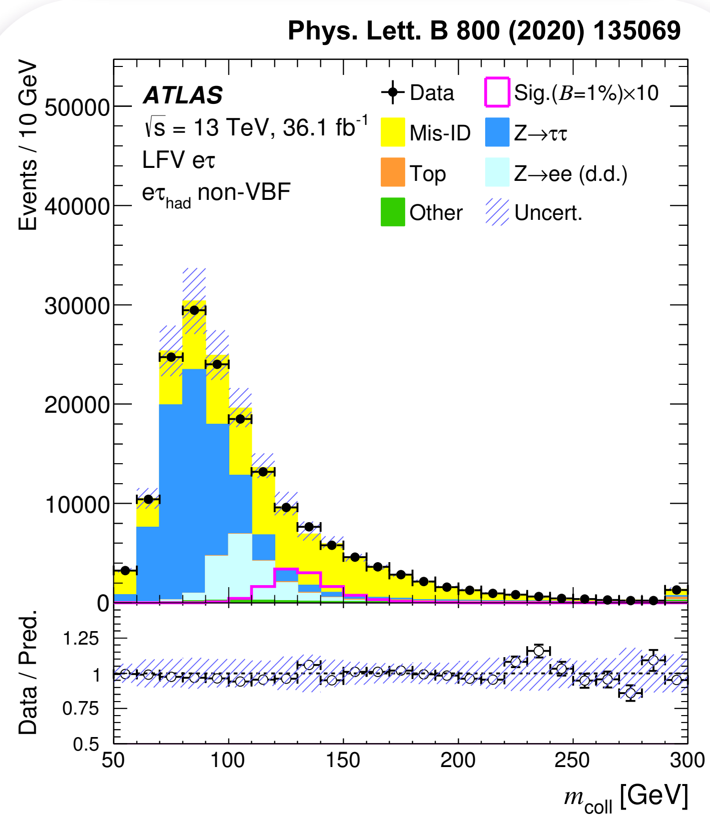

BDT

Discriminants

$\ell\tau_{\ell'}$ Variable	VBF	non-VBF	$\ell\tau_{had}$ Variable	VBF	non-VBF
m_{MMC}	HR	HR	m_{coll}	HR	HR
$p_T^{\ell_1}$	•	•	p_T^{ℓ}	•	HR
$p_T^{\ell_2}$	HR	HR	$p_T^{\tau_{had\text{-}vis}}$	•	HR
$\Delta R(\ell_1, \ell_2)$	HR	•	$\Delta R(\ell, \tau_{had\text{-}vis})$	•	•
$m_T(\ell_1, E_T^{miss})$	•	HR	$m_T(\ell, E_T^{miss})$	HR	•
$m_T(\ell_2, E_T^{miss})$	HR	•	$m_T(\tau_{had\text{-}vis}, E_T^{miss})$	HR	HR
$\Delta\phi(\ell_1, E_T^{miss})$	•	•	$\Delta\phi(\ell, E_T^{miss})$	HR	•
$\Delta\phi(\ell_2, E_T^{miss})$		HR	$\Delta\phi(\tau_{had\text{-}vis}, E_T^{miss})$	•	
$m(j_1, j_2)$	•		$m(j_1, j_2)$	•	
$\Delta\eta(j_1, j_2)$	HR		$\Delta\eta(j_1, j_2)$	•	
$p_T^{\tau}/p_T^{\ell_1}$		HR	$\sum_{i=\ell,\tau_{had\text{-}vis}} \cos\Delta\phi(i, E_T^{miss})$	•	•
			E_T^{miss}	HR	•
			m_{vis}		HR
			$\Delta\eta(\ell, \tau_{had\text{-}vis})$		•
			η^{ℓ}		•
			$\eta^{\tau_{had\text{-}vis}}$		•
			ϕ^{ℓ}		•
			$\phi^{\tau_{had\text{-}vis}}$		•
			$\phi(E_T^{miss})$		•

Bullet: used in training

HR: 5 Highest Ranked Variables

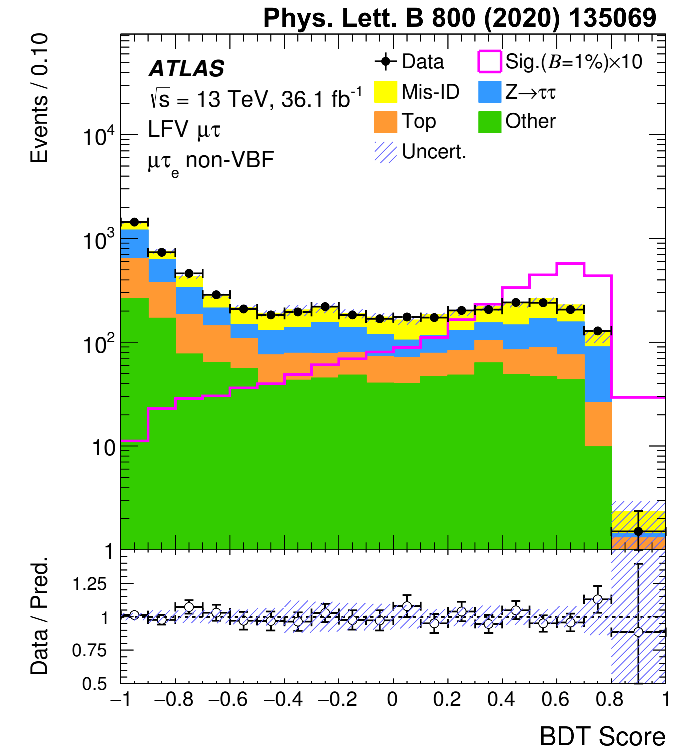

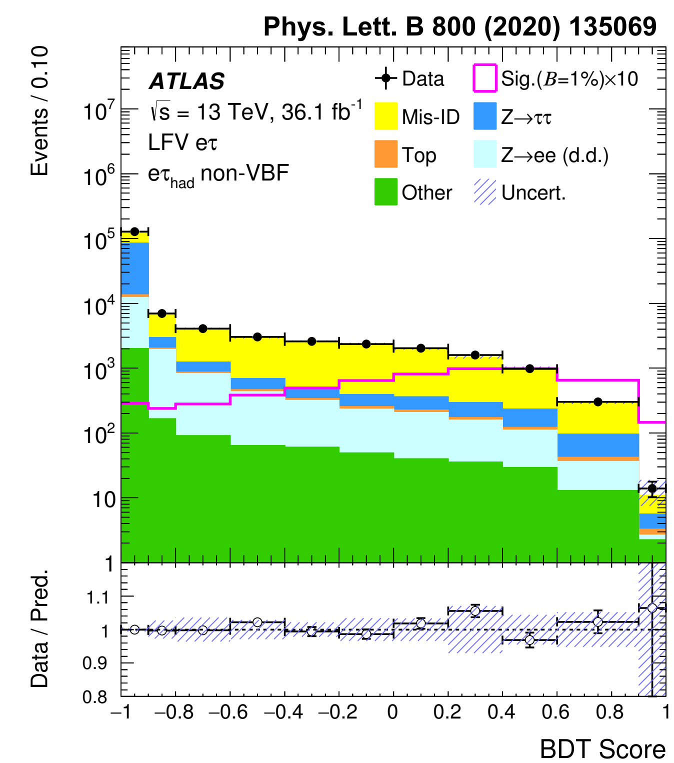

Results H→eτ

- systematic uncertainty dominates
  - data-driven background model
  - jet energy scale & resolution
- observed (exp.) upper limit (CL@95%):
  - **BR(H→eτ) < 4.7×10^{-3} (3.4×10^{-3})**
- **~2× improvement** on ATLAS *Run I* limit of 1.0×10^{-2}

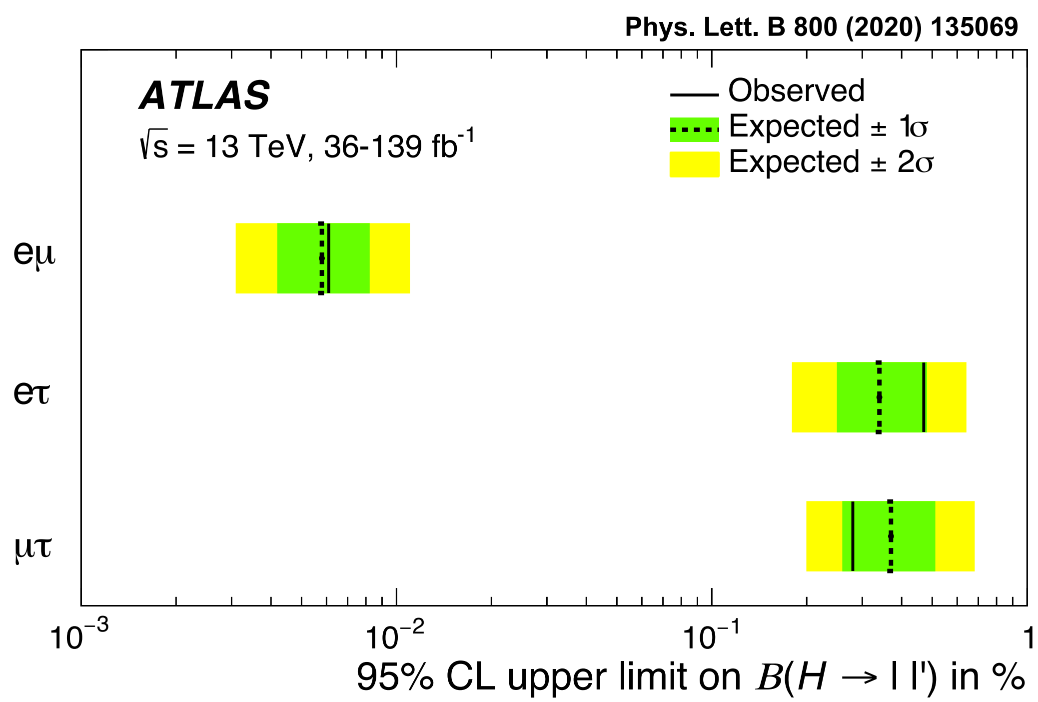

Results H→eτ

- systematic uncertainty dominates
  - data-driven background model
  - jet energy scale & resolution
- observed (exp.) upper limit (CL@95%):
  - **BR(H→eτ) < 4.7×10⁻³ (3.4×10⁻³)**
- **~2× improvement** on ATLAS *Run I* limit of 1.0×10⁻²

Results H→μτ

- systematic uncertainty dominates
  - data-driven background model
  - jet & muon calibration
- observed (exp.) upper limit (CL@95%):
  - **BR(H→μτ) < 2.8×10⁻³ (3.7×10⁻³)**
- **~5× improvement** on ATLAS *Run I* limit of 1.4×10⁻²

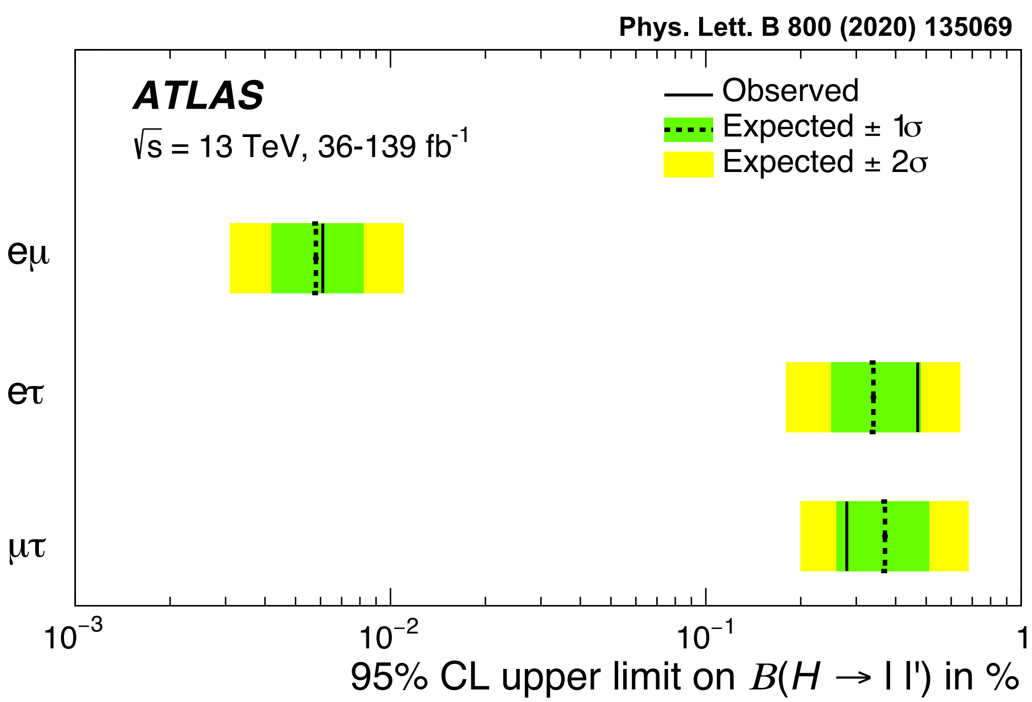

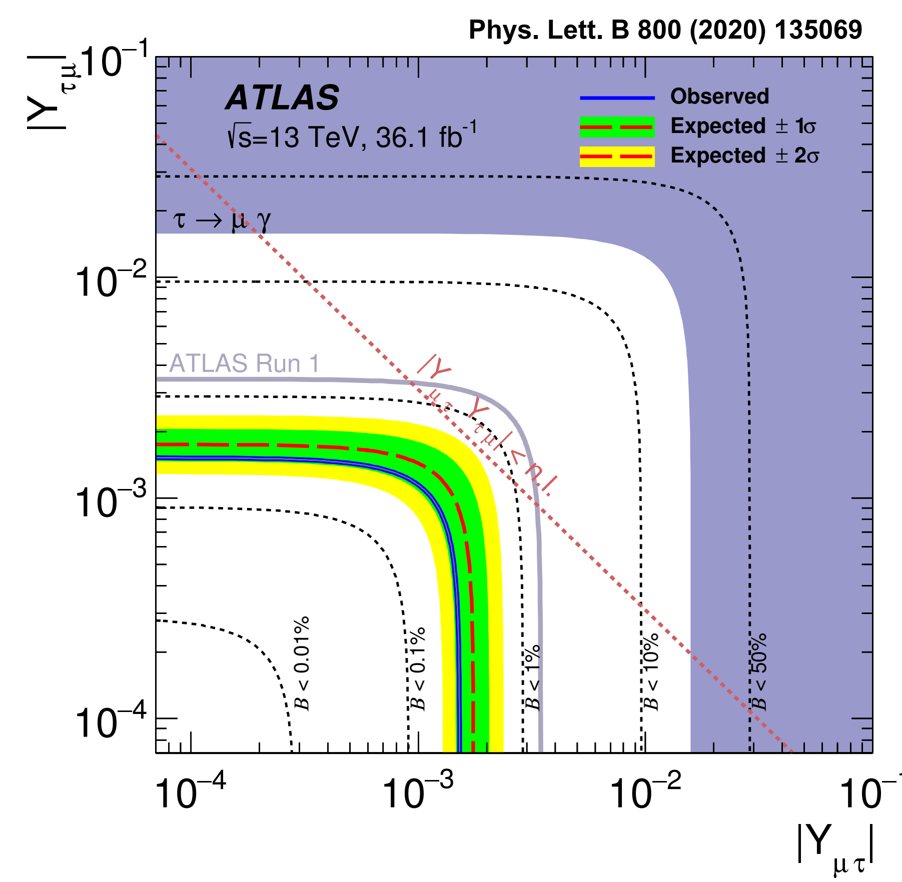

More details in the Backup slides

https://www.particlezoo.net/

	BR^{SM}
$H \to c\bar{c}$	2.9×10^{-2}
$H \to Z\gamma$	1.5×10^{-3}
$H \to \rho\gamma$	1.7×10^{-5}
$H \to \varphi\gamma$	2.3×10^{-6}
$H \to J/\psi\,\gamma$	3.0×10^{-6}

2018: **Search for $H \to J/\psi\gamma$ and $H \to \Upsilon\gamma$ (36 fb^{-1}, $\sqrt{s}$=13 TeV)**
Phys. Lett. B 786 (2018) 134

2018: **Search for $H \to \varphi\gamma$, $H \to \rho\gamma$ (36 fb^{-1}, $\sqrt{s}$=13 TeV)**
JHEP 07 (2018) 127

2018: **Search for $H \to c\bar{c}$ (36 fb^{-1}, $\sqrt{s}$=13 TeV)**
Phys. Rev. Lett. 120 (2018) 211802

2017: **Search for $H \to Z\gamma$ (36 fb^{-1}, $\sqrt{s}$=13 TeV)**
JHEP 10 (2017) 112

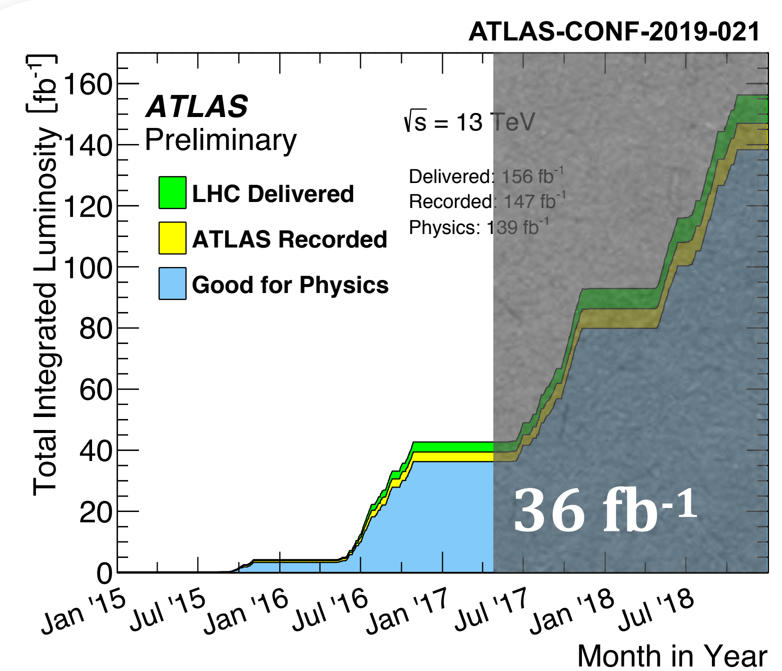

Conclusion

- Higgs boson decays to 1st/2nd generation fermions:
  - **H→ee, H→μμ**
- lepton flavour violating (LFV) Higgs boson decays:
  - **H→eμ, H→eτ, H→μτ**
- other rare decays of the Higgs boson:
  - **H→Zγ, H→cc̄**
  - **H→γ+neutral Meson (qq̄) (q=u,d,s,c,b)**

- no deviations from SM observed
- upper limits in agreement with expectations
- rare searches limited by statistical uncertainty
- new physics might hide in the details
  - increased precision important

Run 3 around the corner!

Prospects

- **H→μμ:**
  - *Run 3* (300 fb^{-1} at $\sqrt{s}$=14 TeV):
    - 2.3 std deviations excess over bkgd
    - 46% error on signal strength
  - ***Run 4* - HL-LHC** (3000 fb^{-1} at $\sqrt{s}$=14 TeV):
    - **9.5 std deviations excess** over bkgd
    - 13% error on signal strength
- upper limits calculated at 95% CL

ATL-PHYS-PUB-2018-006

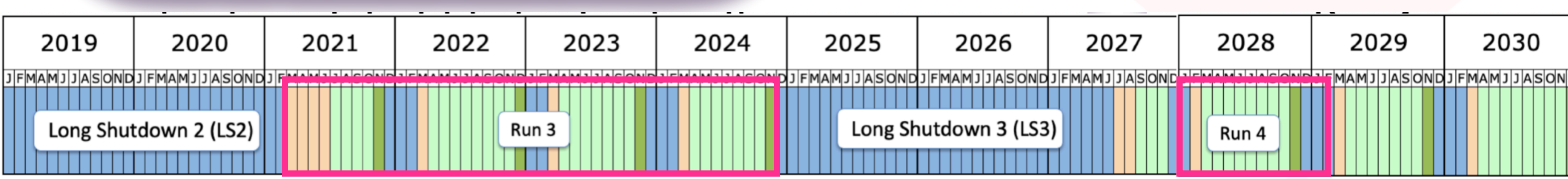

Backup

Channel	SM BR
$H \to \tau\tau$	6.3×10^{-2}
$H \to \mu\mu$	2.2×10^{-4}
$H \to ee$	5.0×10^{-9}
$H \to \ell\ell'$	not allowed

- Higgs boson decays to 1st/2nd generation fermions:
  - **H→ee, H→μμ**
- lepton flavour violating (LFV) Higgs boson decays:
  - **H→eμ, H→eτ, H→μτ**
- other rare decays of the Higgs boson:
  - **H→Zγ, H→c$\bar{c}$**
  - **H→γ+neutral Meson (q$\bar{q}$) (q=u,d,s,c,b)**

- no deviations from SM observed
- upper limits in agreement with expectations
- rare searches limited by statistical uncertainty
- new physics might hide in the details
  - increased precision important

Prospects

- **H→μμ:**
  - Run 3 (300 fb^{-1} at $\sqrt{s}$=14 TeV):
    - 2.3 std deviations excess over bkgd
    - 46% error on signal strength
  - **Run 4** (3000 fb^{-1} at $\sqrt{s}$=14 TeV):
    - **9.5 std deviations excess** over bkgd
    - 13% error on signal strength
- **H→Zγ:**
  - Run 3: upper limit 2.5x SM prediction
  - Run 4: upper limit 0.7x SM prediction
- **H→ J/ψ:**
  - Run3: upper limit 53x SM prediction
  - Run4: upper limit 15x SM prediction
- upper limits calculated at 95% CL

ATL-PHYS-PUB-2018-006
ATL-PHYS-PUB-2013-014
ATL-PHYS-PUB-2015-043

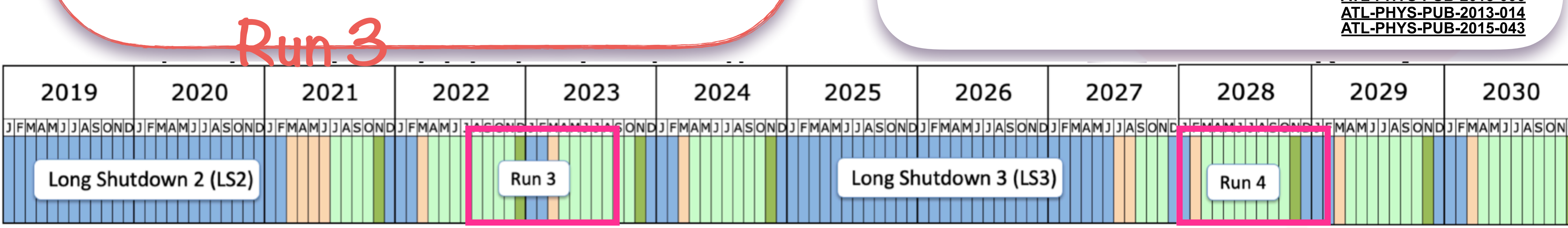

H→Zγ

JHEP 10 (2017) 112

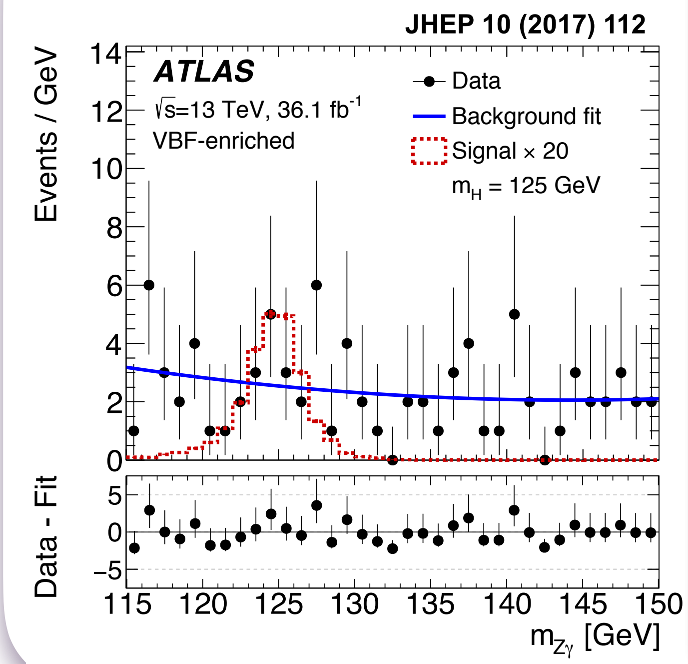

H→φγ, H→ργ
JHEP 07 (2018) 127

H→ J/ψ, H→ Υ(nS)
Phys. Lett. B 786 (2018) 134

H→cc̄
Phys. Rev. Lett. 120 (2018) 211802

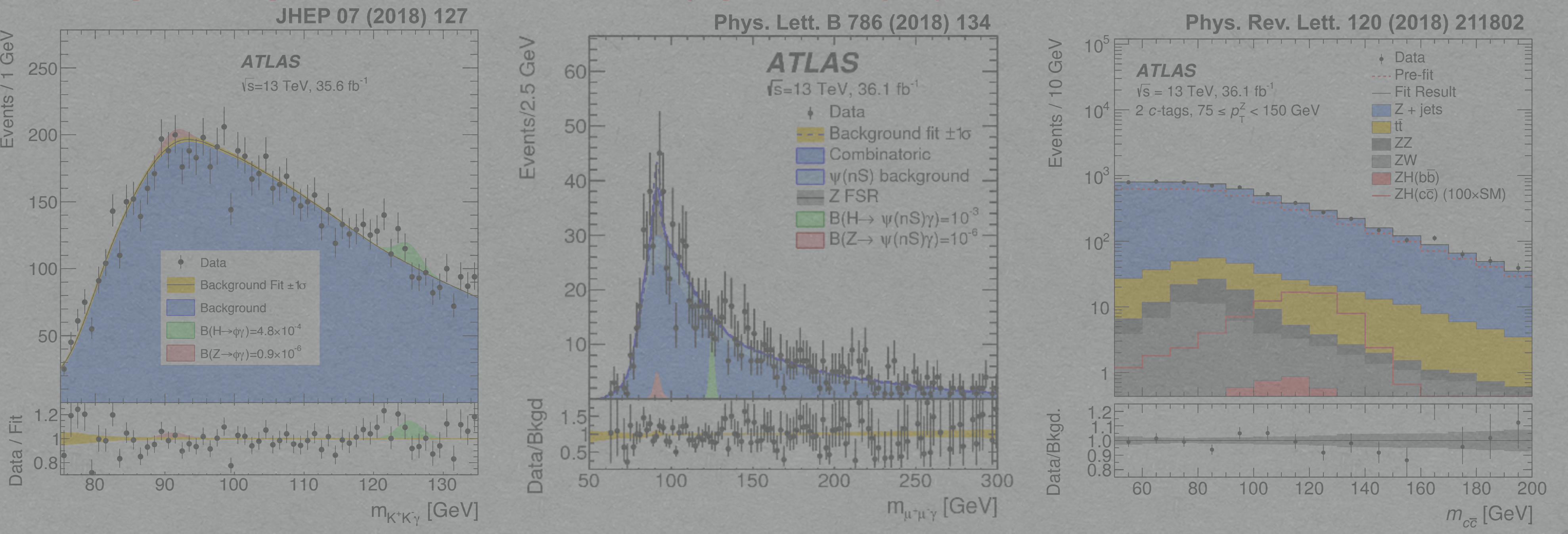

Search for H→Zγ

- sensitive to **new physics in loop**
- targeting subsequent **Z→ee or Z→μμ**
- background-only hypothesis test:
  - 1σ observed (0.5σ expected)
- observed (exp.) upper limit (CL@95%):
  - **B(H→Zγ) < 1.0×10⁻² (0.8×10⁻²)**
- limit at **6.6 times SM** prediction

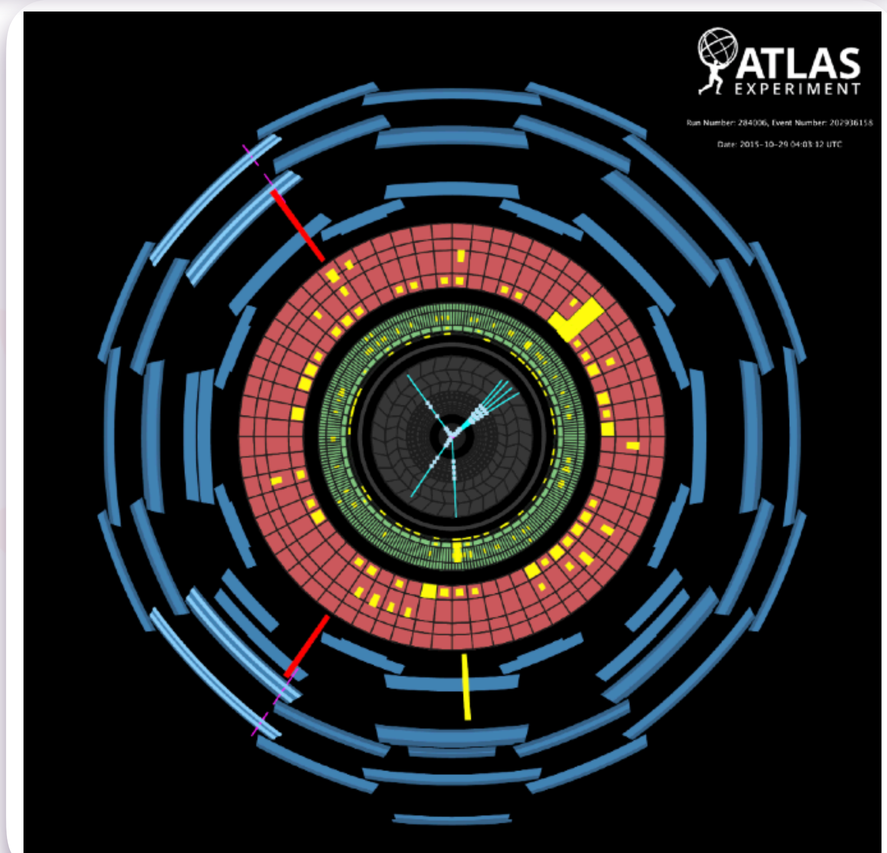

H→(Z→μμ)γ event candidate

H→Zγ

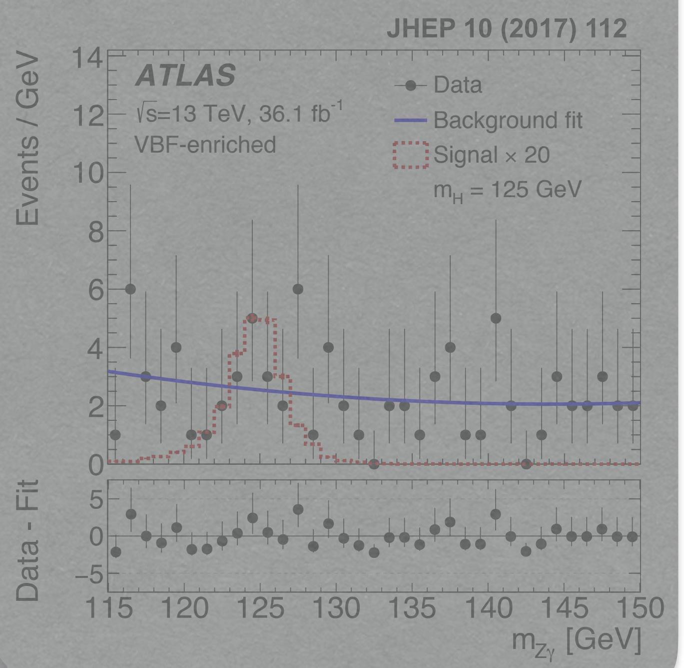

H→φγ, H→ργ

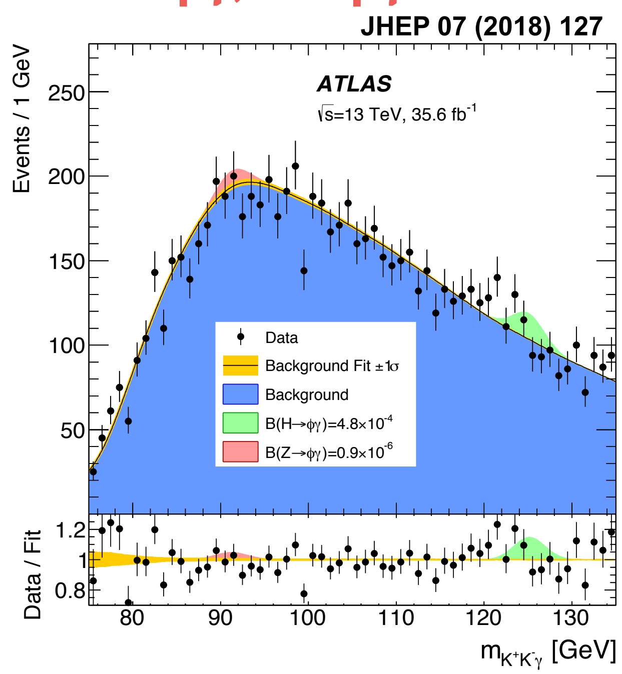

H→ J/ψ, H→ Υ(nS)

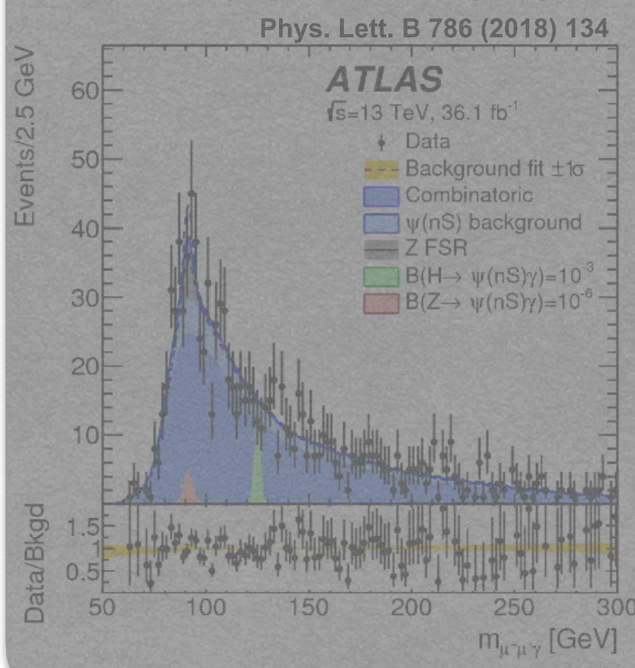

H→cc̄

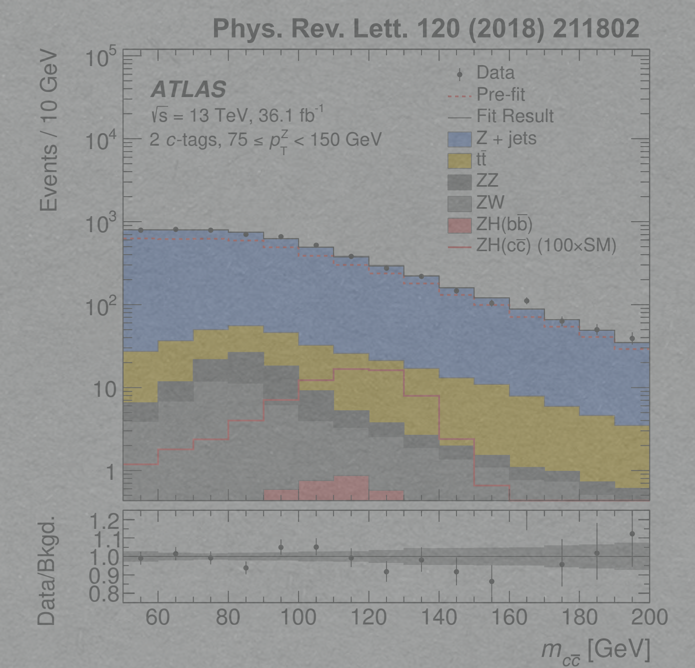

Search for H→φγ and H→ργ

- probing Higgs boson **couplings to light quarks**
- subsequent meson decays:
  - φ (ss̄) decays to Kaons
  - ρ (uū-dd̄) decays to Pions
- upper limits:
  - **H→φγ** at **181 times SM prediction**
  - **H→ργ** at **50 times SM prediction**
- **first experimental constraint on H→ργ**

Branching Fraction Limit (95% CL)	Expected	Observed
$\mathcal{B}(H \to \phi\gamma)\ [\ 10^{-4}\ ]$	$4.2^{+1.8}_{-1.2}$	4.8
$\mathcal{B}(Z \to \phi\gamma)\ [\ 10^{-6}\ ]$	$1.3^{+0.6}_{-0.4}$	0.9
$\mathcal{B}(H \to \rho\gamma)\ [\ 10^{-4}\ ]$	$8.4^{+4.1}_{-2.4}$	8.8
$\mathcal{B}(Z \to \rho\gamma)\ [\ 10^{-6}\ ]$	33^{+13}_{-9}	25

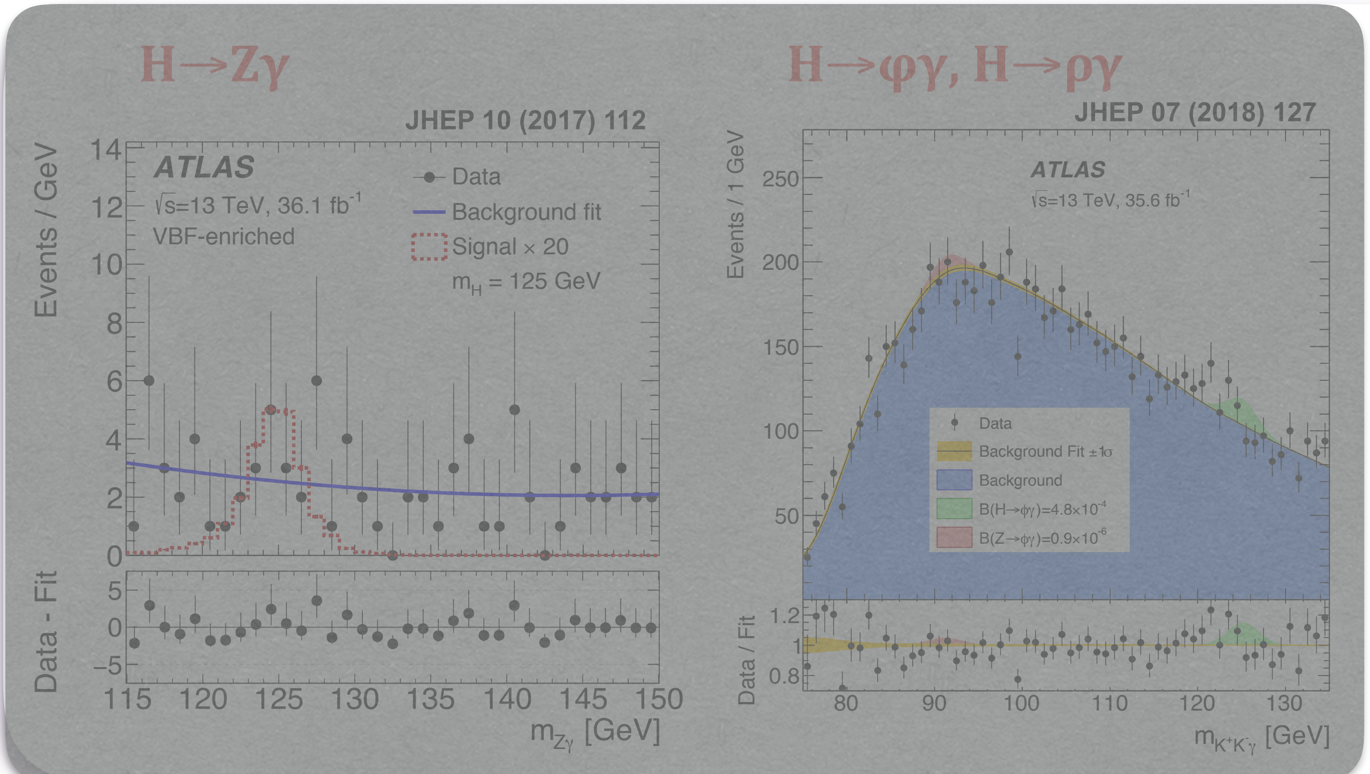

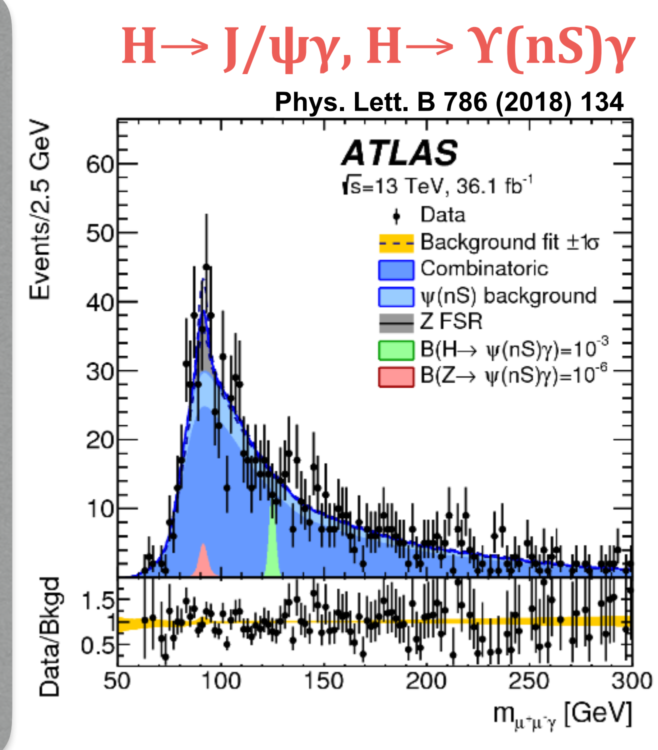

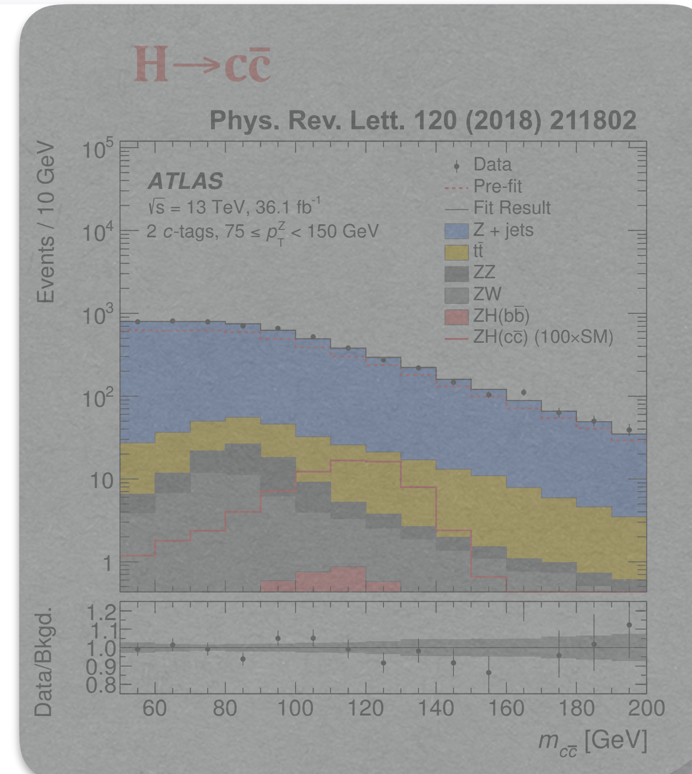

Search for H→ J/ψ and H→ ϒ(nS)

- probing Higgs boson **couplings to c- and b-quarks**
  - Charmonium H→ J/ψ (cc̄-resonance)
  - Bottomium H→ ϒ(nS) (n=1,2,3) (bb̄-resonance)
- subsequent **meson decays to muon pairs**
- upper limits Charmonium resonance
  - **~100 times SM prediction**

Branching fraction limit (95% CL)	Expected	Observed
$\mathcal{B}(H \to J/\psi\,\gamma)\,[\,10^{-4}\,]$	$3.0^{+1.4}_{-0.8}$	3.5
$\mathcal{B}(H \to \psi\,(2S)\;\gamma)\,[\,10^{-4}\,]$	$15.6^{+7.7}_{-4.4}$	19.8
$\mathcal{B}(Z \to J/\psi\,\gamma)\,[\,10^{-6}\,]$	$1.1^{+0.5}_{-0.3}$	2.3
$\mathcal{B}(Z \to \psi\,(2S)\;\gamma)\,[\,10^{-6}\,]$	$6.0^{+2.7}_{-1.7}$	4.5
$\mathcal{B}(H \to \Upsilon(1S)\,\gamma)\,[\,10^{-4}\,]$	$5.0^{+2.4}_{-1.4}$	4.9
$\mathcal{B}(H \to \Upsilon(2S)\,\gamma)\,[\,10^{-4}\,]$	$6.2^{+3.0}_{-1.7}$	5.9
$\mathcal{B}(H \to \Upsilon(3S)\,\gamma)\,[\,10^{-4}\,]$	$5.0^{+2.5}_{-1.4}$	5.7
$\mathcal{B}(Z \to \Upsilon(1S)\,\gamma)\,[\,10^{-6}\,]$	$2.8^{+1.2}_{-0.8}$	2.8
$\mathcal{B}(Z \to \Upsilon(2S)\,\gamma)\,[\,10^{-6}\,]$	$3.8^{+1.6}_{-1.1}$	1.7
$\mathcal{B}(Z \to \Upsilon(3S)\,\gamma)\,[\,10^{-6}\,]$	$3.0^{+1.3}_{-0.8}$	4.8

Phys. Lett. B 786 (2018) 134

$H \to Z\gamma$

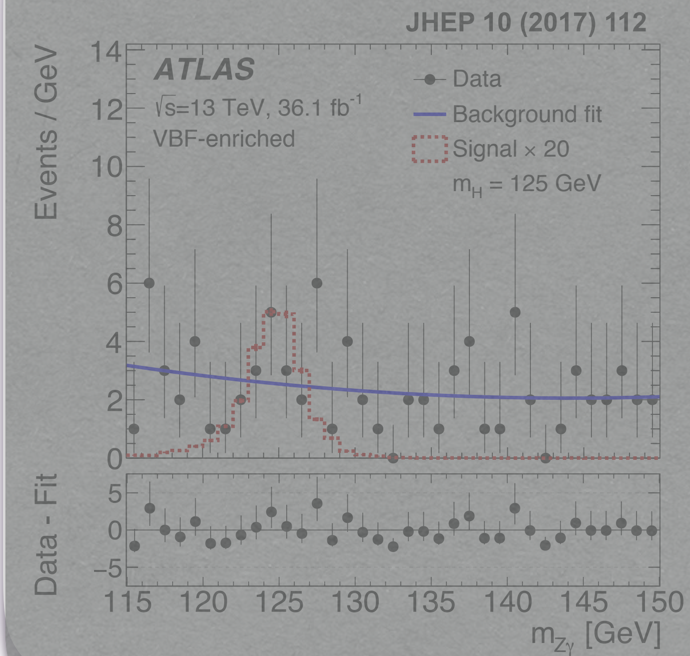

$H \to \phi\gamma$, $H \to \rho\gamma$

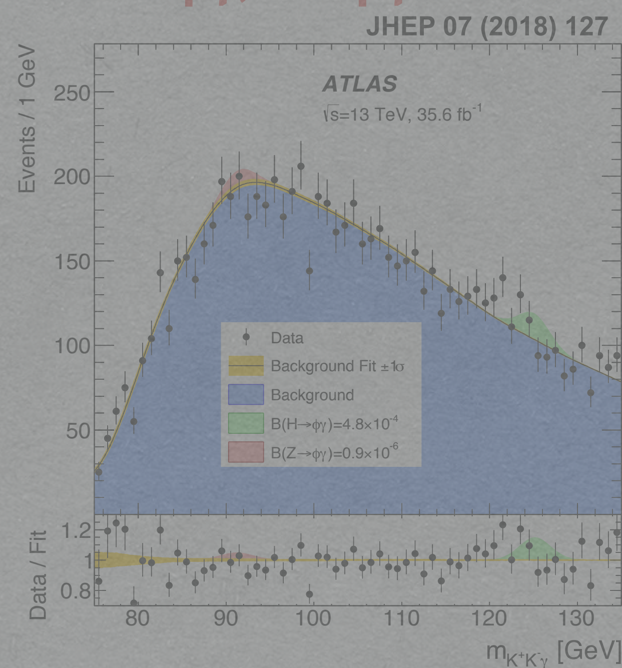

$H \to J/\psi$, $H \to \Upsilon(nS)$

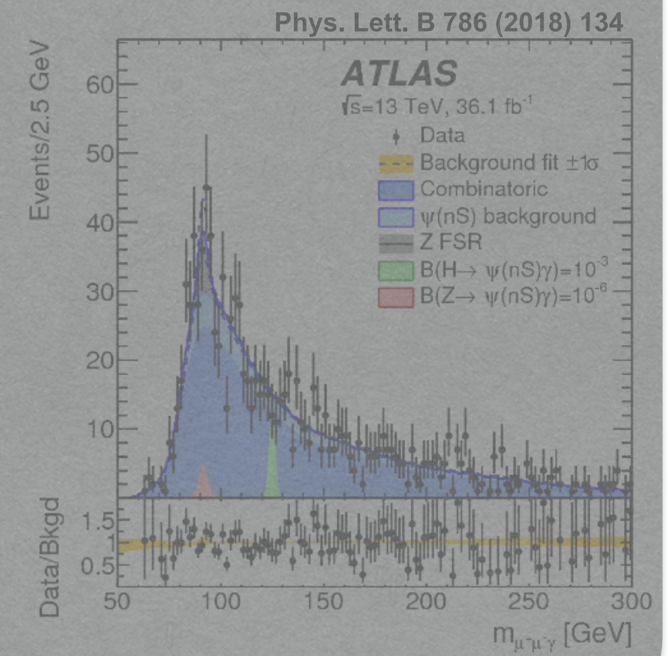

$H \to c\bar{c}$

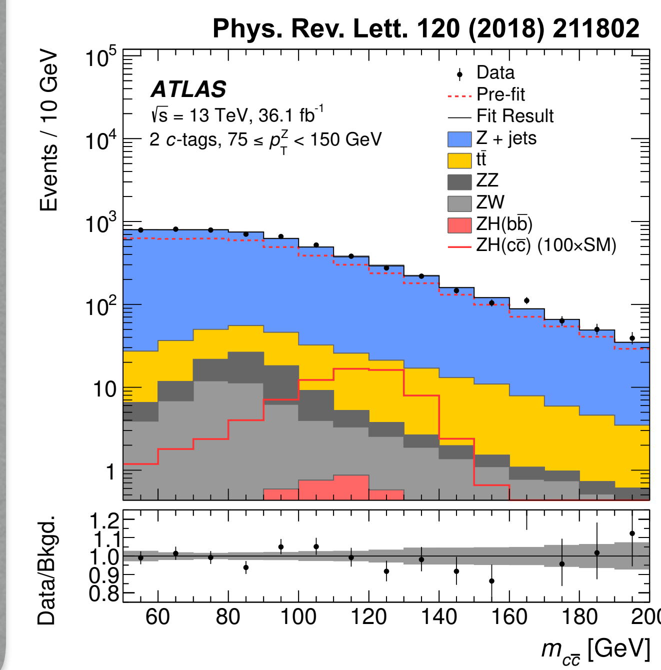

Search for $H \to c\bar{c}$

- **direct** probe of **$H \to c\bar{c}$ coupling**
- "rare" - only in **associated production** with $Z \to ll$ with $l = e, \mu$
- observed (exp.) upper limit (CL@95%):
  - $\sigma(pp \to ZH) \times B(H \to c\bar{c}) < 2.7\ (3.9)$ pb
- limit at **100 times SM prediction**

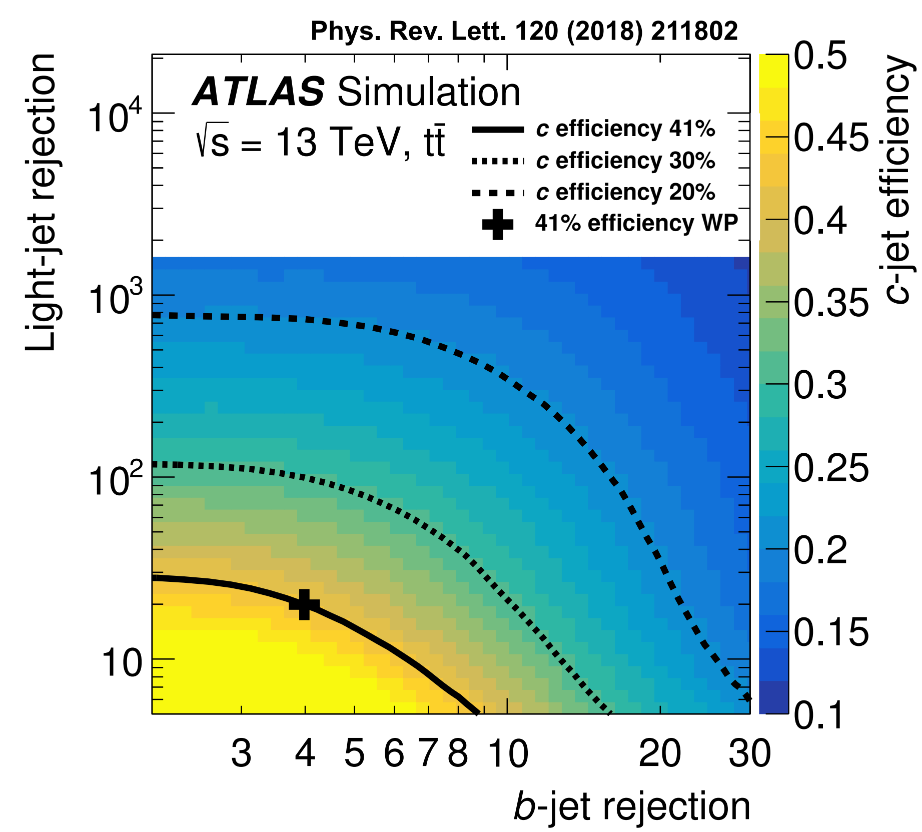

Backup H→μμ

Selection criteria and Categorisation

Table 1: Summary of the main event selection criteria common to all events (top) as well as the criteria applied to the selection of hadronic jets (bottom). The middle section defines three ranges in the dimuon invariant mass $m_{\mu\mu}$ used in the analysis, as described in the text.

	Selection
Common	Primary vertex Two opposite-charge muons Muons: $\lvert\eta\rvert < 2.7$, $p_{\mathrm{T}}^{\mathrm{lead}} > 27$ GeV, $p_{\mathrm{T}}^{\mathrm{sublead}} > 15$ GeV No b-tagged jets
Z region	$76 < m_{\mu\mu} < 106$ GeV
Sideband region	$110 < m_{\mu\mu} < 120$ GeV or $130 < m_{\mu\mu} < 180$ GeV
Fit region	$110 < m_{\mu\mu} < 160$ GeV
Jets	$p_{\mathrm{T}} > 25$ GeV and $\lvert\eta\rvert < 2.5$ or with $p_{\mathrm{T}} > 30$ GeV and $2.5 < \lvert\eta\rvert < 4.5$

Table 2: Summary of BDT boundaries defining the twelve categories.

Category	0-jet	1-jet	VBF	2-jet $O_{\mathrm{VBF}} < 0.60$
High	$O^0_{ggF} \geq 0.75$	$O^1_{ggF} \geq 0.78$	$O_{\mathrm{VBF}} \geq 0.89$	$O^2_{ggF} \geq 0.48$
Medium	$0.35 \leq O^0_{ggF} < 0.75$	$0.38 \leq O^1_{ggF} < 0.78$	$0.77 \leq O_{\mathrm{VBF}} < 0.89$	$0.22 \leq O^2_{ggF} < 0.48$
Low	$O^0_{ggF} < 0.35$	$O^1_{ggF} < 0.38$	$0.60 \leq O_{\mathrm{VBF}} < 0.77$	$O^2_{ggF} < 0.22$

ATLAS-CONF-2019-028

BDT Input Variables

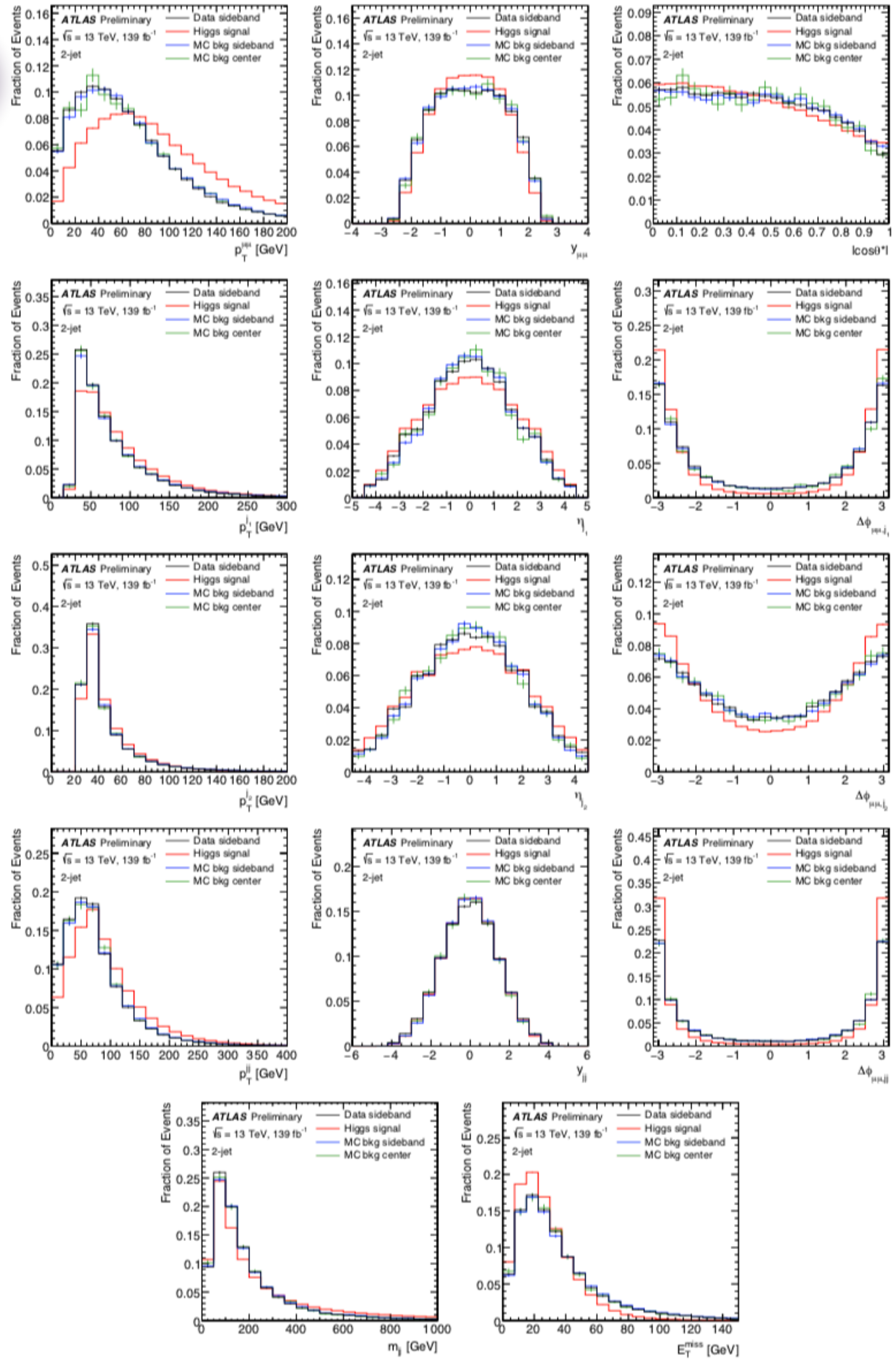

Figure 1: The distributions of the 14 variables used in the VBF BDT for $n_j \geq 2$ events for $H \to \mu\mu$ signal MC (red), data sideband (black) and background MC sideband and center (defined as 120-130 GeV mass range). The background MC includes DY from full simulation, $t\bar{t}$, diboson, single top-quark events.

ATLAS-CONF-2019-028

Analytical Functions

Table 3: List of tested empirical functional forms for the background modelling.

Function	Expression
PowerN	$m_{\mu\mu}^{(a_0+a_1 m_{\mu\mu}+a_2 m_{\mu\mu}^2+\ldots+a_N m_{\mu\mu}^N)}$
EpolyN	$\exp(a_1 m_{\mu\mu} + a_2 m_{\mu\mu}^2 + \ldots + a_N m_{\mu\mu}^N)$

Table 4: Selected empirical background functions in the different analysis categories together with the maximum values of the SS (in the 120–130 GeV mass range) normalised to the expected signal statistical error (δS) and to the SM predictions (S_{SM}) in %.

Category	Empirical Function	max(SS/ δS)[%]	max(SS/S_{SM})[%]
VBF High	Power0	10.6	14.7
VBF Medium	Epoly2	0.51	1.3
VBF Low	Power1	3.6	7.5
2-jet High	Epoly2	8.7	16.3
2-jet Medium	Epoly4	1.2	3.9
2-jet Low	Epoly3	-8.2	-33.2
1-jet High	Power1	6.1	12.1
1-jet Medium	Epoly3	-8.1	-19.8
1-jet Low	Epoly3	-2.5	-5.8
0-jet High	Power1	14.6	26.5
0-jet Medium	Epoly3	-11.6	-39.0
0-jet Low	Epoly3	-18.5	-74.2

ATLAS-CONF-2019-028

Analytical Functions

The core component of the background function is based on the LO DY line-shape (see e.g. Ref. [112]):

$$DY(m_{\mu\mu}) = \sum_q \mathcal{L}_{q\bar{q}}(m_{\mu\mu}) \cdot \sigma_{q\bar{q}}(m_{\mu\mu}),\ q = u,\ s,\ d\,. \quad (1)$$

The parton luminosity contribution $\mathcal{L}_{q\bar{q}}$ in Eq. 1 is derived from PDF4LHC15 as a function of $\hat{s} = m_{\mu\mu}^2$ for the LO DY case using APFEL [113] interfaced to LHAPDF [114] and parameterised using a 6th order polynomial. The matrix element component $\sigma_{q\bar{q}}(\hat{s}) = \sigma_{q\bar{q}}(m_{\mu\mu})/(2m_{\mu\mu})$ can be expressed as

$$\sigma_{q\bar{q}}(\hat{s}) = \frac{4\pi\alpha^2}{3\hat{s}N_c}[Q_q^2 - 2Q_qV_\ell V_q\chi_{Z\gamma}(\hat{s}) + (A_\ell^2 + V_\ell^2)(A_q^2 + V_q^2)\chi_Z(\hat{s})],$$

10

where

$$\chi_{Z\gamma}(\hat{s}) = \kappa\frac{\hat{s}(\hat{s} - m_Z^2)}{(\hat{s} - m_Z^2)^2 + \Gamma_Z^2 m_Z^2},$$

$$\chi_Z(\hat{s}) = \kappa^2\frac{\hat{s}^2}{(\hat{s} - m_Z^2)^2 + \Gamma_Z^2 m_Z^2},$$

$$\kappa = \frac{\sqrt{2}G_F m_Z^2}{4\pi\alpha}.$$

ATLAS-CONF-2019-028

Event yields

Table 5: Number of events observed in the $m_{\mu\mu}$ = 120–130 GeV window in data, the number of signal events expected in the SM (S_{SM}), and events from signal (S) and background (B) as derived from the combined fit. In addition the observed number of signal events over square root of background events ($S/\sqrt{B}$) and the signal-to-background ratio (S/B) in % for each of the twelve BDT categories described in the text are displayed.

Category	Data	S_{SM}	S	B	$S/\sqrt{B}$	S/B [%]
VBF High	40	4.5	2.3	34	0.39	6.6
VBF Medium	109	5.5	2.8	100	0.28	2.8
VBF Low	450	9.6	4.9	420	0.24	1.2
2-jet High	3400	38	19	3440	0.33	0.6
2-jet Medium	13938	70	35	13910	0.30	0.3
2-jet Low	40747	75	38	40860	0.19	0.1
1-jet High	2885	32	16	2830	0.31	0.6
1-jet Medium	24919	107	54	24890	0.35	0.2
1-jet Low	77482	134	68	77670	0.24	0.1
0-jet High	24777	85	43	24740	0.27	0.2
0-jet Medium	85281	155	79	85000	0.27	0.1
0-jet Low	180478	144	73	180000	0.17	<0.1

ATLAS-CONF-2019-028

S+B Fits in Categories

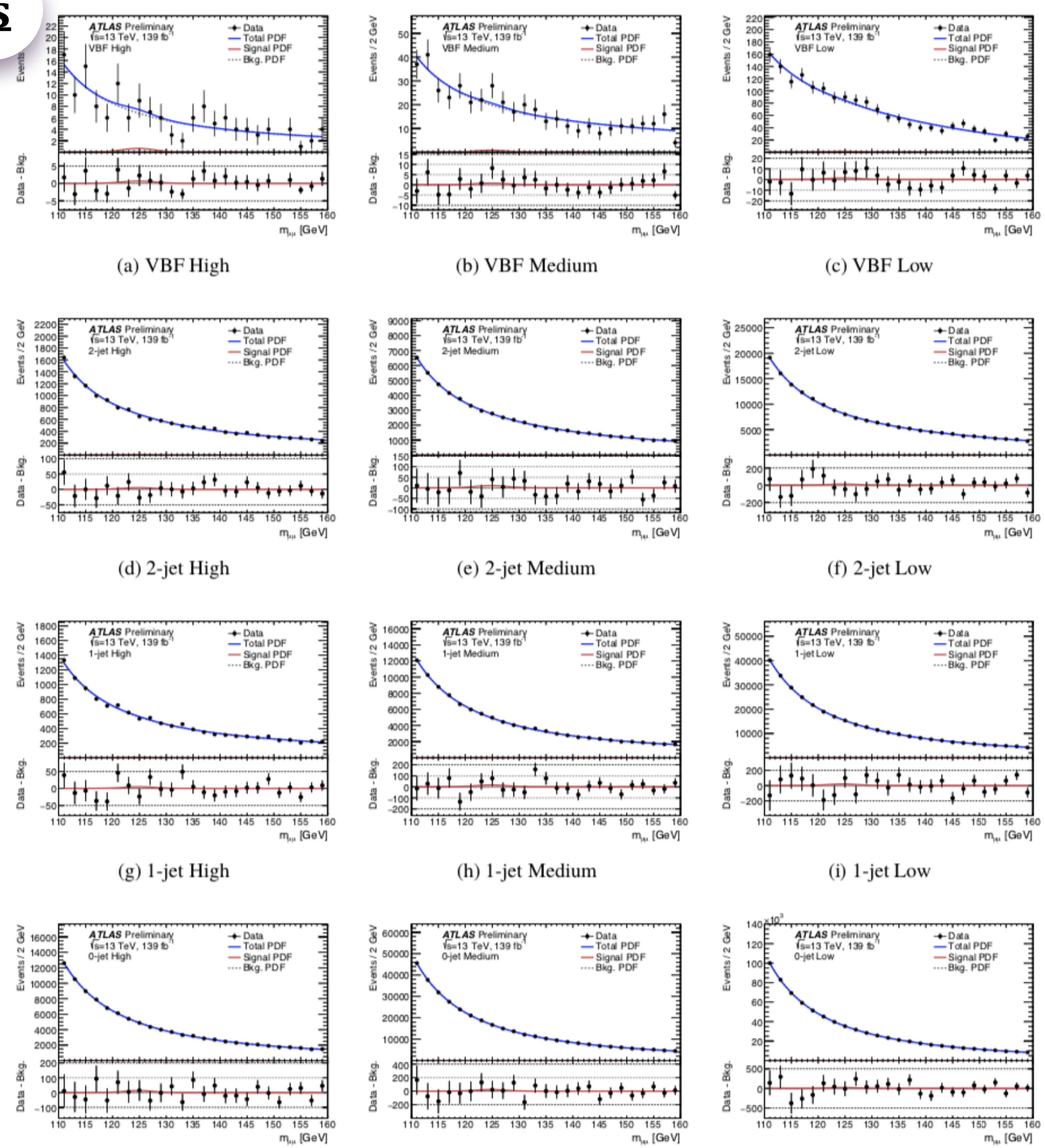

(a) VBF High (b) VBF Medium (c) VBF Low

(d) 2-jet High (e) 2-jet Medium (f) 2-jet Low

(g) 1-jet High (h) 1-jet Medium (i) 1-jet Low

(j) 0-jet High (k) 0-jet Medium (l) 0-jet Low

ATLAS-CONF-2019-028

Figure 2: Signal plus background fits in the twelve BDT analysis categories. In the top panel the signal-plus-background model is shown (blue curve) overlaid to the data points. The signal component is shown separately (red line). In the bottom panel the difference between the data and the background function is shown with overlaid the fitted signal component (red curve).

S+B Combined

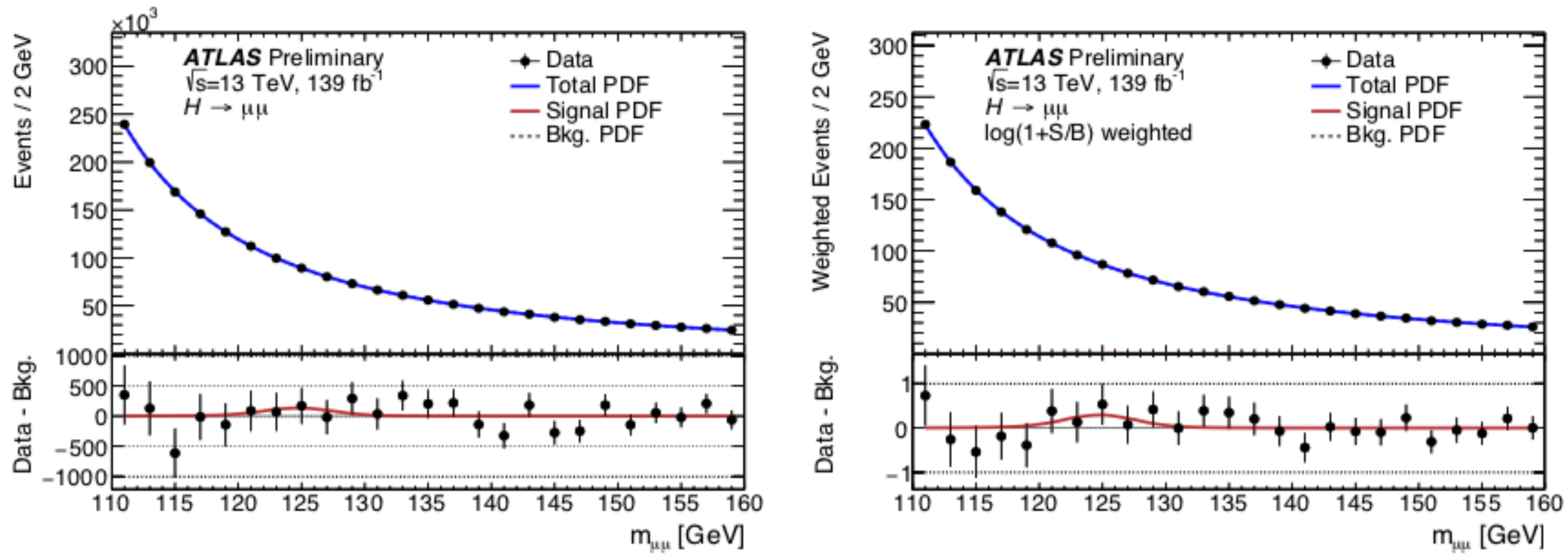

(a) (b)

Figure 3: Dimuon invariant mass spectrum in all the analysis categories observed in data. In (a) the unweighted sum of all events and signal plus background probability density functions (PDF) are shown, while in (b) events and PDFs are weighted by $\log(1 + S/B)$, where S and B are signal and background yields in the $m_{\mu\mu}$ = 120–130 GeV window derived from the combined fit to data.

ATLAS-CONF-2019-028

A search for the dimuon decay of the Standard Model Higgs boson in pppp collisions at s√=13s=13 TeV with the ATLAS Detector

FSR recovery

ATLAS-CONF-2019-028

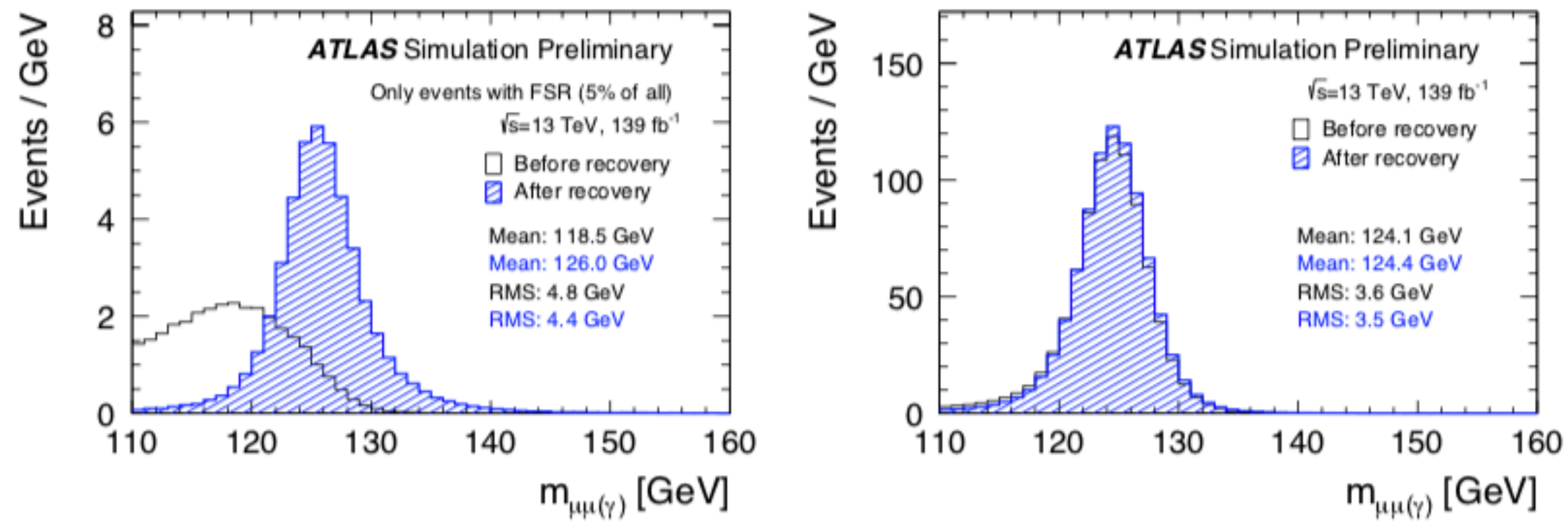

Figure 4: Invariant mass of $\mu\mu(\gamma)$ final states for events with a reconstructed FSR photon candidate (left) and for all ggF signal events (right). The black and blue histograms represent the distributions before and after the FSR recovery, respectively. Histograms are scaled to 139 fb^{-1}.

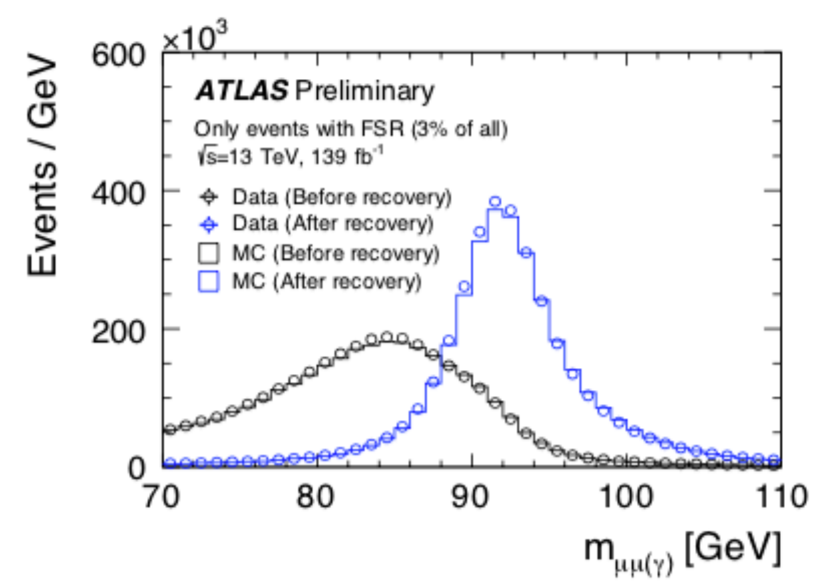

Figure 5: The invariant mass of $\mu\mu(\gamma)$ final states for events with a reconstructed FSR photon candidate in the region around the Z-boson resonance. The black and blue histograms represent the distributions before and after the FSR recovery for $Z \rightarrow \mu\mu$ MC events scaled to 139 fb^{-1}. The black and blue circles represent data before and after the FSR recovery respectively.

Fit results

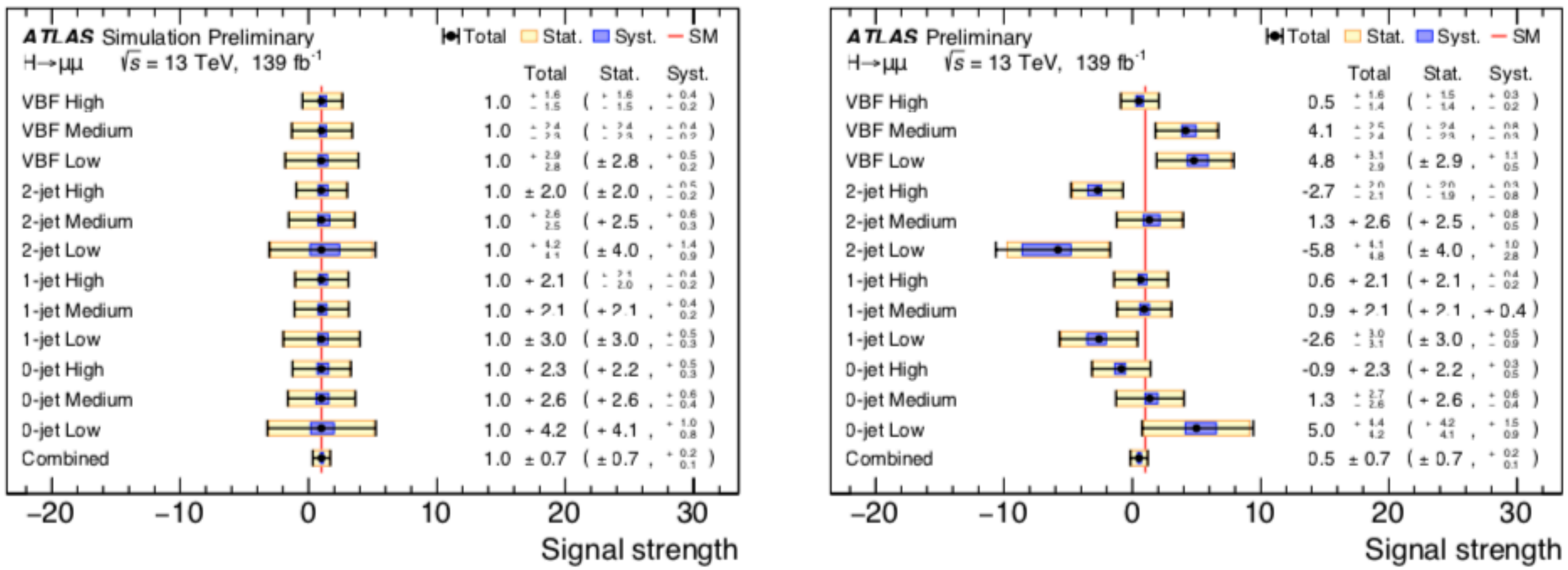

Figure 9: Expected (left) and observed (right) signal strengths in each category and combined for all categories.

ATLAS-CONF-2019-028

Signal Mass spectrum

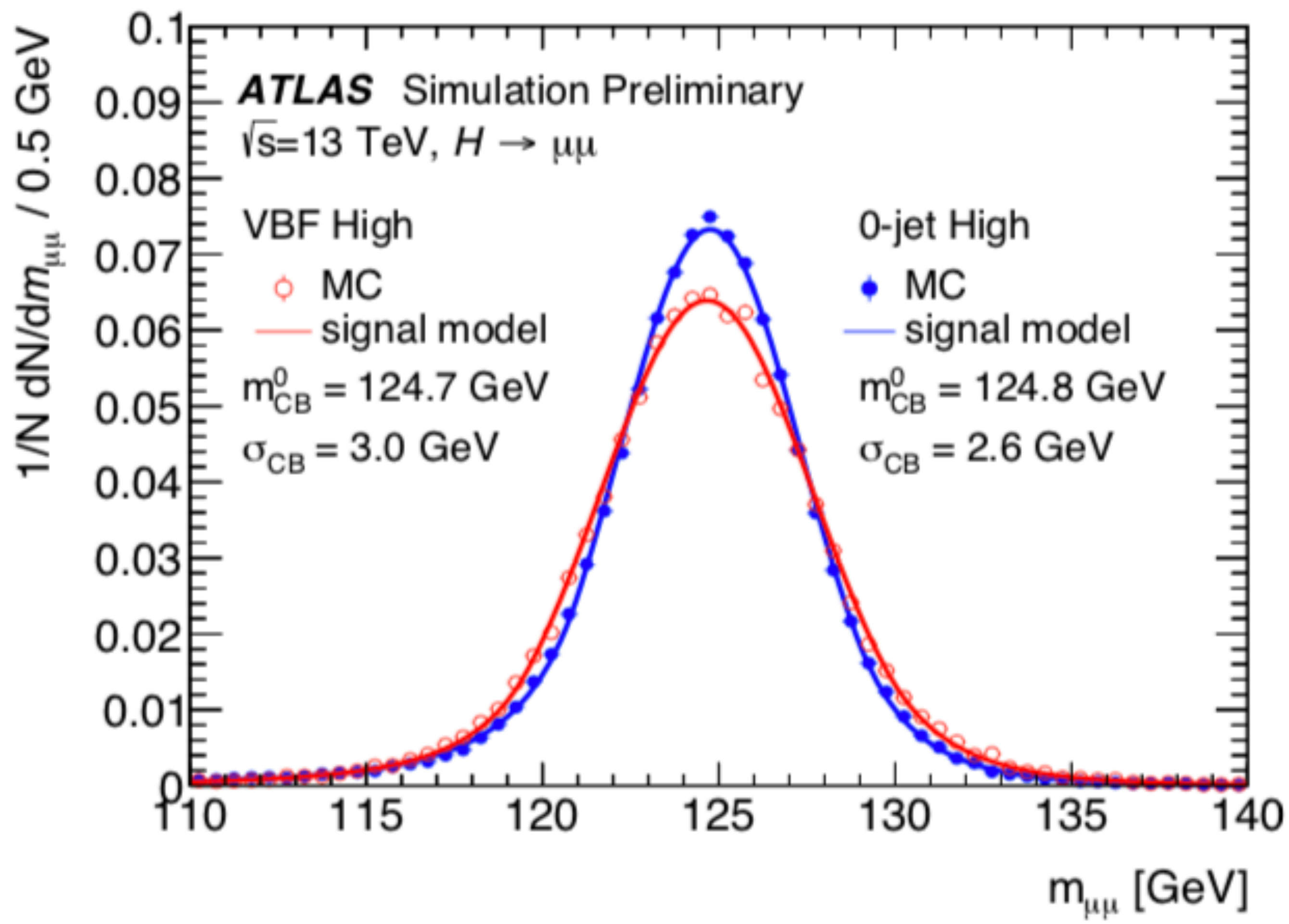

Figure 13: Dimuon invariant mass spectra of signal $H \rightarrow \mu\mu$ events in two specific BDT categories of the analysis. For both categories the distribution from the signal simulation is shown in points and the parametric signal model fitted to the distributions is shown as line. The central values m^0_{CB} as well as the width σ_{CB} of the signal model Crystal-Ball functions are also shown.

ATLAS-CONF-2019-028

\

Backup $H \rightarrow ee$ and $H \rightarrow e\mu$

Event Yields

Category	S	B	S/B	Data
Central Low $p_T^{\ell\ell}$	230	39200	0.0057	39872
Forward Low $p_T^{\ell\ell}$	390	98500	0.0039	100844
Central Medium $p_T^{\ell\ell}$	420	30700	0.014	31182
Forward Medium $p_T^{\ell\ell}$	710	74900	0.0095	76477
Central High $p_T^{\ell\ell}$	380	13400	0.028	13625
Forward High $p_T^{\ell\ell}$	590	29900	0.020	30164
VBF	120	2530	0.049	2561

- 120 < mee < 130 GeV. The signal is shown for a branching fraction of B(H → ee) = 0.1%.

Category	S	B	S/B	Data
Central Low $p_T^{\ell\ell}$	210	150	1.35	171
Forward Low $p_T^{\ell\ell}$	400	560	0.72	532
Central Medium $p_T^{\ell\ell}$	250	290	0.86	277
Forward Medium $p_T^{\ell\ell}$	450	830	0.54	854
Central High $p_T^{\ell\ell}$	180	280	0.65	299
Forward High $p_T^{\ell\ell}$	300	700	0.43	707
VBF	83	100	0.82	102
Low p_T^{ℓ}	89	600	0.15	558

- 120 < meμ < 130 GeV. The signal is shown for a branching fraction of B(H → eμ) = 0.1%

Mass spectra

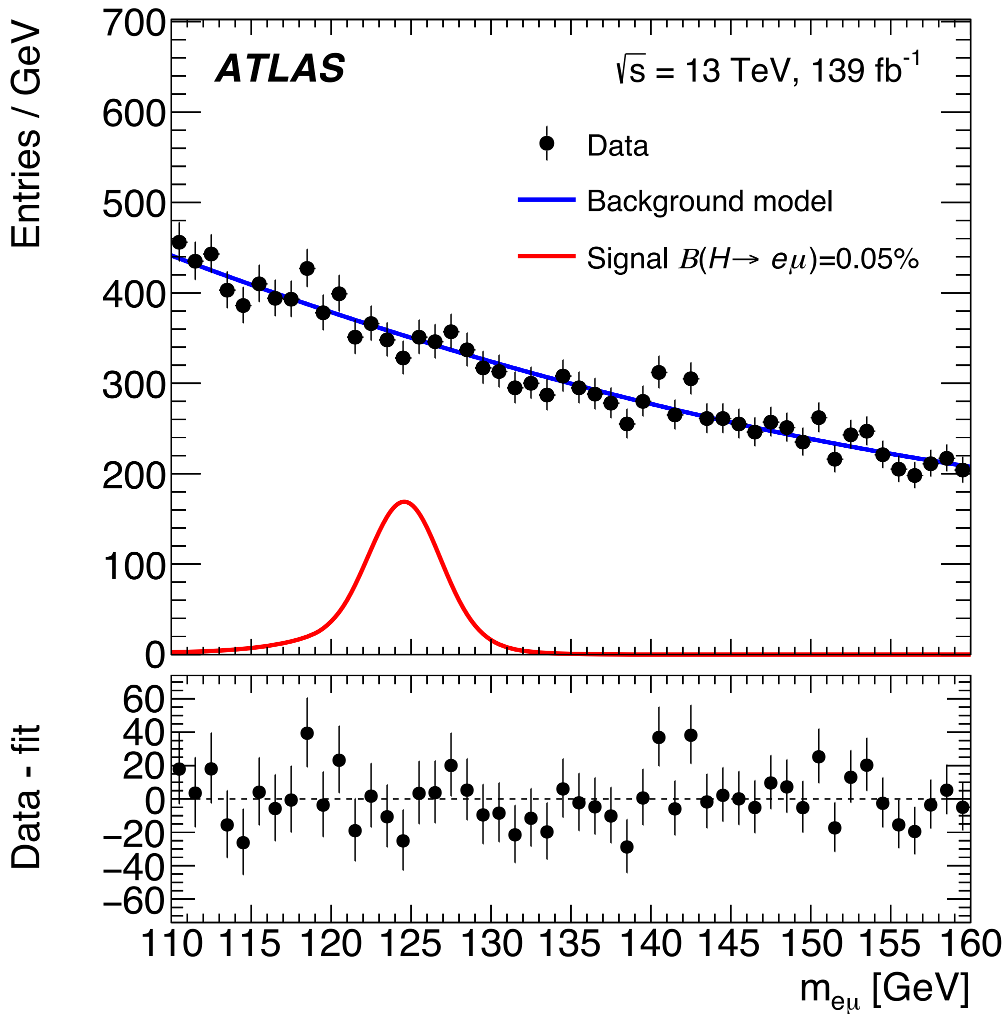

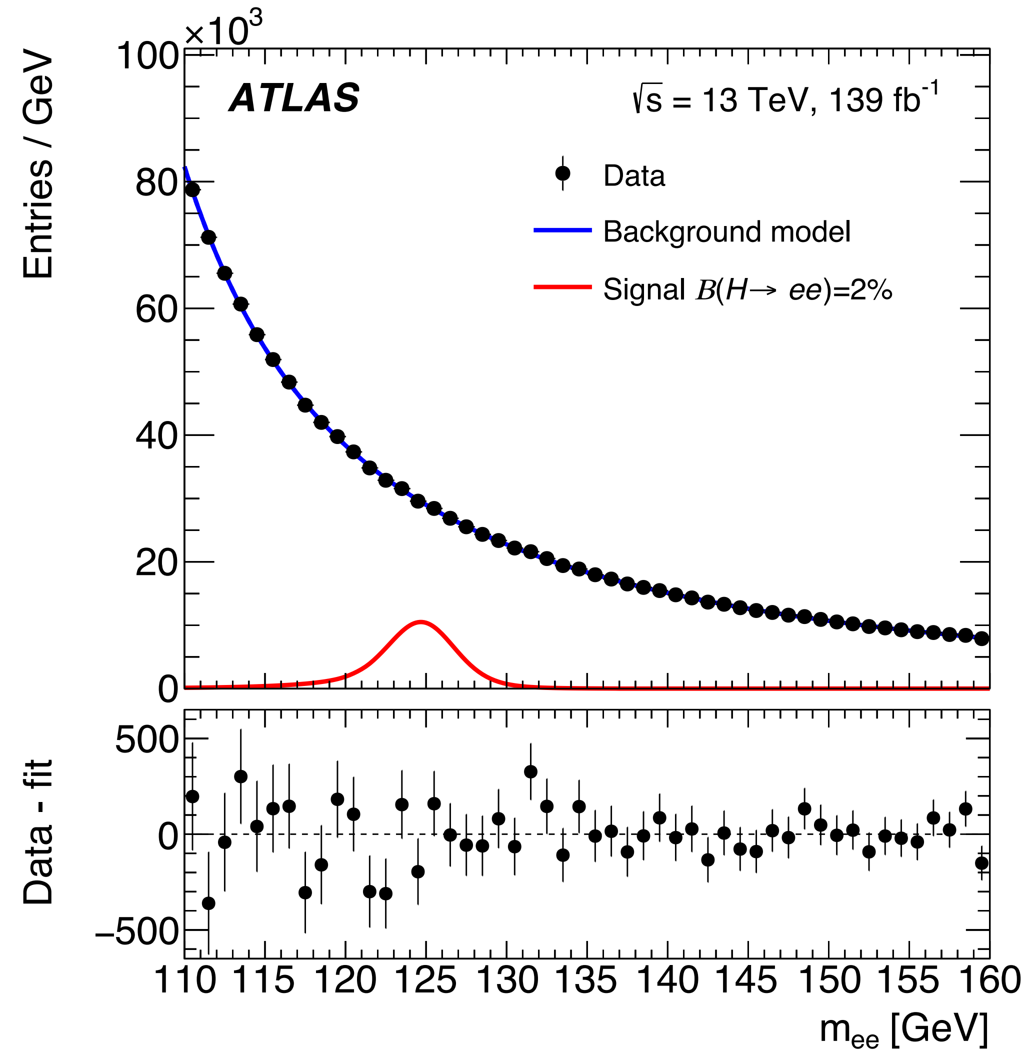

- B(H → ee) = 2% and B(H → eμ) = 0.05%

Yukawa constraints

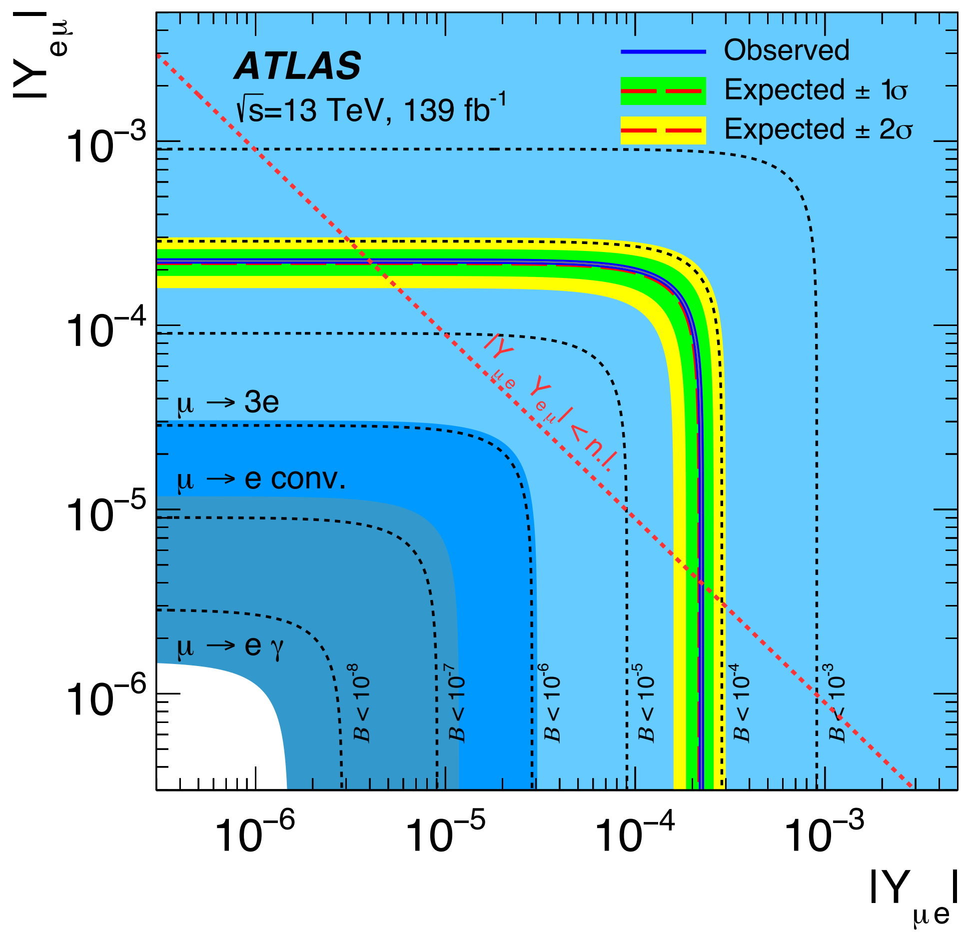

- Constraints on the flavour violating Yukawa couplings Yeμ and Yμe that are related to the branching ratio of the LFV Higgs boson decay B(H → eμ) following Ref. [14] as |Yeμ|2+|Yμ e|2=8πΓHSM/mH · B(H → eμ)/(1-B(H → eμ)) , where mH=125.09 GeV and ΓHSM = 4.07 MeV are the mass and SM width of the Higgs boson. The expected (red dashed line) and observed (blue solid line) limits are derived from the limits on B(H → eμ) from the present analysis. The green (yellow) band indicates the range that is expected to contain 68% (95%) of all observed limit excursions. The shaded regions show the indirect constraints derived using the model calculations of Ref. [14] from null searches for μ→ eγ [MEG Collaboration, Eur. Phys. J. C 76 (2016) 434], μ→ 3e [SINDRUM Collaboration, Nucl. Phys. B 299 (1988) 1] and μ→ e conversions on gold nuclei [SINDRUM II Collaboration, Eur. Phys. J. C 47 (2006) 337]. For these calculations the flavour diagonal Yukawa couplings are taken to be the SM values. The diagonal line indicates the so-called 1 naturalness limit |YeμYμe| < me mμ /v2, where v=246 GeV is the vacuum expectation value of the Higgs field.
-

Selection criteria

- trigger:
  - isolated electron or muon PT> 26 GeV
- e: |η| < 2.47 , muons |η| < 2.5
- exactly two OS e or OS e and mu
- lead lep: pT > 27 GeV to ensure a high trigger efficiency
- sublead lep: pT > 15 GeV.
- Requirements on jets are used in this analysis to suppress background and define a category that has a high sensitivity to signal produced in the VBF production mode.
- Jets in the range |η| < 4.5 and pT > 30 GeV antikt R0.4. jvt
- top quark bg: btagging of jets within |η| < 2.5
  - different WP used for ee and eμ (larger top bg)
- ee (eμ) channel the b-jet identification efficiency is about 60% (85%)
- Emiss/√HT < 3.5 (1.75) GeV1/2 for the ee (eμ) channel - surpression of MET backgrounds
  - Ht proportional Etmiss
- H → γγ bg neglected in Hee (~ 0.07% in Hee channel)
- dilepton invariant mass 110 < mll < 160 GeV,
  - background determination with analytic functions
  - constrained by the sidebands

Categorisation

- seven (eight) categories for the ee (eμ) channel
  - based on Hmumu
  - low-pT lepton category ‘Low plT (eμ)
    - subleading lepton has pT < 27 GeV.
    - fake leptons enriched
    - not for Hee, smaller fake contribution
  - VBF categories:
    - opposite hemisphere, |Δηj j | > 3, mj j > 500 GeV.
  - Centrality
    - fail VBF and lowPT
    - ‘central’: both leptons |ηl | < 1, ’Non-central’ otherwise
    - three ranges in the dilepton transverse momentum pll are considered:
    - ‘Low pll’ (pll ≤ 15 GeV),
    - ‘Mid ll ll llllT TT pT ’(15<pT ≤50GeV)
    - `HighpT ’(pT >50GeV).

Baseline

- object selection
- MET suppression
- 110 GeV < m_{ll} < 160 GeV

Low-p_T H→eμ only

- subleading lepton p_T < 27 GeV
- fake leptons enriched

VBF

- opposite hemisphere
- pseudorapidity gap $|\Delta\eta_{jj}|$>3.
- m_{jj} > 500 GeV

Central

- each lepton: $|\eta|$ < 1

Low-p_T(ll)

- p_T(ll) ≤ 15 GeV

Mid-p_T(ll)

- 15 <p_T(ll) ≤ 50 GeV

High-p_T(ll)

- p_T(ll) >50 GeV

Non-Central

- otherwise

Low-p_T(ll)

- p_T(ll) ≤ 15 GeV

Mid-p_T(ll)

- 15 <p_T(ll) ≤ 50 GeV

High-p_T(ll)

- p_T(ll) >50 GeV

H→ee

Category	S	B	S/B	Data
Central Low $p_T^{\ell\ell}$	230	39200	0.0057	39872
Forward Low $p_T^{\ell\ell}$	390	98500	0.0039	100844
Central Medium $p_T^{\ell\ell}$	420	30700	0.014	31182
Forward Medium $p_T^{\ell\ell}$	710	74900	0.0095	76477
Central High $p_T^{\ell\ell}$	380	13400	0.028	13625
Forward High $p_T^{\ell\ell}$	590	29900	0.020	30164
VBF	120	2530	0.049	2561

Phys. Lett. B 801 (2020) 135148

H→eμ

Category	S	B	S/B	Data
Central Low $p_T^{\ell\ell}$	210	150	1.35	171
Forward Low $p_T^{\ell\ell}$	400	560	0.72	532
Central Medium $p_T^{\ell\ell}$	250	290	0.86	277
Forward Medium $p_T^{\ell\ell}$	450	830	0.54	854
Central High $p_T^{\ell\ell}$	180	280	0.65	299
Forward High $p_T^{\ell\ell}$	300	700	0.43	707
VBF	83	100	0.82	102
Low p_T^{ℓ}	89	600	0.15	558

Phys. Lett. B 801 (2020) 135148

Analytic Functions

- analytic functions to model mll distributions
- signals: narrow resonances
- detector resolution determines signal shapes
  - parameterised with crystal ball function and Gaussian function
  - parameters determined by fitting simulated signal mll in each category

$$P_{\mathrm{S}}(m_{\ell\ell}) = f_{\mathrm{CB}} \times F_{\mathrm{CB}}(m_{\ell\ell}|m_{\mathrm{CB}}, \sigma_{\mathrm{CB}}, \alpha, n) + (1 - f_{\mathrm{CB}}) \times F_{\mathrm{GS}}\left(m_{\ell\ell}|m_{\mathrm{GS}}, \sigma_{\mathrm{GS}}^{\mathrm{S}}\right)$$

- background for Hee
  - breit wigner convolved with gaussian plus exponential fct/cubic
  - parameters determined in final fit+from signal fit
  - parameters uncorrelated across categories

$$P_{\mathrm{B}}(m_{ee}) = f \times [F_{\mathrm{BW}}(m_{ee}|m_{\mathrm{BW}}, \Gamma_{\mathrm{BW}}) \otimes F_{\mathrm{GS}}(m_{ee}|\sigma_{\mathrm{GS}}^{\mathrm{B}})] + (1 - f) \times C e^{A \cdot m_{ee}} / m_{ee}^3,$$

- background for Hemu
  - Bernstein polynomial with degree 2
  - parameters uncorrelated across categories
- final fit/channel
  - MLE fit simultaneously all categories
  - bkgd norm and BR(sig) free parameters (plus background-parameters above)

Systematics I

- Systematics
  - total experimental unc VBF
    - 2015-18 luminosity 1.7%
    - E miss T soft term and pileup effects (eμ>ee tighter E miss T / √ HT selection)
    - others: e,mu trigger, reco, id, isol eff, btag eff, pileup modelling, JES, JER,
    - uncertainties in e/mu-scale/res
  - ggF signal yield: 2-3% (ee), 4-6% (emu)
  - VBF 7-15% (ee), 6-22% emu (contributions from JES, JER)
- theoretical uncertainties:
    - production cross section of the Higgs boson
    - modelling uncertainties acceptance for the signals (separately VBF/ggf/each category)
    - VH acceptance uncertainty neglected
    - renormalisation and factorisation scales variation perturbative QCD
      - ggF: 1-11%
      - VBF: small
    - alpha_S PDF4LHC15 recommendations very small.
    - PS,UE and hadronisation: acceptance difference PYTHIA or HERWIG shower generators
      - ggF 1% to 11%
      - VBF 1% to 8%

Systematics II

- Background uncertainties:
  - potential bias on signal measurement due to choice of bg function
  - ee:
    - S+B fit repeated on DY simulated data (high stat)
    - signal yield/category taken as uncertainty
    - uncorrelated between categories
    - NP acting on signal norm/category
    - 8% effect on limit
  - emu:
    - change fit function to standard polynomial
    - evaluate signal yield differences on simulation between default and changed
    - <1% effect on limit

Results H→ee

- statistical uncertainty dominates
- main systematic uncertainty: bkgd modelling
- observed (exp.) upper limit (CL@95%):
  - **BR(H → ee) < 3.6×10^{-4} (3.5×10^{-4})**
- best fit branching ratio:
  - BR(H→ee)=(0.0 ± 1.7 (stat.) ± 0.6 (syst.))$\times10^{-4}$
- **~5× improvement** on CMS Run I limit of 1.9×10^{-3}

Phys. Lett. B 744 (2015) 184

Results H→eμ

- statistical uncertainty dominates
- main systematic unc.: Higgs boson production xsec
- observed (exp.) upper limit (CL@95%):
  - **BR(H → eμ) < 6.1×10^{-5} (5.8×10^{-5})**
- best fit branching ratio:
  - BR(H→eμ)=(0.4 ± 2.9 (stat.) ± 0.3(syst.))$\times10^{-5}$
- **~6× improvement** on CMS Run I limit of 3.5×10^{-4}

Phys. Lett. B 763 (2016) 472

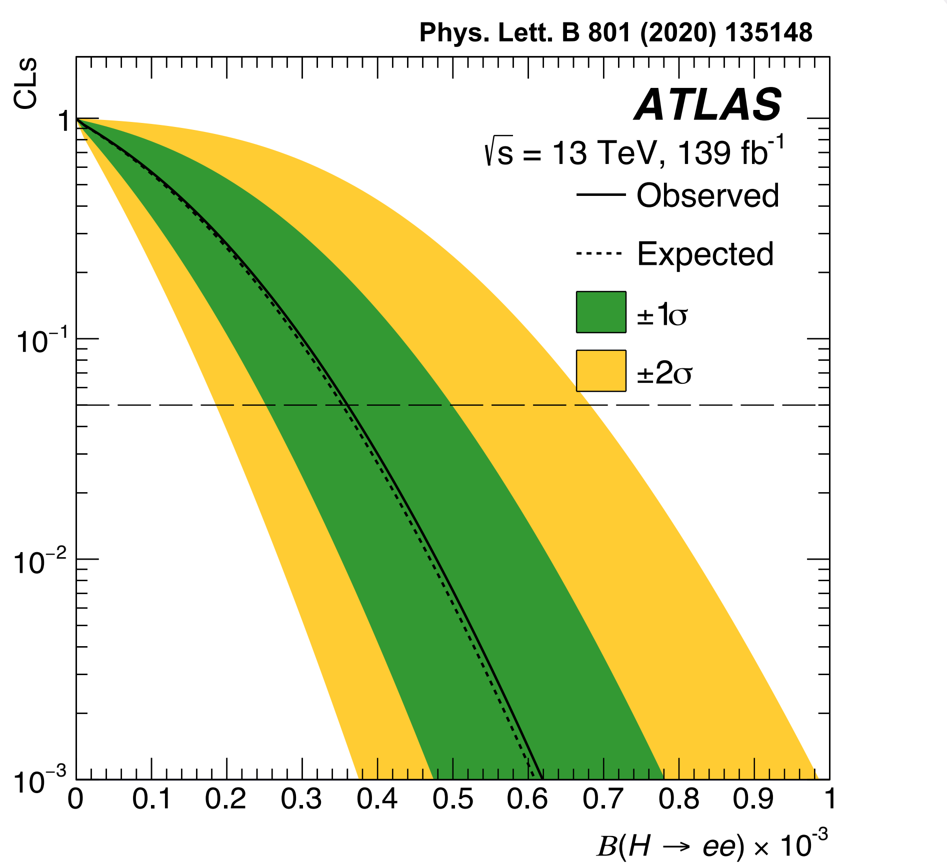

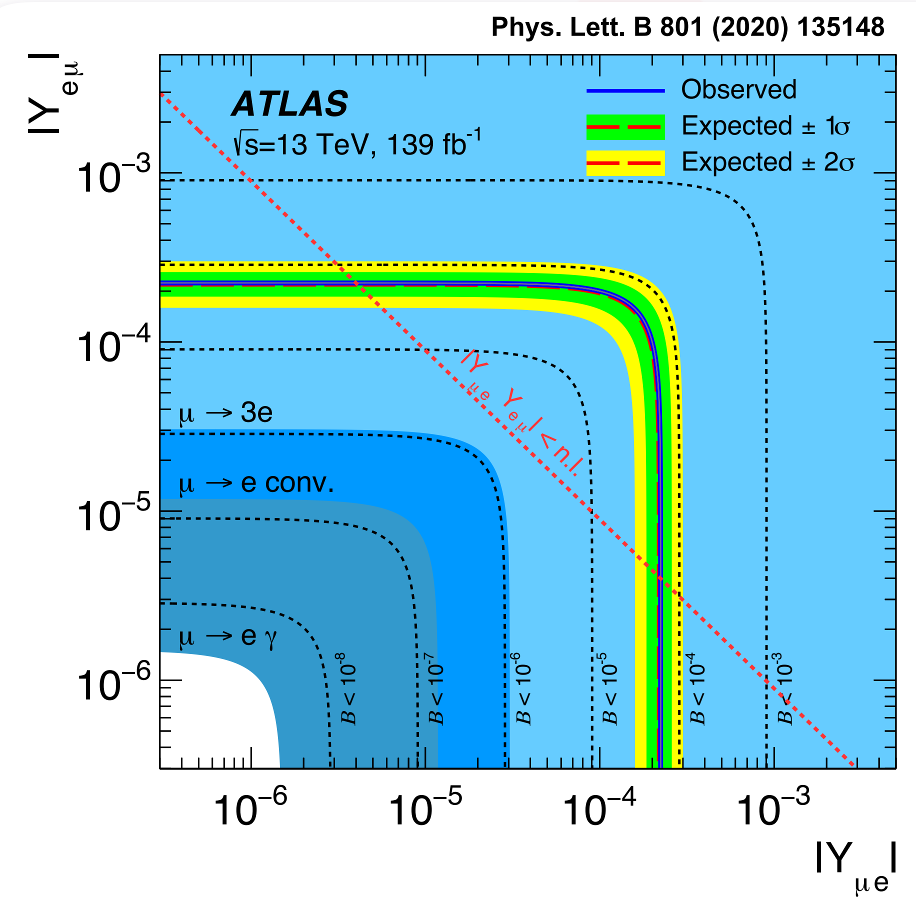

Search for Rare and Lepton Flavour Violating Decays of the Higgs Boson with the ATLAS Detector

Backup LFV H→τl

Signal Mass spectrum

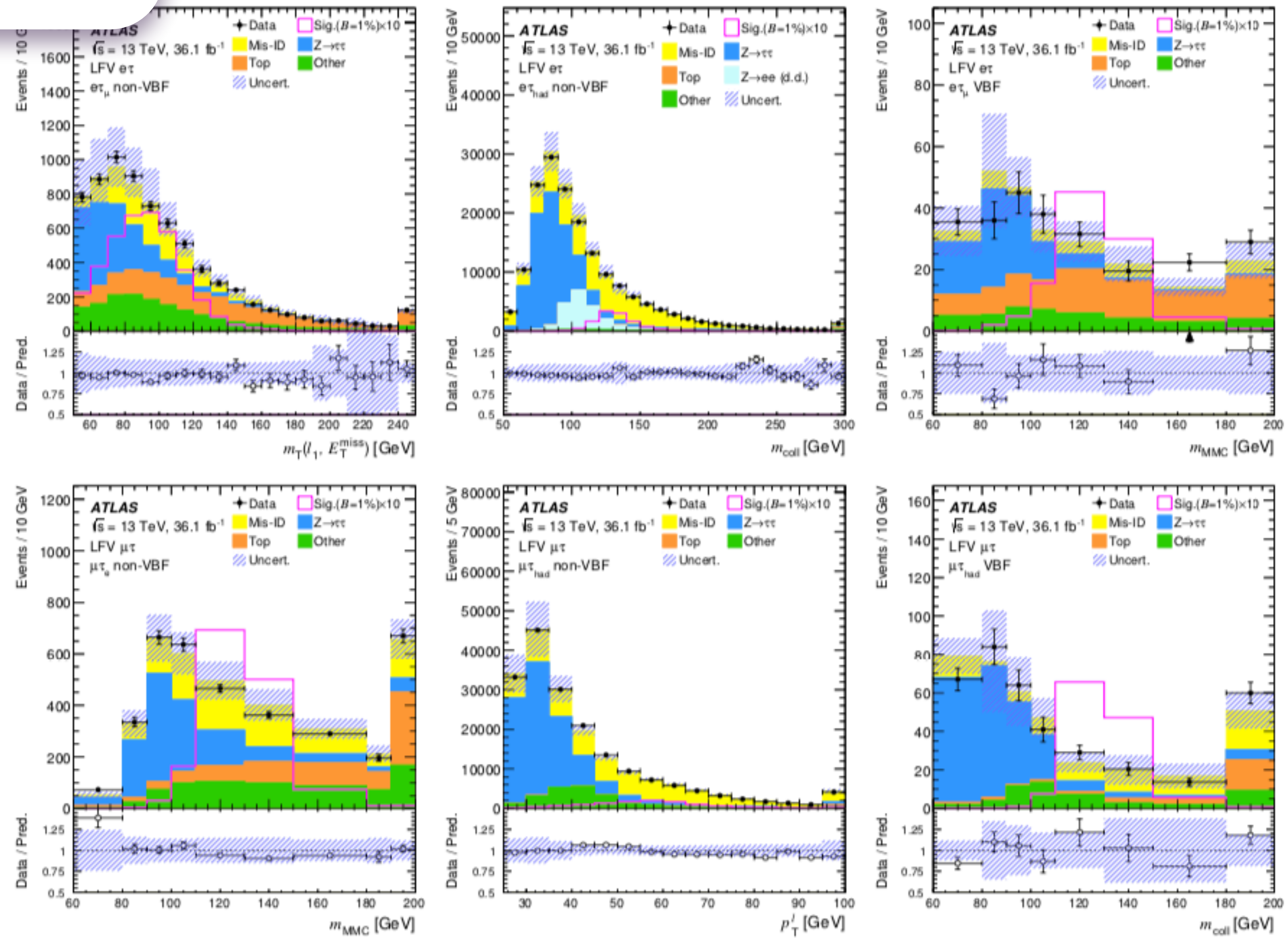

Figure 1: Pre-fit distributions of representative kinematic quantities for different searches, channels and categories. Top row: transverse mass $m_{\mathrm{T}}(\ell_1, E_{\mathrm{T}}^{\mathrm{miss}})$ ($e\tau_\mu$ non-VBF), collinear mass m_{coll} ($e\tau_{\mathrm{had}}$ non-VBF) and m_{MMC} ($e\tau_\mu$ VBF). Bottom row: m_{MMC} ($\mu\tau_e$ non-VBF), muon p_{T} ($\mu\tau_{\mathrm{had}}$ non-VBF) and m_{coll} ($\mu\tau_{\mathrm{had}}$ VBF). Entries with values that would exceed the x-axis range are included in the last bin of each distribution. The size of the combined statistical, experimental and theoretical uncertainties in the background is indicated by the hatched bands. The $H \to e\tau$ ($H \to \mu\tau$) signal overlaid in top (bottom) plots assumes $\mathcal{B}(H \to \ell\tau) = 1\%$ and is enhanced by a factor 10. In the data/background prediction ratio plots, points outside the displayed y-axis range are shown by arrows.

Phys. Lett. B 800 (2020) 135069

Signal Mass spectrum

Phys. Lett. B 800 (2020) 135069

Table 1: Generators used to describe the signal and background processes, parton distribution function (PDF) sets for the hard process, and models used for parton showering, hadronization and the underlying event (UEPS). The orders of the total cross-sections used to normalize the events are also given. More details are given in Ref. [10].

Process	Generator	PDF	UEPS	Cross-section order
ggF	Powheg-Box v2 [19–23] NNLOPS [24]	PDF4LHC15 [25] NNLO	Pythia 8.212 [18]	N^3LO QCD + NLO EW [26–29]
VBF	Powheg-Box v2 MiNLO [23]	PDF4LHC15 NLO	Pythia 8.212	~NNLO QCD + NLO EW [30–32]
WH, ZH	Powheg-Box v2 MiNLO	PDF4LHC15 NLO	Pythia 8.212	NNLO QCD + NLO EW [33–35]
W/Z+jets	Sherpa 2.2.1 [36]	NNPDF30NNLO [37]	Sherpa 2.2.1 [38]	NNLO [39, 40]
$VV/V\gamma^*$	Sherpa 2.2.1	NNPDF30NNLO	Sherpa 2.2.1	NNLO
$t\bar{t}$	Powheg-Box v2 [19–21, 41]	CT10 [42]	Pythia 6.428 [43]	NNLO+NNLL [44]
Single t	Powheg-Box v1 [45, 46]	CT10	Pythia 6.428	NLO [47–49]

Signal Mass spectrum

event selection and further categorization for the $\ell\tau_{\ell'}$ and $\ell\tau_{\text{had}}$ channels. The same criteria are also used for the control region (CR) definitions in the $\ell\tau_{\ell'}$ channel (Section 5), but one requirement of the baseline selection is inverted to achieve orthogonal event selection. There is no CR in the $\ell\tau_{\text{had}}$ channel.

Selection	$\ell\tau_{\ell'}$	$\ell\tau_{\text{had}}$
Baseline	exactly $1e$ and 1μ, OS $p_T^{\ell_1} > 45$ GeV $p_T^{\ell_2} > 15$ GeV $30\,\text{GeV} < m_{\text{vis}} < 150\,\text{GeV}$ $p_T^e(\text{track})/p_T^e(\text{cluster}) < 1.2$ ($\mu\tau_e$ only)	exactly 1ℓ and $1\tau_{\text{had-vis}}$, OS $p_T^{\ell} > 27.3$ GeV $p_T^{\tau_{\text{had-vis}}} > 25$ GeV, $\lvert\eta^{\tau_{\text{had-vis}}}\rvert < 2.4$ $\sum_{i=\ell,\tau_{\text{had-vis}}} \cos\Delta\phi(i, E_T^{\text{miss}}) > -0.35$ $\lvert\Delta\eta(\ell, \tau_{\text{had-vis}})\rvert < 2$
	b-veto (for jets with $p_T > 25$ GeV and $\lvert\eta\rvert < 2.4$)	
VBF	Baseline ≥ 2 jets, $p_T^{j_1} > 40$ GeV, $p_T^{j_2} > 30$ GeV $\lvert\Delta\eta(j_1, j_2)\rvert > 3$, $m(j_1, j_2) > 400$ GeV	
	–	$p_T^{\tau_{\text{had-vis}}} > 45$ GeV
Non-VBF	Baseline plus fail VBF categorization	
	$m_T(\ell_1, E_T^{\text{miss}}) > 50$ GeV $m_T(\ell_2, E_T^{\text{miss}}) < 40$ GeV $\lvert\Delta\phi(\ell_2, E_T^{\text{miss}})\rvert < 1.0$ $p_T^{\tau}/p_T^{\ell_1} > 0.5$	– – – –
Top-quark CR VBF and non-VBF	inverted b-veto: ≥ 1 b-tagged jet ($p_T > 25$ GeV and $\lvert\eta\rvert < 2.4$)	
$Z \to \tau\tau$ CR VBF and non-VBF	inverted $p_T^{\ell_1}$ requirement: $35\,\text{GeV} < p_T^{\ell_1} < 45\,\text{GeV}$	

Phys. Lett. B 800 (2020) 135069

Signal Mass spectrum

Table 3: BDT input variables used in the analysis. For each channel and category, used input variables are marked with HR (indicating the five variables with the highest rank) or a bullet. Analogous variables between the two channels are listed on the same line.

	$\ell\tau_{\ell'}$			$\ell\tau_{\text{had}}$	
Variable	VBF	non-VBF	Variable	VBF	non-VBF
m_{MMC}	HR	HR	m_{coll}	HR	HR
$p_{\text{T}}^{\ell_1}$	•	•	p_{T}^{ℓ}	•	HR
$p_{\text{T}}^{\ell_2}$	HR	HR	$p_{\text{T}}^{\tau_{\text{had-vis}}}$	•	HR
$\Delta R(\ell_1, \ell_2)$	HR	•	$\Delta R(\ell, \tau_{\text{had-vis}})$	•	•
$m_{\text{T}}(\ell_1, E_{\text{T}}^{\text{miss}})$	•	HR	$m_{\text{T}}(\ell, E_{\text{T}}^{\text{miss}})$	HR	•
$m_{\text{T}}(\ell_2, E_{\text{T}}^{\text{miss}})$	HR	•	$m_{\text{T}}(\tau_{\text{had-vis}}, E_{\text{T}}^{\text{miss}})$	HR	HR
$\Delta\phi(\ell_1, E_{\text{T}}^{\text{miss}})$	•	•	$\Delta\phi(\ell, E_{\text{T}}^{\text{miss}})$	HR	•
$\Delta\phi(\ell_2, E_{\text{T}}^{\text{miss}})$		HR	$\Delta\phi(\tau_{\text{had-vis}}, E_{\text{T}}^{\text{miss}})$	•	
$m(\text{j}_1, \text{j}_2)$	•		$m(\text{j}_1, \text{j}_2)$	•	
$\Delta\eta(\text{j}_1, \text{j}_2)$	HR		$\Delta\eta(\text{j}_1, \text{j}_2)$	•	
$p_{\text{T}}^{\tau}/p_{\text{T}}^{\ell_1}$		HR	$\sum_{i=\ell,\tau_{\text{had-vis}}} \cos\Delta\phi(i, E_{\text{T}}^{\text{miss}})$	•	•
			$E_{\text{T}}^{\text{miss}}$	HR	•
			m_{vis}		HR
			$\Delta\eta(\ell, \tau_{\text{had-vis}})$		•
			η^{ℓ}		•
			$\eta^{\tau_{\text{had-vis}}}$		•
			ϕ^{ℓ}		•
			$\phi^{\tau_{\text{had-vis}}}$		•
			$\phi(E_{\text{T}}^{\text{miss}})$		•

Phys. Lett. B 800 (2020) 135069

Signal Mass spectrum

Event yields and predictions as determined by the background-only fit in different signal regions of the $H \to e\tau$ analysis. Uncertainties include both the statistical and systematic contributions. "Other" contains diboson, $Z \to \ell\ell$, $H \to \tau\tau$ and $H \to WW$ background processes. For the $e\tau_{had}$ channel the "$Z \to ee$ (d.d.)" component corresponds to electrons misidentified as $\tau_{had\text{-}vis}$. This contribution is summed with "Other" since there are few events in the VBF category. The uncertainty of the total background includes all correlations between channels. The normalizations of top-quark ($\ell\tau_{\ell'}$ channel only) and $Z \to \tau\tau$ background components are determined by the fit, while the expected signal event yields are given for $\mathcal{B}(H \to e\tau) = 1\%$.

	$e\tau_\mu$ non-VBF	$e\tau_\mu$ VBF	$e\tau_{had}$ non-VBF	$e\tau_{had}$ VBF
Signal	379 ± 31	19.8 ± 2.7	1180 ± 110	25 ± 4
$Z \to \tau\tau$	2470 ± 230	221 ± 34	73 800 ± 1900	290 ± 40
Top-quark	1640 ± 140	490 ± 40	1580 ± 190	56 ± 12
Mis-identified	1330 ± 250	73 ± 33	74 400 ± 1600	140 ± 50
$Z \to ee$ (d.d.)			15 900 ± 1800	
Other	1700 ± 80	220 ± 15	2960 ± 200	82 ± 13
Total background	7130 ± 100	1003 ± 33	168 700 ± 1000	570 ± 40
Data	7128	992	168 883	572

Table 5: Event yields and predictions as determined by the background-only fit in different signal regions of the $H \to \mu\tau$ analysis. Uncertainties include both the statistical and systematic contributions. "Other" contains diboson, $Z \to \ell\ell$, $H \to \tau\tau$ and $H \to WW$ background processes.The uncertainty of the total background includes all correlations between channels. The normalizations of top-quark ($\ell\tau_{\ell'}$ channel only) and $Z \to \tau\tau$ background components are determined by the fit, while the expected signal event yields are given for $\mathcal{B}(H \to \mu\tau) = 1\%$.

	$\mu\tau_e$ non-VBF	$\mu\tau_e$ VBF	$\mu\tau_{had}$ non-VBF	$\mu\tau_{had}$ VBF
Signal	287 ± 23	14.6 ± 1.9	1200 ± 120	25 ± 5
$Z \to \tau\tau$	1860 ± 130	144 ± 26	96 100 ± 2000	274 ± 33
Top quark	1260 ± 130	390 ± 34	1620 ± 210	51 ± 10
Misidentified	1340 ± 210	41 ± 21	63 900 ± 1600	149 ± 33
Other	1180 ± 140	168 ± 18	23 000 ± 1000	104 ± 15
Total background	5640 ± 100	743 ± 29	184 500 ± 1200	580 ± 30
Data	5664	723	184 508	583

Phys. Lett. B 800 (2020) 135069

Signal Mass spectrum

Table 6: Summary of the systematic uncertainties and their impact on the best-fit value of $\mathcal{B}$ in the $H \to e\tau$ and $H \to \mu\tau$ searches. The measured values are obtained by the fit to data, while the expected values are determined by the fit to a background-only sample.

Source of uncertainty	Impact on $\mathcal{B}(H \to e\tau)$ [%] Measured	Impact on $\mathcal{B}(H \to e\tau)$ [%] Expected	Impact on $\mathcal{B}(H \to \mu\tau)$ [%] Measured	Impact on $\mathcal{B}(H \to \mu\tau)$ [%] Expected
Electron	+0.05/−0.05	+0.06/−0.06	+0.03/−0.03	+0.02/−0.02
Muon	+0.04/−0.04	+0.04/−0.04	+0.10/−0.10	+0.08/−0.10
$\tau_{\text{had-vis}}$	+0.02/−0.02	+0.02/−0.02	+0.04/−0.04	+0.04/−0.05
Jet	+0.09/−0.08	+0.09/−0.09	+0.11/−0.12	+0.11/−0.12
$E_{\text{T}}^{\text{miss}}$	+0.02/−0.02	+0.02/−0.03	+0.05/−0.08	+0.03/−0.05
b-tag	+0.02/−0.03	+0.03/−0.03	+0.01/−0.01	+0.01/−0.01
Mis-ID backg. ($\ell\tau_{\ell'}$)	+0.08/−0.07	+0.09/−0.08	+0.07/−0.07	+0.07/−0.07
Mis-ID backg. ($\ell\tau_{\text{had}}$)	+0.12/−0.11	+0.11/−0.12	+0.11/−0.11	+0.10/−0.10
Pile-up modelling	+0.02/−0.01	+0.01/−0.01	+0.05/−0.03	+0.08/−0.06
Luminosity	< 0.01	< 0.01	< 0.01	< 0.01
Background norm.	+0.05/−0.04	+0.05/−0.03	+0.04/−0.02	+0.05/−0.03
Theor. uncert. (backg.)	+0.04/−0.03	+0.04/−0.03	+0.08/−0.07	+0.09/−0.09
Theor. uncert. (signal)	+0.01/−0.01	+0.01/−0.01	+0.04/−0.02	+0.02/−0.02
MC statistics	+0.04/−0.04	+0.03/−0.03	+0.04/−0.04	+0.05/−0.04
Full systematic	+0.17/−0.16	+0.17/−0.17	+0.18/−0.18	+0.19/−0.20
Data statistics	+0.07/−0.07	+0.07/−0.07	+0.07/−0.07	+0.08/−0.08
Total	+0.18/−0.17	+0.18/−0.18	+0.19/−0.19	+0.20/−0.21

Phys. Lett. B 800 (2020) 135069

BDT

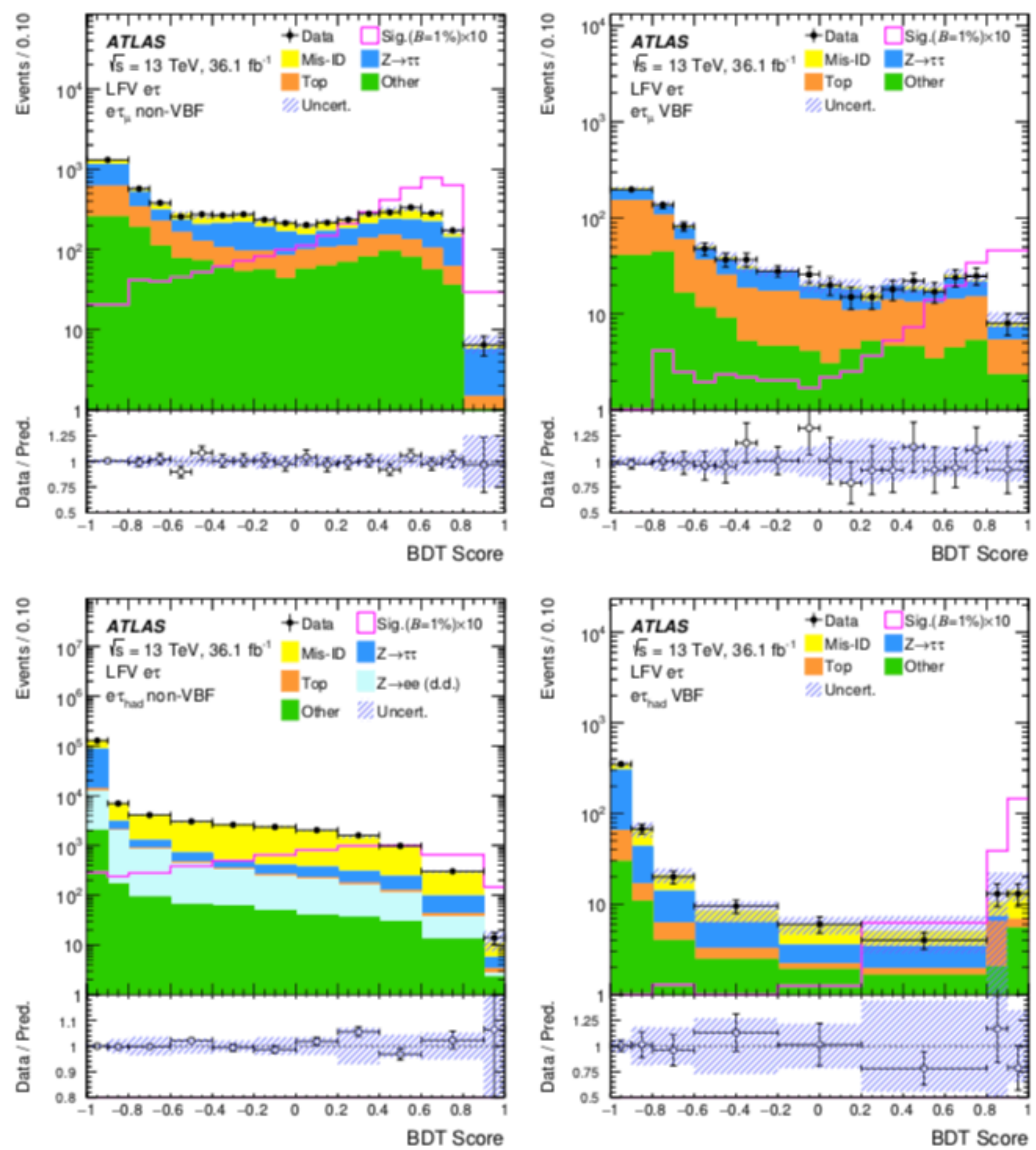

Figure 2: Distributions of the BDT score after the background+signal fit in each signal region of the $e\tau$ search, with the LFV signal overlaid, normalized with $\mathcal{B}(H \to e\tau) = 1\%$ and enhanced by a factor 10 for visibility. The top and bottom plots display $e\tau_{\mu}$ and $e\tau_{\mathrm{had}}$ BDT scores respectively, the left (right) column corresponds to the non-VBF (VBF) category. The size of the combined statistical, experimental and theoretical uncertainties of the background is indicated by the hatched bands. The binning is shown as in the statistical analysis.

Phys. Lett. B 800 (2020) 135069

Signal Mass spectrum

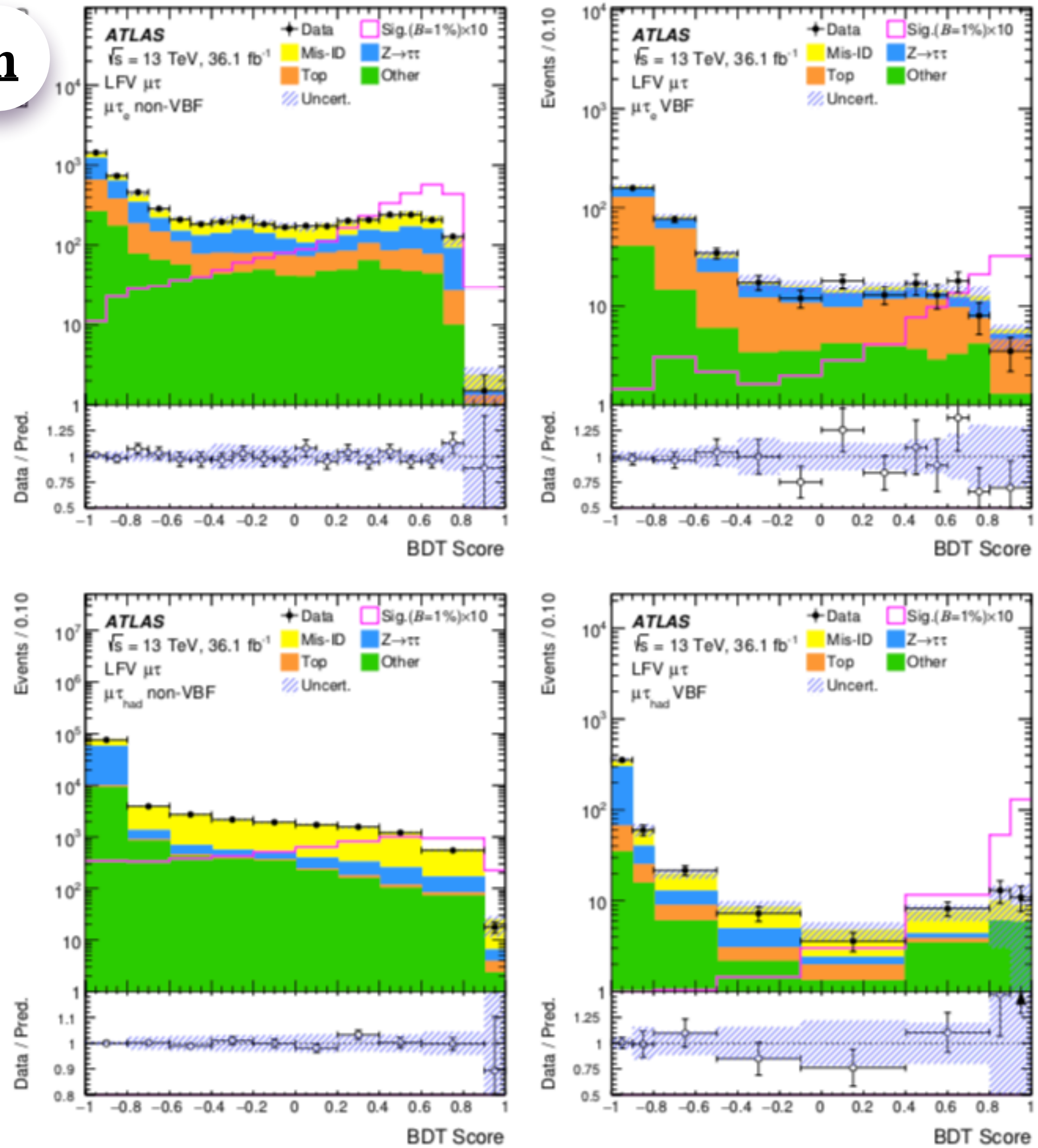

Figure 3: Distributions of the BDT score after the background+signal fit in each signal region of the $\mu\tau$ search, with the LFV signal overlaid, normalized with $\mathcal{B}(H \rightarrow \mu\tau) = 1\%$ and enhanced by a factor 10 for visibility. The top and bottom plots display $\mu\tau_e$ and $\mu\tau_{\text{had}}$ BDT scores respectively, the left (right) column corresponds to the non-VBF (VBF) category. The size of the combined statistical, experimental and theoretical uncertainties of the background is indicated by the hatched bands. The binning is shown as in the statistical analysis. In the data/background prediction ratio plots, points outside the displayed y-axis range are shown by arrows.

Phys. Lett. B 800 (2020) 135069

Signal Mass spectrum

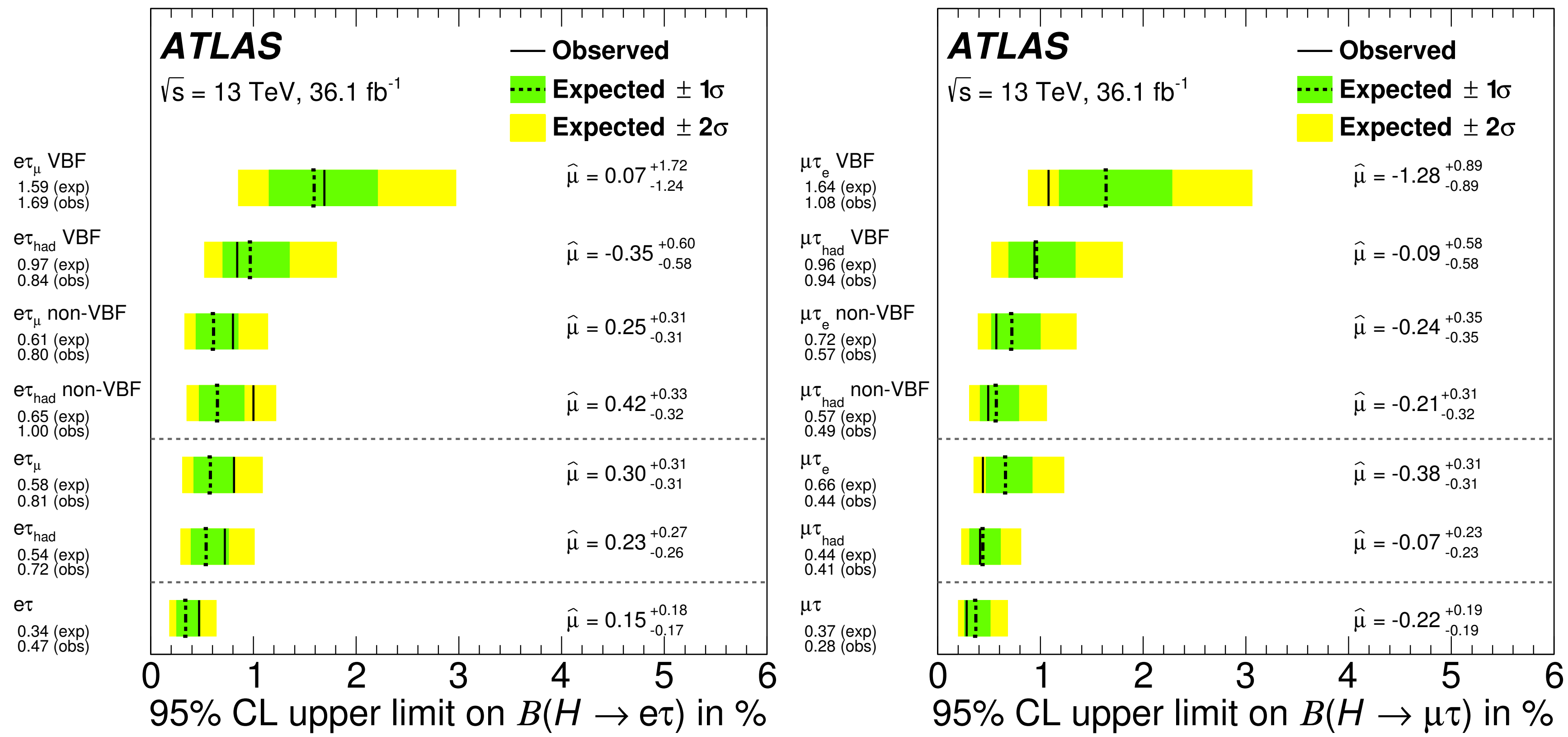

Figure 4: Upper limits at 95% CL on the LFV branching ratios of the Higgs boson, $H \to e\tau$ (left) and $H \to \mu\tau$ (right), indicated by solid and dashed lines. Best-fit values of the branching ratios ($\hat{\mu}$) are also given, in %. The limits are computed while assuming that either $\mathcal{B}(H \to \mu\tau) = 0$ (left) or $\mathcal{B}(H \to e\tau) = 0$ (right). First, the results of the fits are shown, when only the data of an individual channel or of an individual category are used; in these cases the signal and control regions from all other channels/categories are removed from the fit. These results are finally compared with the full fit displayed in the last row.

Phys. Lett. B 800 (2020) 135069

Signal Mass spectrum

$$|Y_{\ell\tau}|^2 + |Y_{\tau\ell}|^2 = \frac{8\pi}{m_H}\frac{\mathcal{B}(H\to\ell\tau)}{1-\mathcal{B}(H\to\ell\tau)}\Gamma_H(\mathrm{SM}),$$

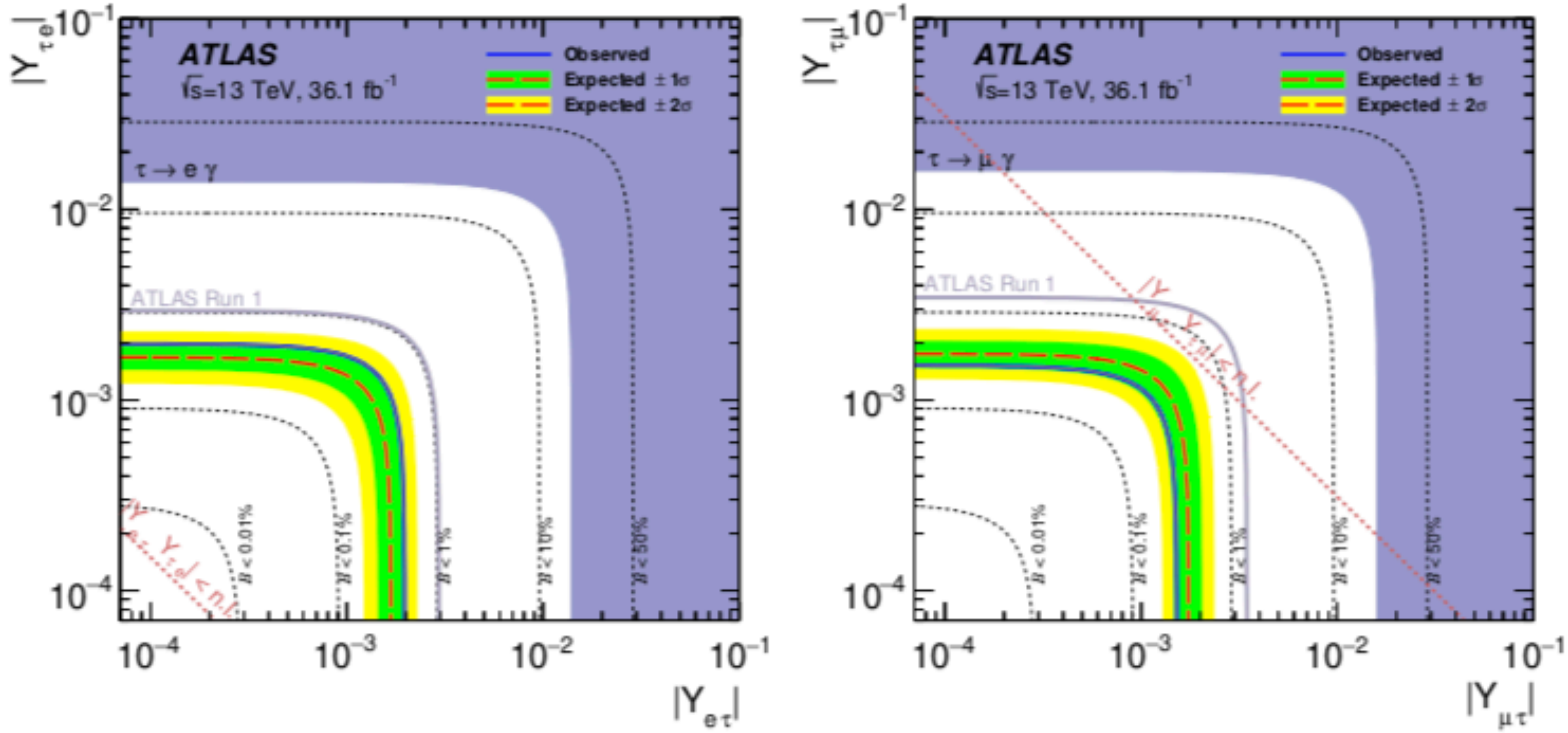

Figure 5: Upper limits on the absolute value of the couplings $Y_{\tau\ell}$ and $Y_{\ell\tau}$ together with the limits from the ATLAS Run 1 analysis (light grey line) and the most stringent indirect limits from $\tau\to\ell\gamma$ searches (dark purple region). Also indicated are limits corresponding to different branching ratios (0.01%, 0.1%, 1%, 10% and 50%) and the naturalness limit (denoted n.l.) $|Y_{\tau\ell}Y_{\ell\tau}| \lesssim \frac{m_\tau m_\ell}{v}$ [84] where v is the vacuum expectation value of the Higgs field.

Phys. Lett. B 800 (2020) 135069

Backup Others

2018: **Search for H→ J/ψγ and H→ϒγ (36 fb^{-1}, $\sqrt{s}$=13 TeV)**

Phys. Lett. B 786 (2018) 134

2018: **Search for H→φγ, H→ργ (36 fb^{-1}, $\sqrt{s}$=13 TeV)**

JHEP 07 (2018) 127

2018: **Search for H→c$\bar{c}$ (36 fb^{-1}, $\sqrt{s}$=13 TeV)**

Phys. Rev. Lett. 120 (2018) 211802

2017: **Search for H→ Zγ (36 fb^{-1}, $\sqrt{s}$=13 TeV)**

JHEP 10 (2017) 112

Search for H→ J/ψγ and H→ϒγ

Truth Pt Spectra

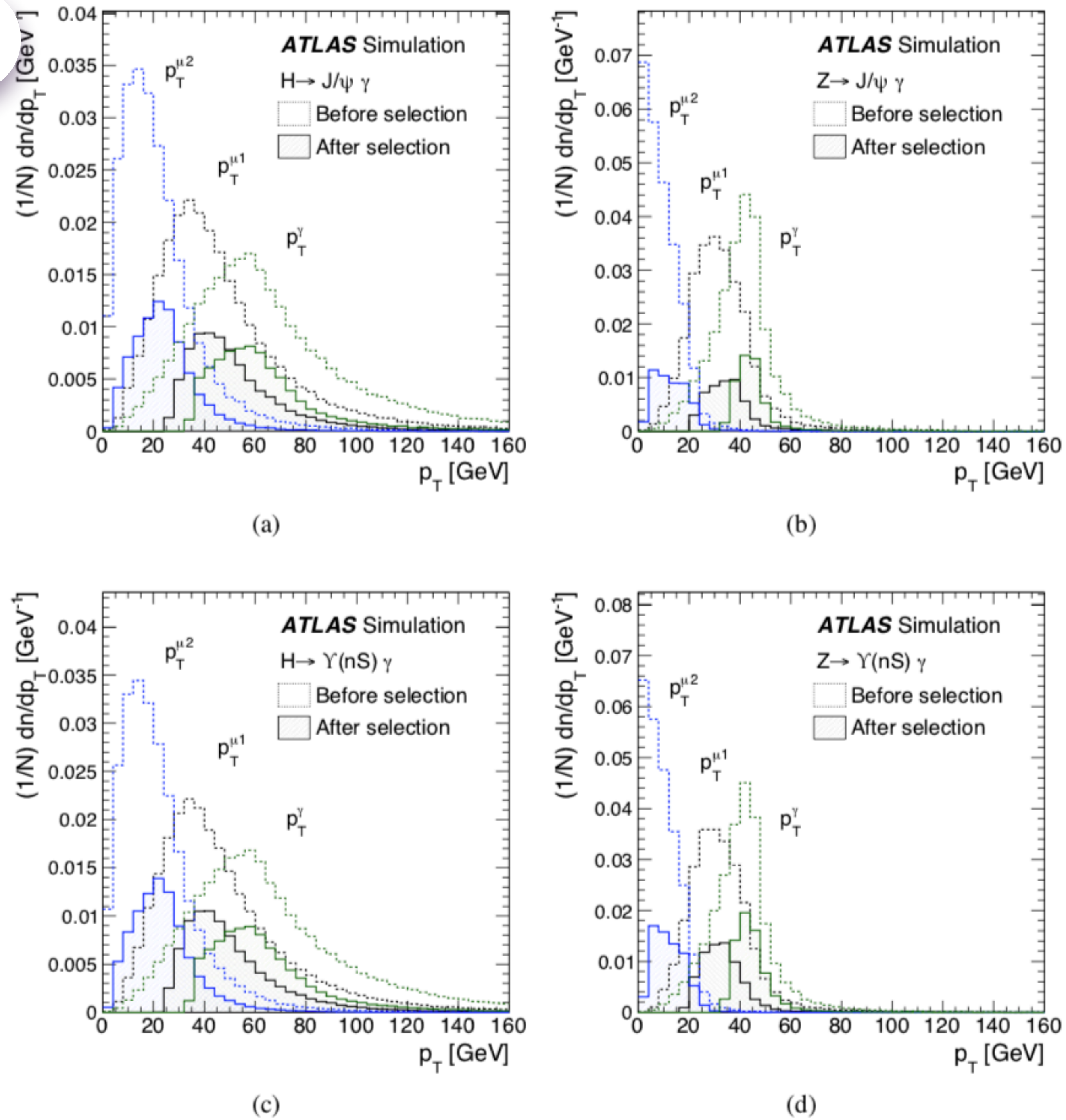

Figure 1: Generator-level transverse momentum (p_T) distributions of the photon and of the muons, ordered in p_T, for (a) $H \to J/\psi\,\gamma$, (b) $Z \to J/\psi\,\gamma$, (c) $H \to \Upsilon(nS)\,\gamma$ and (d) $Z \to \Upsilon(nS)\,\gamma$ simulated signal events, respectively. The leading muon candidate is denoted by $p_T^{\mu 1}$ and the subleading candidate by $p_T^{\mu 2}$. The hatched histograms denote the full event selection while the dashed histograms show the events at generator level that fall within the analysis geometric acceptance (both muons are required to have $|\eta^{\mu}| < 2.5$ while the photon is required to have $|\eta^{\gamma}| < 2.37$, excluding the region $1.37 < |\eta^{\gamma}| < 1.52$). The dashed histograms are normalised to unity, and the relative difference between the two sets of distributions corresponds to the effects of reconstruction, trigger, and event selection efficiencies.

ys. Lett. B 786 (2018) 134

Mass Spectra

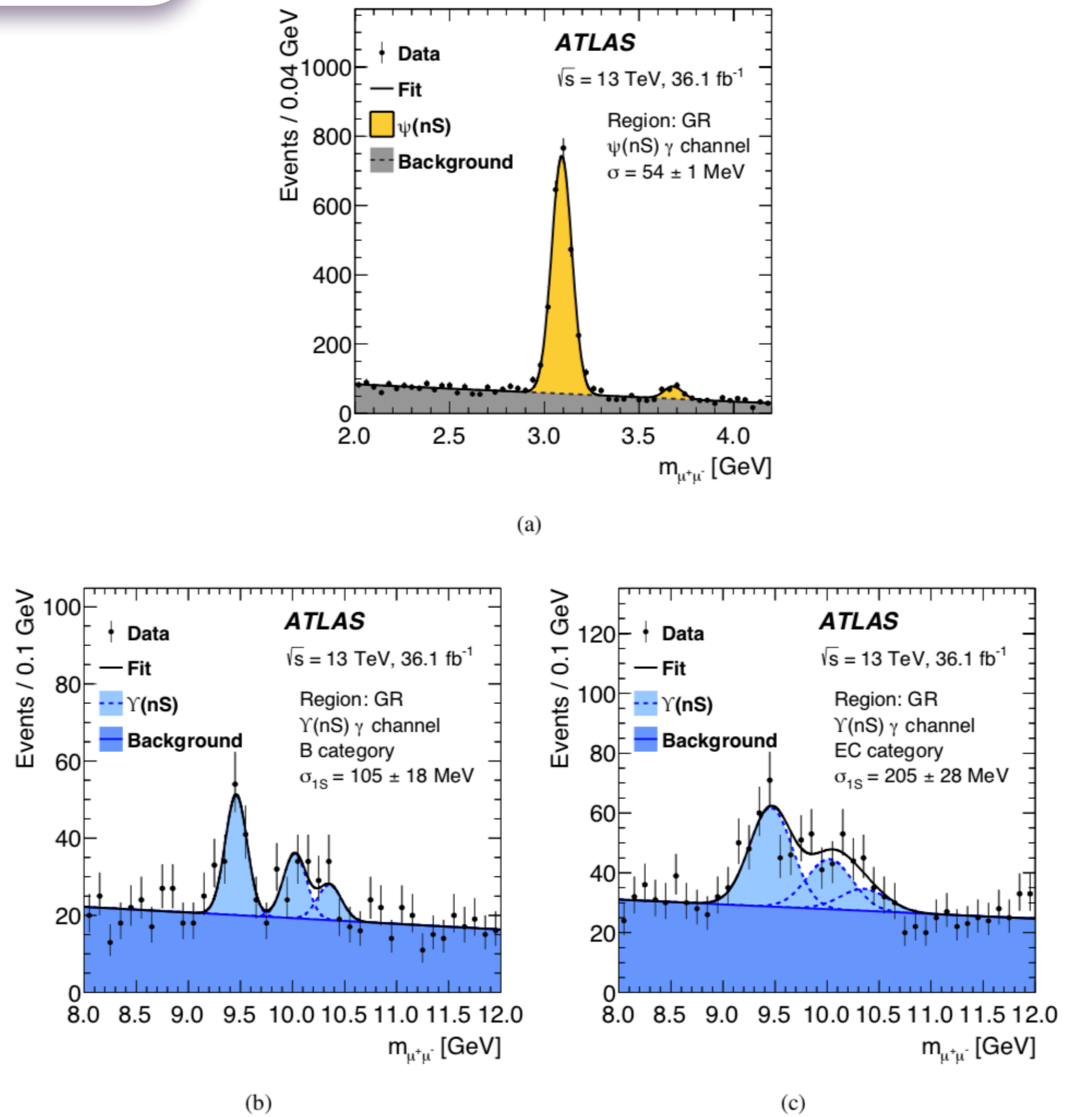

Figure 2: Distribution of $\mu^+\mu^-$ invariant mass for (a) $\psi(nS)\gamma$ and $\Upsilon(nS)\gamma$ ((b) barrel and (c) endcap categories) candidates. The candidates satisfy the event selection but without the nominal isolation requirements and with a looser minimum p_T^Q requirement of 30 GeV. These events constitute the background "generation region" defined in Section 6.

Phys. Lett. B 786 (2018) 134

Background Mass spectra

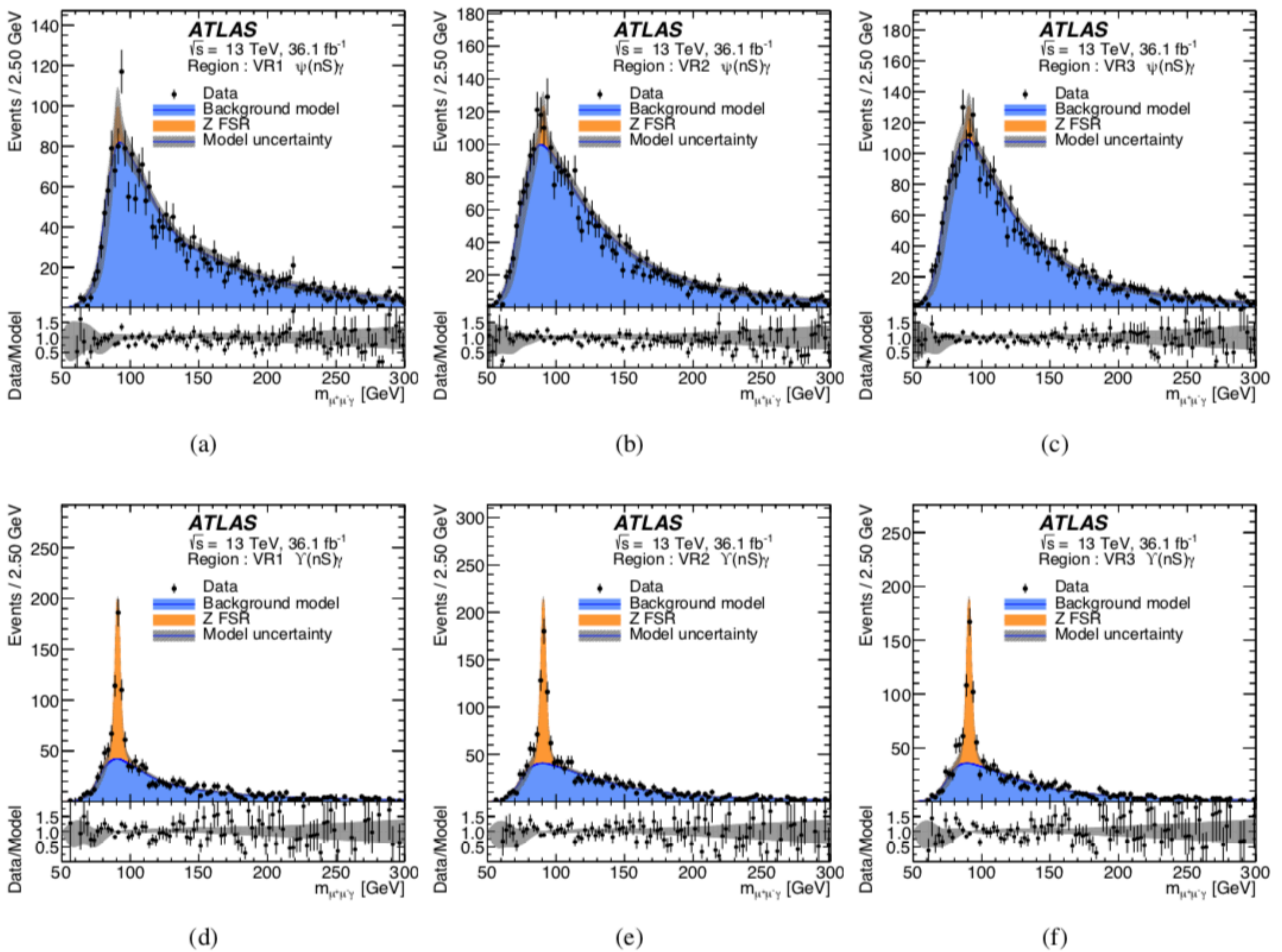

Figure 3: The distribution of $m_{\mu^+\mu^-\gamma}$ in data compared to the prediction of the background model for ((a), (b) and (c)) $H(Z) \to \psi(nS)\,\gamma$ and ((d), (e) and (f)) $H(Z) \to \Upsilon(nS)\,\gamma$ in the VR1, VR2 and VR3 validation regions. Z FSR refers to the $Z \to \mu^+\mu^-\gamma$ background contribution. The background model is normalised to the observed number of events within the region shown. The uncertainty band corresponds to the uncertainty envelope derived from variations in the background modelling procedure.

Phys. Lett. B 786 (2018) 134

Systematics & Yields

Table 1: Summary of the systematic uncertainties in the expected signal yields.

Source of systematic uncertainty	Yield uncertainty $H(Z) \to Q\gamma$
Total $H(Z)$ cross section	7.0% (2.9%)
Integrated luminosity	2.1%
$H(Z)$ QCD modelling	1.8% (6%)
Trigger efficiency	2.0%
Photon identification	1.4%
Muon identification and reconstruction	2.8%
Photon energy scale	0.3%
Muon momentum scale	0.2%

Table 2: The number of observed events and the mean expected background, with its total uncertainty, for the $m_{Q\gamma}$ ranges of interest. The expected Z and Higgs boson contributions are shown for branching fraction values of 10^{-6} and 10^{-3}, respectively. These values are motivated by the expected sensitivity of the search to the respective branching fractions.

	$m_{\mu^+\mu^-}$ mass range [GeV]	Observed (expected background) $m_{\mu^+\mu^-\gamma}$ mass range [GeV] 81–101		Observed (expected background) $m_{\mu^+\mu^-\gamma}$ mass range [GeV] 120–130		Z signal for $\mathcal{B} = 10^{-6}$	H signal for $\mathcal{B} = 10^{-3}$
$J/\psi\,\gamma$	2.9–3.3	92	(89 ± 6)	20	(23.6 ± 1.3)	13.7 ± 1.1	22.2 ± 1.9
$\psi(2S)\,\gamma$	3.5–3.9	43	(42 ± 5)	8	(10.0 ± 0.8)	1.82 ± 0.14	2.96 ± 0.25
$\Upsilon(1S)\,\gamma$	9.0–10.0	115	(126 ± 8)	9	(13.6 ± 1.2)	7.8 ± 0.6	10.7 ± 0.9
$\Upsilon(2S)\,\gamma$	9.5–10.5	106	(121 ± 8)	8	(12.6 ± 1.4)	5.9 ± 0.5	8.1 ± 0.7
$\Upsilon(3S)\,\gamma$	10.0–11.0	112	(113 ± 8)	7	(10.6 ± 1.2)	7.1 ± 0.6	9.2 ± 0.8

Phys. Lett. B 786 (2018) 134

S+B Postfit Mass spectra

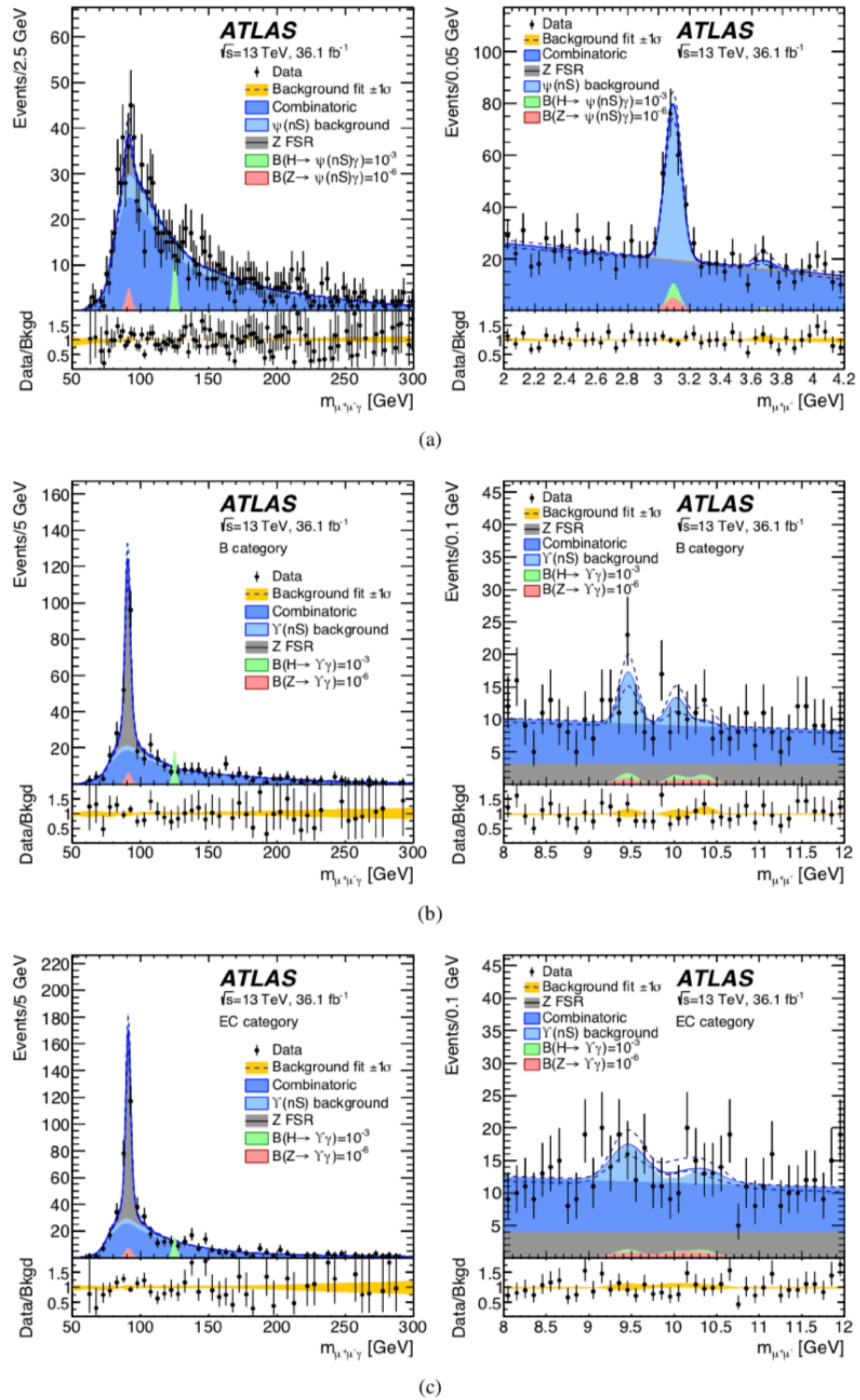

Phys. Lett. B 786 (2018) 134

Figure 4: The $m_{\mu^+\mu^-\gamma}$ and $m_{\mu^+\mu^-}$ distributions for the selected (a) $\psi(nS)\,\gamma$ and $\Upsilon(nS)\,\gamma$ ((b) barrel and (c) endcap categories) candidates along with the results of the maximum-likelihood fits with background-only models. Z FSR refers to the $Z \to \mu^+\mu^-\gamma$ background contribution. The solid blue line denotes the full fit result and the dashed blue lines correspond to its $\pm 1\sigma$ uncertainty band. The ratios of the data to the background-only fits are also shown.

Search for H→ Zγ

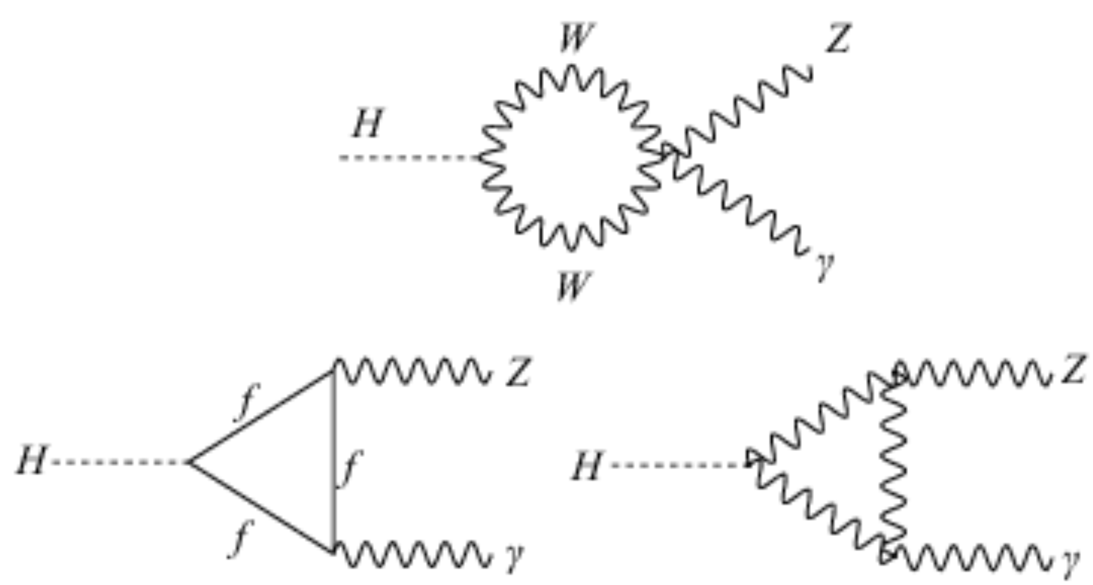

Simulators & Plots

Table 1: Higgs boson production processes produced with POWHEG Box with the techniques used and their precision in α_s for the event generation (gen.). The total cross section is known with higher precision in QCD and electroweak (norm.) than available in the event generation. The events were reweighted to reproduce the more precise total cross section.

Process	Technique	QCD (gen.)	QCD (norm.)	EW (norm.)
ggF	MiNLO & NNLOPS	NNLO (incl.), NLO (H + 1-jet)	NNNLO	NLO
VBF	POWHEG	NLO	approx. NNLO	NLO
VH	MiNLO	NLO (incl. and H + 1-jet)	NNLO	NLO

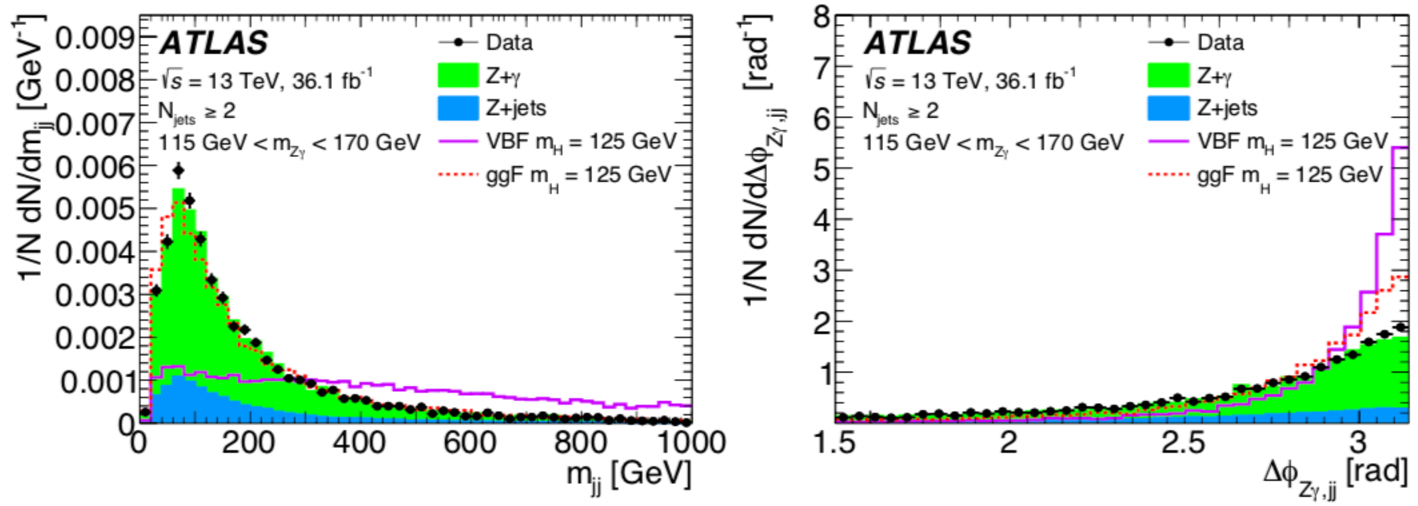

(a) (b)

Figure 2: Kinematic variables used in the BDT used to define the VBF-enriched category: (a) the invariant mass of the two jets with the highest transverse momenta, m_{jj} and (b) the azimuthal separation of the $Z\gamma$ and the dijet system, $\Delta\phi_{Z\gamma,jj}$ for events with at least two jets and 115 GeV $< m_{Z\gamma} <$ 170 GeV. The observed distribution (normalised to unity) is shown as data points. The contributions from $Z + \gamma$ events (obtained from simulation) and the contribution from Z+jets (obtained from data control regions described in the text) are shown as stacked histograms. The corresponding expected distributions for Higgs bosons produced via gluon–gluon fusion and vector-boson fusion production for m_H = 125 GeV are shown as open histograms. The $\Delta\phi_{Z\gamma,jj}$ distribution is shown before the suppression of the shape information for $\Delta\phi_{Z\gamma,jj} > 2.94$.

JHEP 10 (2017) 112 \
Searches for the Zγ decay mode of the Higgs boson and for new high-mass resonances in pp collisions at √s = 13 TeV with the ATL

Signal Eff & Yields

Table 2: The expected signal efficiency times acceptance, denoted by ϵ, per production mode for each category after the full event selection, as well as the expected fraction f of each production process relative to the total signal yield, for simulated SM Higgs boson production assuming m_H = 125 GeV. The expected number of signal events per production process is also given.

	ggF		VBF		WH		ZH	
Category	$\epsilon[\%]$	$f[\%]$	$\epsilon[\%]$	$f[\%]$	$\epsilon[\%]$	$f[\%]$	$\epsilon[\%]$	$f[\%]$
VBF-enriched	0.25	30.5	6.5	67.5	0.34	1.3	0.24	0.6
High relative p_T	1.1	71.5	2.6	14.3	4.0	8.3	4.1	5.3
ee high p_{Tt}	1.7	80.8	2.8	11.0	3.2	4.7	3.6	3.3
ee low p_{Tt}	7.1	93.2	3.6	4.1	3.7	1.5	4.2	1.1
$\mu\mu$ high p_{Tt}	2.2	80.4	3.6	11.3	4.1	4.8	4.2	3.1
$\mu\mu$ low p_{Tt}	9.2	93.4	4.7	4.1	4.6	1.5	4.8	1.0
Total efficiency (%)	21.5		23.8		20.2		21.0	
Expected events	35		3.3		1.0		0.7	

Table 3: The number of data events selected in the mass range used for the background fit to the $m_{Z\gamma}$ spectrum (115–150 GeV) per category. In addition, the following numbers are given: the expected number of Higgs boson signal events in an interval around the peak position for a signal of m_H = 125.09 GeV, expected to contain 90% of the SM signal (S_{90}), the half-width of the S_{90} interval (w_{90}), as well as the expected signal-to-background ratio in the S_{90} window (S_{90}/B_{90}) with B_{90} determined from data, and the expected significance estimate $S_{90}/\sqrt{S_{90}+B_{90}}$.

Category	Events	S_{90}	w_{90} [GeV]	S_{90}/B_{90} $[10^{-2}]$	$S_{90}/\sqrt{S_{90}+B_{90}}$
VBF-enriched	88	1.2	3.9	9.5	0.32
High relative p_T	443	2.3	3.9	3.0	0.26
ee high p_{Tt}	1053	3.3	3.9	1.1	0.19
ee low p_{Tt}	11707	11.2	4.2	0.3	0.18
$\mu\mu$ high p_{Tt}	1413	4.0	3.7	1.2	0.22
$\mu\mu$ low p_{Tt}	16529	14.5	3.8	0.3	0.21

JHEP 10 (2017) 112 \
Searches for the Zγ decay mode of the Higgs boson and for new high-mass resonances in pp collisions at √s = 13 TeV with the ATL

Mass spectra

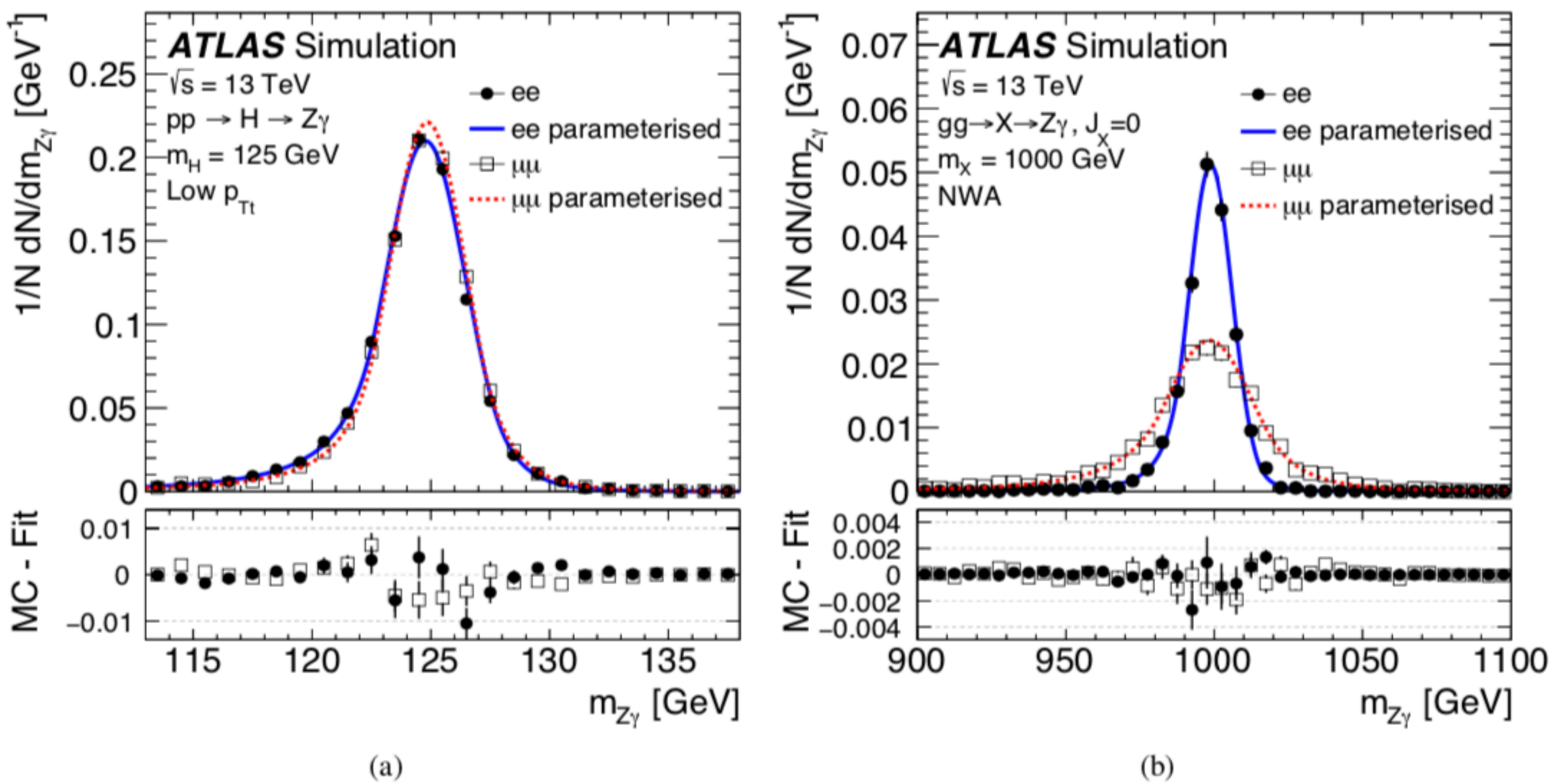

Figure 3: The differential distribution of the invariant $Z\gamma$ mass ($m_{Z\gamma}$) for (a) Higgs bosons with $m_H = 125$ GeV in the low p_{Tt} categories and (b) high-mass spin-0 particles produced via gluon–gluon fusion and with $m_X = 1000$ GeV, using the narrow width assumption (NWA). The markers show the $m_{Z\gamma}$ distributions and the solid and dotted lines the fitted parameterisations used in the searches. The bottom part of the figures shows the residuals between the markers and the parameterisation.

JHEP 10 (2017) 112 \
Searches for the Zγ decay mode of the Higgs boson and for new high-mass resonances in pp collisions at √s = 13 TeV with the ATL

Systematics

Table 5: The main sources of theoretical and modelling uncertainties for the $H \to Z\gamma$ search. For the uncertainties in the total efficiency and the acceptance of the different categories, the gluon–gluon fusion samples produced with Powheg Box v1 with and without MPI are used, as well as the nominal Powheg Box v2 gluon–gluon fusion signal sample along with the sample generated with MadGraph5_aMC@NLO, as described in the text. The combined uncertainty on the total cross section and efficiency is given assuming the cross sections predicted by the SM. The ranges for the uncertainties cover the variations among different categories. The uncertainty values are given as relative uncertainties.

Sources	
Total cross section and efficiency [%]	
Underlying event	5.3
ggF perturbative order	3.9
ggF PDF and α_s	3.2
VBF perturbative order	0.4
VBF PDF and α_s	2.1
WH (ZH) perturbative order	0.5 (3.8)
WH (ZH) PDF and α_s	1.9 (1.6)
Interference	5.0
$B(H \to Z\gamma)$	5.9
Total (total cross section and efficiency)	10
Category acceptance [%]	
ggF H + 2-jets in VBF-enriched category	0.5–45
ggF BDT variables	0.2–15
ggF Higgs p_T	8.4–22
PDF and α_s	0.2–2.0
Underlying event	2.9–25
Total (category acceptance)	9.5–49

Table 4: The main sources of experimental uncertainty for the $H/X \to Z\gamma$ searches. The gluon–gluon fusion signal samples produced at m_H = 125 GeV and m_X = [300–2500] GeV are used to estimate the systematic uncertainty. The ranges for the uncertainties span the variations among different categories and different m_X resonance masses. The uncertainty values are given as fractions of the total predictions, except for the spurious signal uncertainty, which is reported as the absolute number of events. Values are not listed if systematic sources are negligible or not applicable.

Sources	$H \to Z\gamma$	$X \to Z\gamma$
Luminosity [%]		
Luminosity	3.2	3.2
Signal efficiency [%]		
Modelling of pile-up interactions	0.02–0.03	< 0.01–0.2
Photon identification efficiency	0.7–1.7	2.0–2.6
Photon isolation efficiency	0.07–0.4	0.6–0.6
Electron identification efficiency	0.0–1.6	0.0–2.6
Electron isolation efficiency	0.0–0.2	0.0–3.5
Electron reconstruction efficiency	0.0–0.4	0.0–1.0
Electron trigger efficiency	0.0–0.1	0.0–0.2
Muon selection efficiency	0.0–1.6	0.0–0.7
Muon trigger efficiency	0.0–3.5	0.0–4.2
MC statistical uncertainty	–	1.2–2.0
Jet energy scale, resolution, and pile-up	0.2–10	–
Total (signal efficiency)	2.1–10	4.0–6.3
Signal modelling on σ_{CB} [%]		
Electron and photon energy scale	0.6–3.5	1.0–4.0
Electron and photon energy resolution	1.1–4.0	4.0–30
Muon momentum scale	0.0–0.5	0.0–3.0
Muon ID resolution	0.0–3.7	0.0–2.0
Muon MS resolution	0.0–1.7	0.0–4.0
Signal modelling on μ_{CB} [%]		
Electron and photon energy scale	0.1–0.2	0.2–0.6
Muon momentum scale	0.0–0.03	0.0–0.03
Higgs mass	0.2	–
Background modelling [Events]		
Spurious signal	1.7–25	0.005–6.1

JHEP 10 (2017) 112 \
Searches for the Zγ decay mode of the Higgs boson and for new high-mass resonances in pp collisions at √s = 13 TeV with the ATL

Postfit Mass spectra/ Category

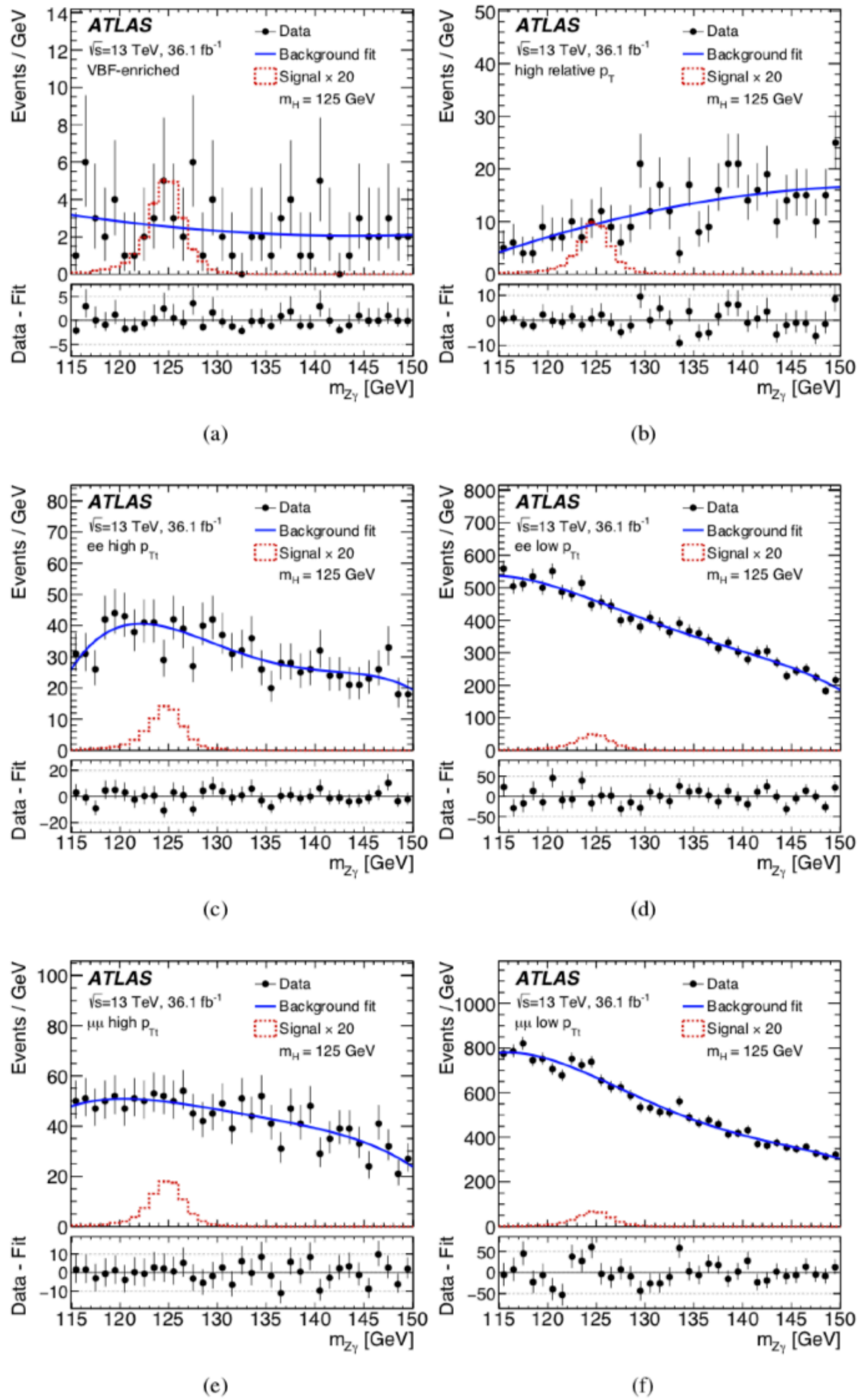

Figure 5: The invariant $Z\gamma$ mass ($m_{Z\gamma}$) distributions of events satisfying the $H \to Z\gamma$ selection in data for the six event categories: (a) VBF-enriched, (b) high p_{Tt}^{γ}, (c) ee high p_{Tt}, (d) ee low p_{Tt}, (e) $\mu\mu$ high p_{Tt}, and (f) $\mu\mu$ low p_{Tt}. The points represent the data and the statistical uncertainty. The solid lines show the background-only fits to the data, performed independently in each category. The dashed histogram corresponds to the expected signal for a SM Higgs boson with $m_H = 125$ GeV decaying to $Z\gamma$ with a rate 20 times the SM prediction. The bottom part of the figures shows the residuals of the data with respect to the background-only fit.

JHEP 10 (2017) 112 \
ıigh-mass resonances in pp collisions at √s = 13 TeV with the ATL

Mass spectra

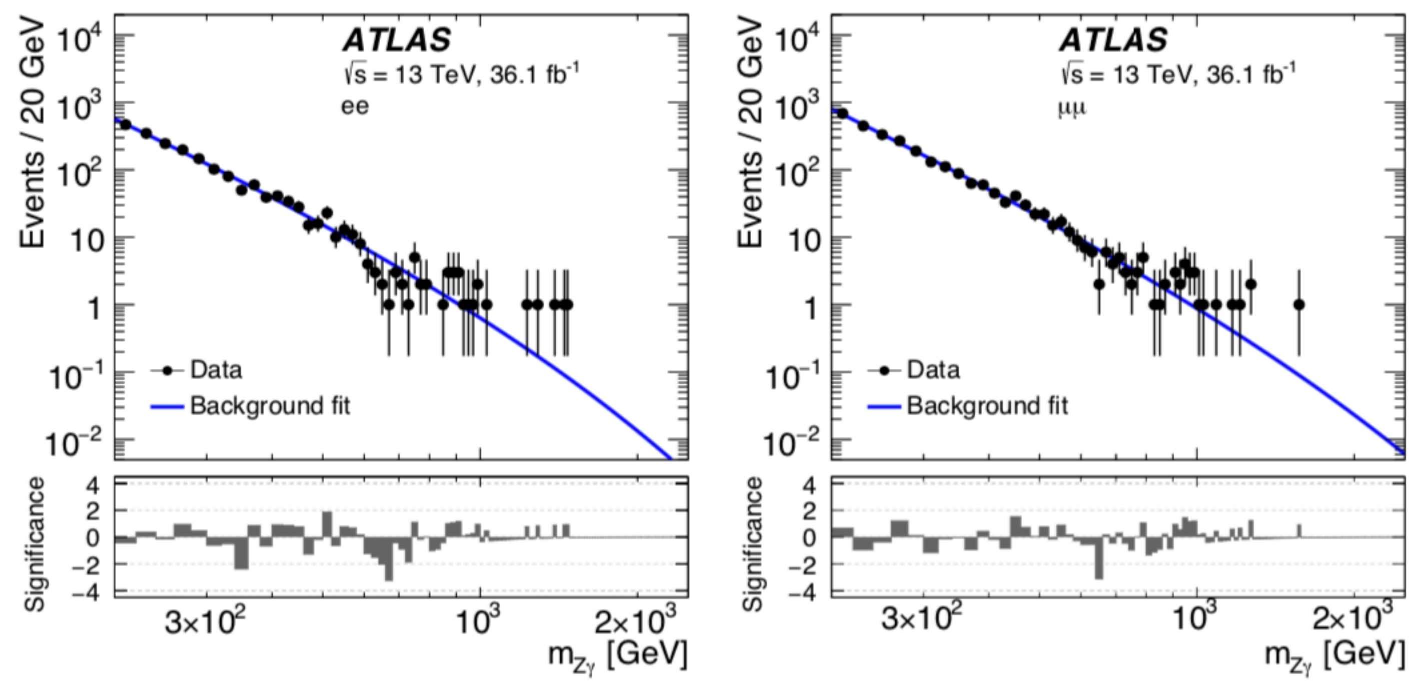

(a) (b)

Figure 6: The invariant $Z\gamma$ mass ($m_{Z\gamma}$) distributions of events satisfying the high-mass selection in data for the two event categories: (a) ee and (b) $\mu\mu$. The points represent the data and the statistical uncertainty. The solid lines show the background-only fit to the data, performed independently in each category. The bottom part of the figures shows the significance, here defined as the residual of the data with respect to the background-only fit divided by the statistical uncertainty of the data.

JHEP 10 (2017) 112 \
Searches for the Zγ decay mode of the Higgs boson and for new high-mass resonances in pp collisions at √s = 13 TeV with the ATL

CL Exclusion

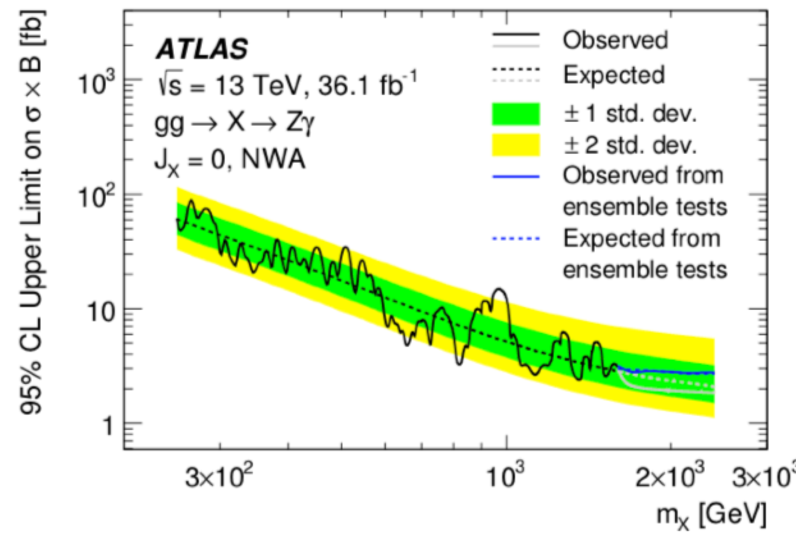

Figure 7: The observed (solid line) and expected (dashed line) upper limit derived at the 95% CL on $\sigma(pp \to X) \cdot B(X \to Z\gamma)$ at $\sqrt{s}$ = 13 TeV as a function of the high-mass spin-0 resonance's mass, assuming production via gluon–gluon fusion and using the narrow width assumption (NWA). For m_X > 1.6 TeV results are derived from ensemble tests in addition to the results obtained using closed-form asymptotic formulae. The shaded regions correspond to the ±1 and ±2 standard deviation bands for the expected exclusion limit derived using asymptotic formulae.

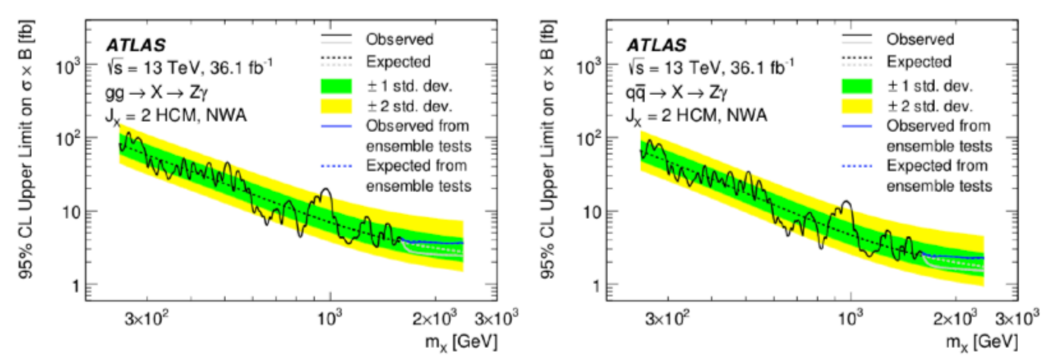

(a) (b)

Figure 8: The observed (solid line) and expected (dashed line) upper limit derived at the 95% CL on $\sigma(pp \to X) \cdot B(X \to Z\gamma)$ at $\sqrt{s}$ = 13 TeV as a function of the spin-2 resonance mass produced via (a) gluon–gluon initial states and (b) $q\bar{q}$ initial states modelled using the Higgs Characterisation Model (HCM), using the narrow width assumption (NWA). For m_X > 1.6 TeV results are derived from ensemble tests in addition to the results obtained using closed-form asymptotic formulae. The shaded regions correspond to the ±1 and ±2 standard deviation bands for the expected exclusion limit derived using asymptotic formulae.

JHEP 10 (2017) 112 \

Search for $H \rightarrow c\bar{c}$

Generators

Table 1: The configurations used for event generation of the signal and background processes. If two parton distribution functions (PDFs) are shown, the first is for the matrix element calculation and the second for the parton shower, otherwise the same is used for both. Alternative event generators and configurations, used to estimate systematic uncertainties, are in parentheses. Tune refers to the underlying-event tuned parameters of the parton shower event generator. MG5_aMC refers to MadGraph5_aMC@NLO 2.2.2 [30]; Pythia 8 refers to version 8.212 [31]. Heavy-flavor hadron decays modeled by EvtGen 1.2.0 [32] are used for all samples except those generated using Sherpa. The order of the calculation of the cross-sections used to normalize the predictions is indicated. The $q\bar{q} \to ZH$ cross-section is estimated by subtracting the $gg \to ZH$ cross-section from the $pp \to ZH$ cross-section. The asterisk (*) in the last column denotes that the indicated order is for the $pp \to ZH$ cross-section. NNLO denotes next-to-next-to-leading order; NLL denotes next-to-leading-log and NNLL denotes next-to-next-to-leading log.

Process	Event Generator (alternative)	Parton Shower (alternative)	PDF (alternative)	Tune	Cross-section
$q\bar{q} \to ZH$	Powheg-BOX v2 [28] +GoSaM [35] +MiNLO [45, 46]	Pythia 8 (Herwig 7 [47])	PDF4LHC15NLO [33] /CTEQ6L1 [36, 37]	AZNLO [34] (A14 [48])	NNLO (QCD)* +NLO (EW) [38–44]
$gg \to ZH$	Powheg-BOX v2	Pythia 8 (Herwig 7)	PDF4LHC15NLO /CTEQ6L1	AZNLO (A14)	NLO+NLL (QCD) [17, 49–51]
$t\bar{t}$	Powheg-BOX v2	Pythia 8 (Herwig 7)	NNPDF3.0NLO [52] /NNPDF2.3LO	A14	NNLO+NNLL [53]
ZW, ZZ	Sherpa 2.2.1 [29] (Powheg-BOX)	Sherpa (Pythia 8)	NNPDF3.0NNLO	Sherpa	NLO
Z+jets	Sherpa 2.2.1 (MG5_aMC)	Sherpa (Pythia 8)	NNPDF3.0NNLO (NNPDF2.3LO)	Sherpa (A14)	NNLO [54]

Phys. Rev. Lett. 120 (2018) 211802
Search for the Decay of the Higgs Boson to Charm Quarks with the ATLAS Experiment

Tagging efficiency

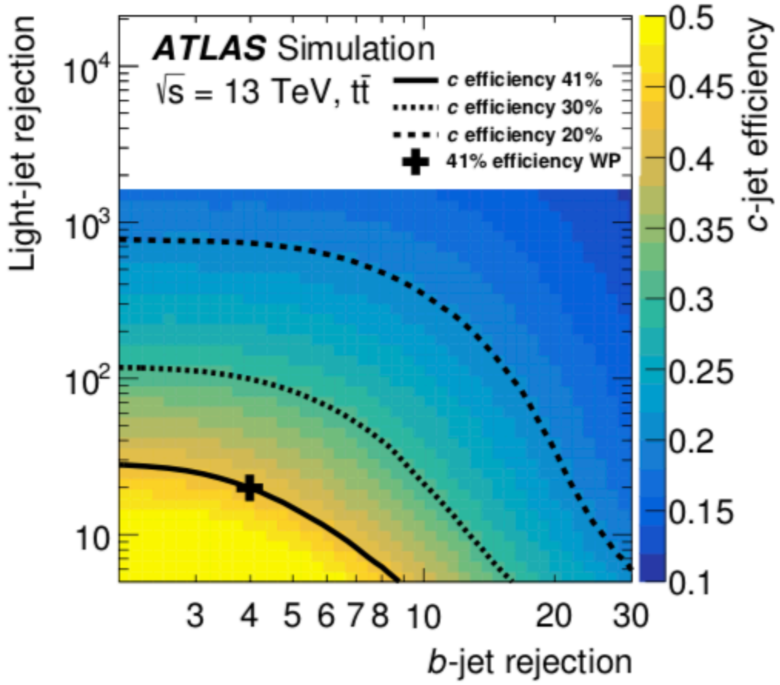

Figure 1: The c-jet tagging efficiency (colored scale) as a function of the b-jet and l-jet rejection as obtained from simulated $t\bar{t}$ events. The cross, labeled as working point, WP, denotes the selection criterion used in this analysis. The solid and dotted black lines indicate the contours in rejection space for the fixed c-tagging efficiency used in the analysis and two alternatives.

Phys. Rev. Lett. 120 (2018) 211802

Systematics & Yields

Table 2: Breakdown of the relative contributions to the total uncertainty in μ. The statistical uncertainty includes the contribution from the floating Z+jets normalization parameters. The sum in quadrature of the individual components differs from the total uncertainty due to correlations between the components.

Source	$\sigma/\sigma_{\text{tot}}$
Statistical	**49%**
Floating Z + jets normalization	31%
Systematic	**87%**
Flavor tagging	73%
Background modeling	47%
Lepton, jet and luminosity	28%
Signal modeling	28%
MC statistical	6%

Table 3: Post-fit yields for the signal and background processes in each category from the profile likelihood fit. Uncertainties include statistical and systematic contributions. The pre-fit SM expected $ZH(c\bar{c})$ signal yields are indicated in parenthesis.

Sample	Yield, 50 GeV < $m_{c\bar{c}}$ < 200 GeV			
	1 c-tag		2 c-tags	
	$75 \leq p_T^Z < 150$ GeV	$p_T^Z \geq 150$ GeV	$75 \leq p_T^Z < 150$ GeV	$p_T^Z \geq 150$ GeV
Z + jets	69400 ± 500	15650 ± 180	5320 ± 100	1280 ± 40
ZW	750 ± 130	290 ± 50	53 ± 13	20 ± 5
ZZ	490 ± 70	180 ± 28	55 ± 18	26 ± 8
$t\bar{t}$	2020 ± 280	130 ± 50	240 ± 40	13 ± 6
$ZH(b\bar{b})$	32 ± 2	19.5 ± 1.5	4.1 ± 0.4	2.7 ± 0.2
$ZH(c\bar{c})$ (SM)	-143 ± 170 (2.4)	-84 ± 100 (1.4)	-30 ± 40 (0.7)	-20 ± 29 (0.5)
Total	72500 ± 320	16180 ± 140	5650 ± 80	1320 ± 40
Data	72504	16181	5648	1320

Phys. Rev. Lett. 120 (2018) 211802
Search for the Decay of the Higgs Boson to Charm Quarks with the ATLAS Experiment

Mass spectra

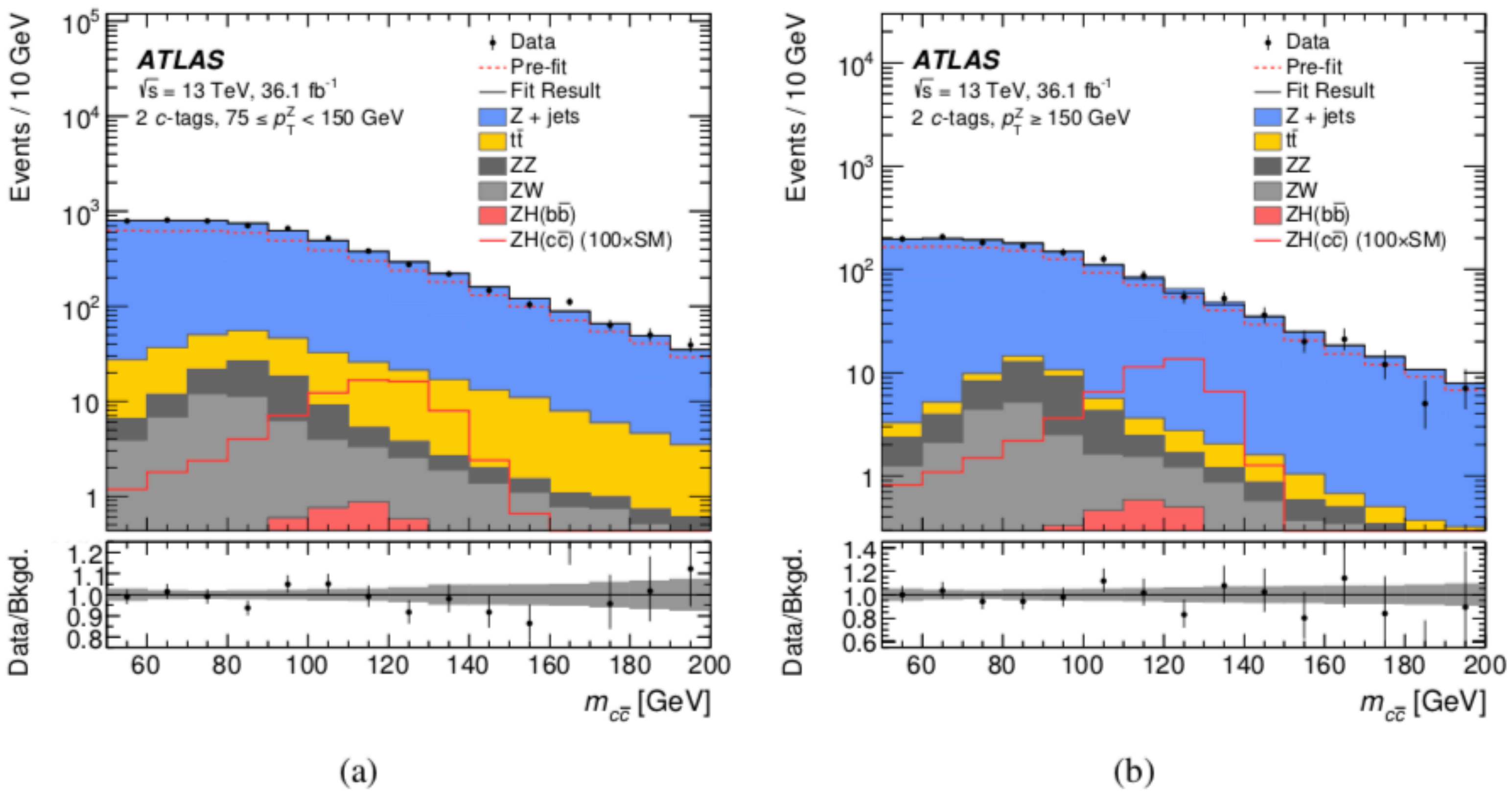

Figure 2: Observed and predicted $m_{c\bar{c}}$ distributions in the 2 c-tag analysis categories. The expected signal is scaled by a factor of 100. Backgrounds are corrected to the results of the fit to the data. The predicted background from the simulation is shown as red dashed histograms. The ratios of the data to the fitted background are shown in the lower panels. The error bands indicate the sum in quadrature of the statistical and systematic uncertainties in the background prediction.

Phys. Rev. Lett. 120 (2018) 211802
Search for the Decay of the Higgs Boson to Charm Quarks with the ATLAS Experiment

Results

A search for the decay of the Higgs boson to charm quarks has been performed using 36.1 fb^{-1} of data collected with the ATLAS detector in pp collisions at $\sqrt{s}$ = 13 TeV at the LHC. No significant excess of $ZH(c\bar{c})$ production is observed over the SM background expectation. The observed upper limit on $\sigma(pp \to ZH) \times \mathcal{B}(H \to c\bar{c})$ is 2.7 pb at the 95% CL. The corresponding expected upper limit is $3.9^{+2.1}_{-1.1}$ pb. This is the most stringent limit to date in direct searches for the inclusive decay of the Higgs boson to charm quarks.

Phys. Rev. Lett. 120 (2018) 211802

Search for H→φγ, H→ργ

Truth pt spectra

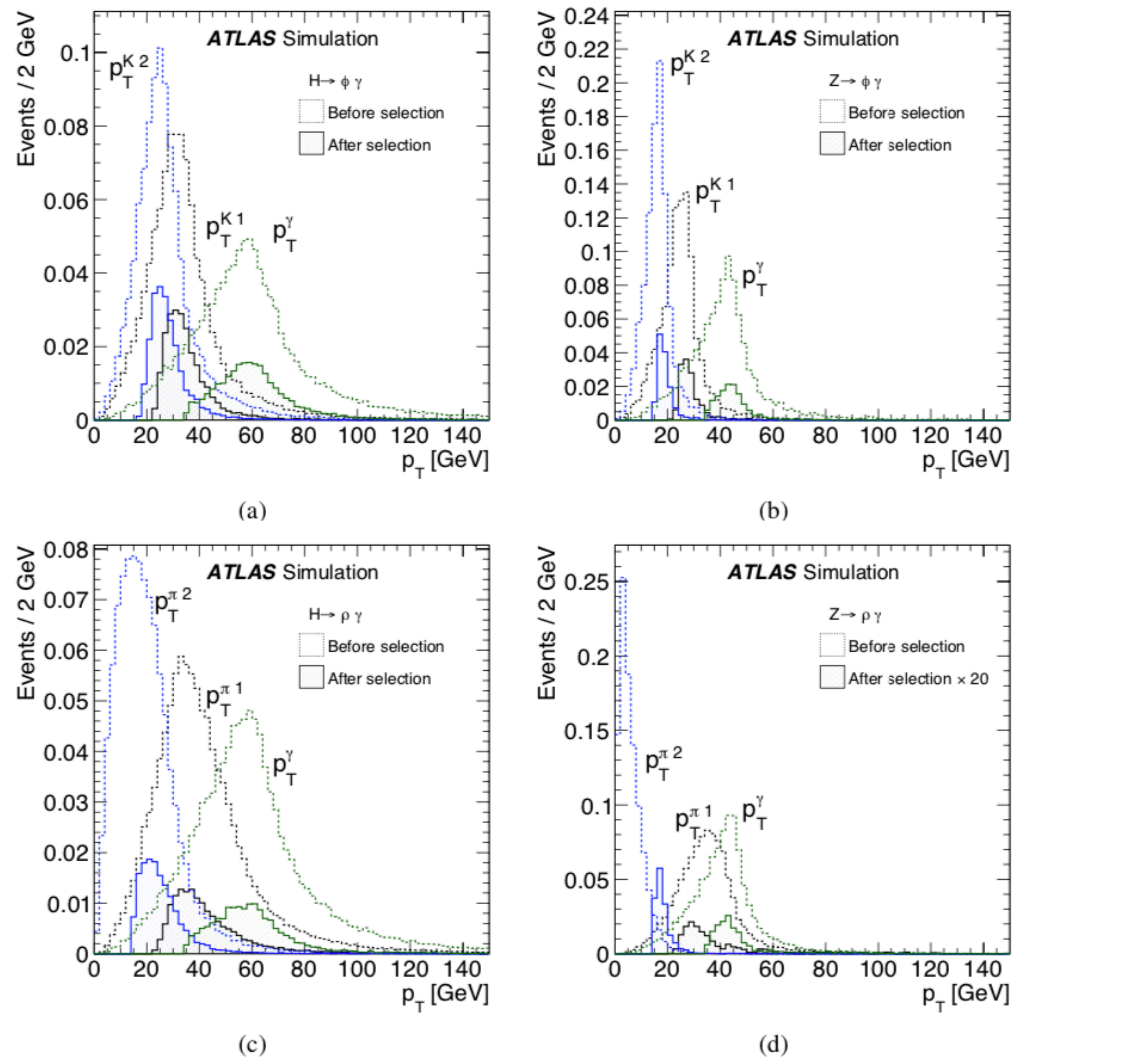

Figure 1: Generator-level transverse momentum (p_T) distributions of the photon and of the charged-hadrons, ordered in p_T, for (a) $H \to \phi\gamma$, (b) $Z \to \phi\gamma$, (c) $H \to \rho\gamma$ and (d) $Z \to \rho\gamma$ simulated signal events, respectively. The hatched histograms denote the full event selection while the dashed histograms show the events at generator level that fall within the analysis geometric acceptance (both charged-hadrons are required to have $|\eta| < 2.5$ while the photon is required to have $|\eta| < 2.37$, excluding the region $1.37 < |\eta| < 1.52$). The dashed histograms are normalised to unity, and the relative difference between the two sets of distributions corresponds to the effects of reconstruction, trigger, and event selection efficiencies. The leading charged-hadron candidate $h = K, \pi$ is denoted by p_T^{h1} and the sub-leading candidate by p_T^{h2}.

JHEP 07 (2018) 127

Search for exclusive Higgs and Z boson decays to ϕγ and ϱγ with the ATLAS detector

Mass spectra

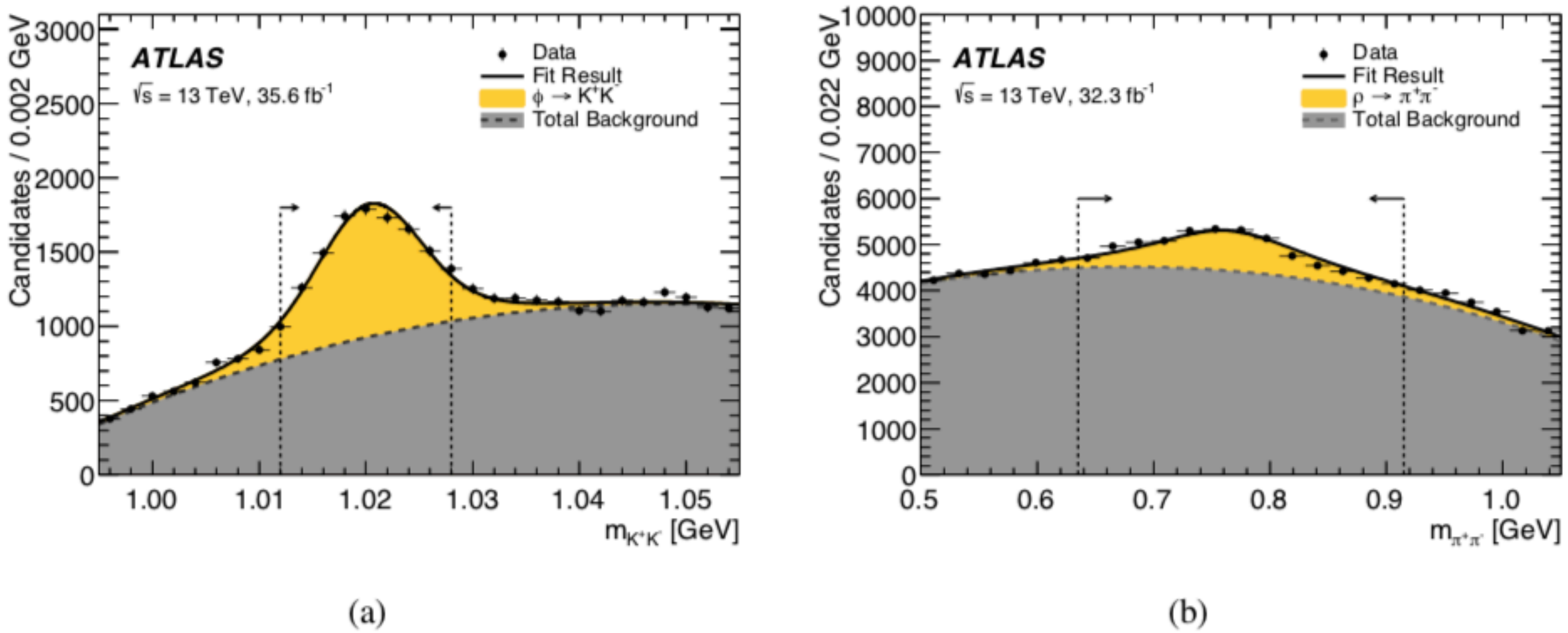

Figure 2: The (a) $m_{K^+K^-}$ and (b) $m_{\pi^+\pi^-}$ distributions for $\phi\gamma$ and $\rho\gamma$ candidates, respectively. The candidates fulfil the complete event selection (see text), apart from requirements on $m_{K^+K^-}$ or $m_{\pi^+\pi^-}$. These requirements are marked on the figures with dashed lines topped with arrows indicating the included area. The signal and background models are discussed in the text.

JHEP 07 (2018) 127
Search for exclusive Higgs and Z boson decays to ϕγ and ϱγ with the ATLAS detector

Mass spectra

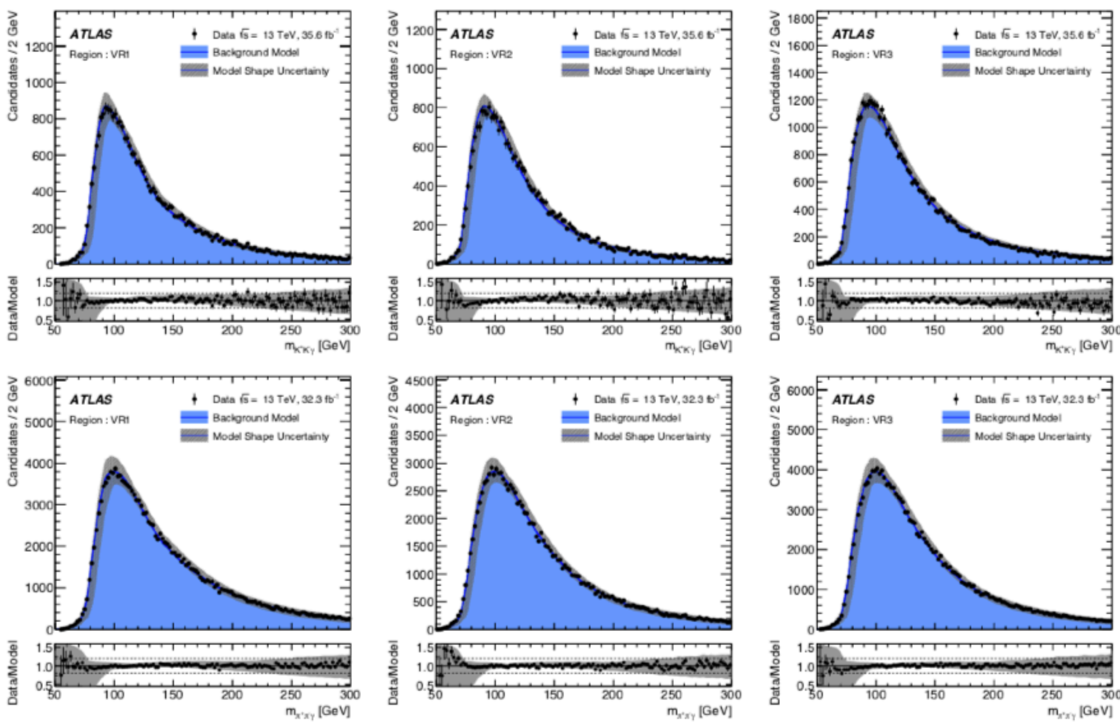

Figure 3: The distribution of $m_{K^+K^-\gamma}$ top ($m_{\pi^+\pi^-\gamma}$ bottom) in data compared to the prediction of the background model for the VR1, VR2 and VR3 validation regions. The background model is normalised to the observed number of events within the region shown. The uncertainty band corresponds to the uncertainty envelope derived from variations in the background modelling procedure. The ratio of the data to the background model is shown below the distributions.

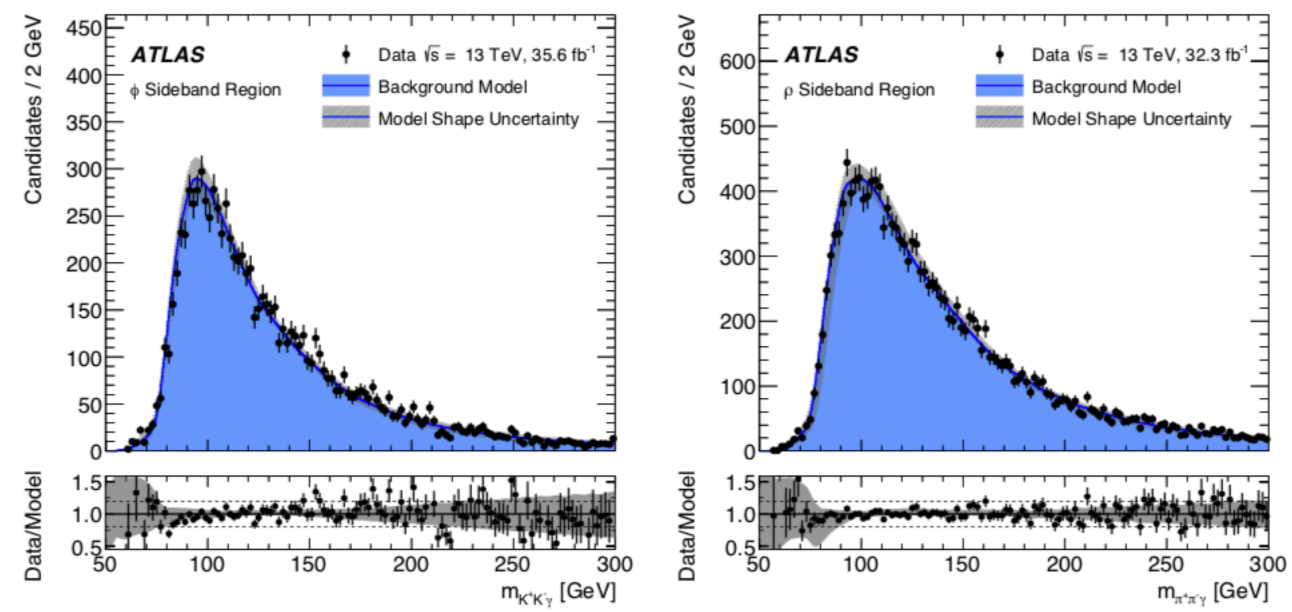

(a) (b)

Figure 4: The distribution of $m_{M\gamma}$ for the (a) $\phi\gamma$ and (b) $\rho\gamma$ selections in the sideband control region. The background model is normalised to the observed number of events within the region shown. The uncertainty band corresponds to the uncertainty envelope derived from variations in the background modelling procedure. The ratio of the data to the background model is shown below the distributions.

JHEP 07 (2018) 127

Search for exclusive Higgs and Z boson decays to ϕγ and ϱγ with the ATLAS detector

Mass spectra

Table 1: Summary of the relative systematic uncertainties in the expected signal yields. The magnitude of the effects are the same for both the $\phi\gamma$ and $\rho\gamma$ selections.

Source of systematic uncertainty	Yield uncertainty
Total H cross section	6.3%
Total Z cross section	2.9%
Integrated luminosity	3.4%
Photon ID efficiency	2.5%
Trigger efficiency	2.0%
Tracking efficiency	6.0%

Table 2: The number of observed events and the mean expected background, estimated from the maximum-likelihood fit and shown with the associated total uncertainty, for the $m_{M\gamma}$ ranges of interest. The expected Higgs and Z boson signal yields, along with the total systematic uncertainty, for $\phi\gamma$ and $\rho\gamma$, estimated using simulations, are also shown in parentheses.

	Observed yields (Mean expected background)					Expected signal yields	
	Mass range [GeV]					H	Z
	All	81–101		120–130		$[\mathcal{B} = 10^{-4}]$	$[\mathcal{B} = 10^{-6}]$
$\phi\gamma$	12051	3364	(3500 ± 30)	1076	(1038 ± 9)	15.6 ± 1.5	83 ± 7
$\rho\gamma$	58702	12583	(12660 ± 60)	5473	(5450 ± 30)	17.0 ± 1.7	7.5 ± 0.6

JHEP 07 (2018) 127

Search for exclusive Higgs and Z boson decays to ϕγ and ϱγ with the ATLAS detector

Search for H→φγ, H→ργ

Mass spectra

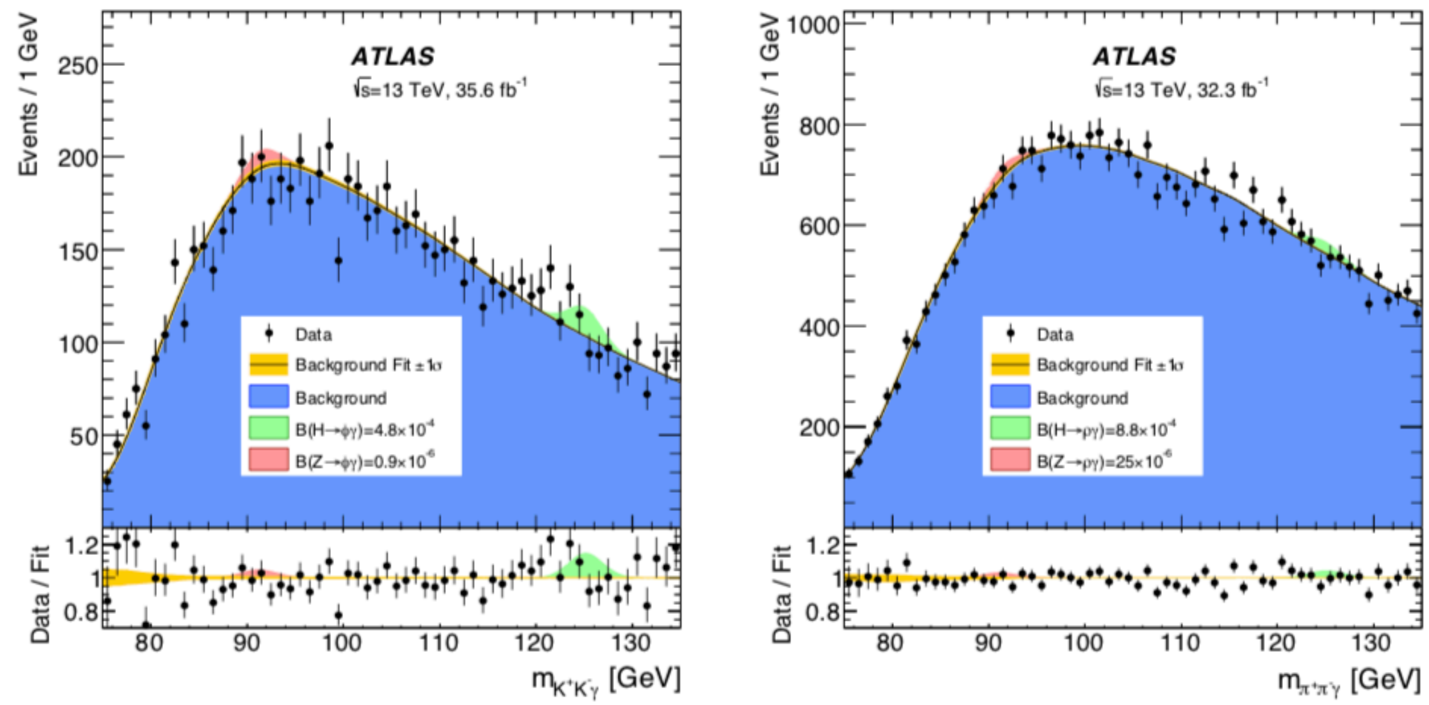

(a) (b)

Figure 5: The (a) $m_{K^+K^-\gamma}$ and (b) $m_{\pi^+\pi^-\gamma}$ distributions of the selected $\phi\gamma$ and $\rho\gamma$ candidates, respectively, along with the results of the maximum-likelihood fits with a background-only model. The Higgs and Z boson contributions for the branching fraction values corresponding to the observed 95% CL upper limits are also shown. Below the figures the ratio of the data to the background-only fit is shown.

Table 3: Expected and observed branching fraction upper limits at 95% CL for the $\phi\gamma$ and $\rho\gamma$ analyses. The $\pm 1\sigma$ intervals of the expected limits are also given.

Branching Fraction Limit (95% CL)	Expected	Observed
$\mathcal{B}(H \to \phi\gamma)\,[\,10^{-4}\,]$	$4.2^{+1.8}_{-1.2}$	4.8
$\mathcal{B}(Z \to \phi\gamma)\,[\,10^{-6}\,]$	$1.3^{+0.6}_{-0.4}$	0.9
$\mathcal{B}(H \to \rho\gamma)\,[\,10^{-4}\,]$	$8.4^{+4.1}_{-2.4}$	8.8
$\mathcal{B}(Z \to \rho\gamma)\,[\,10^{-6}\,]$	33^{+13}_{-9}	25

JHEP 07 (2018) 127